



**Comparative Assessment of Possible Topologies of
Offshore Transmission Network in the North Sea:
Role of the North Sea Wind Power Hub at the Dogger Bank**

Qinghan Chen

February 21, 2018

COMPARATIVE ASSESSMENT OF POSSIBLE TOPOLOGIES OF OFFSHORE TRANSMISSION NETWORK IN THE NORTH SEA: ROLE OF THE NORTH SEA WIND POWER HUB AT THE DOGGER BANK

by

Qinghan Chen

in partial fulfillment of the requirements for the degree of

Master of Science

in **Electrical Engineering**

at Delft University of Technology,

to be defended publicly on Wednesday February 28th, 2018 at 15:00 PM

Student number: 4508874
Project duration: Nov 16, 2016 – Feb 28, 2018
Thesis committee: Prof.ir. Mart van der Meijden, TU Delft & TenneT
Dr.ir. Jose Rueda Torres, TU Delft
Dr. Domenico Lahaye, TU Delft

An electronic version of this thesis is available at <http://repository.tudelft.nl/>.

ACKNOWLEDGEMENTS

First and foremost, I would like to express gratitude to my supervisors, Prof.ir. Mart A.M.M. van der Meijden and Dr.ir. Jose L. Rueda Torres. Throughout the whole process of the thesis project, I received tremendous guidance and help w.r.t technical problems and research methodologies from them, as well as encouragement and patience. It is always a pleasure to discuss with and learn from them, professionally and personally.

Thanks to Dr. Domenico J.P. Lahaye for joining the thesis committee.

Also, I would like to thank the main author of PowerGAMA, Harald Svendsen and the main author of PowerGIM, Martin Kristiansen for their help.

Many thanks to the friends I met in the Netherlands during the past two years. Their company has been inspiring and fun.

Finally, I specifically acknowledge my parents and my girlfriend for their constant support and love.

Qinghan Chen
Delft, February 2018

ABSTRACT

TenneT's vision of the North Sea Infrastructure (NSI) creates a basis for a joint European approach up to 2050 which focuses specifically on developing the North Sea as a source and distribution hub for Europe's energy transition. High wind speed, central location and shallow water qualify the Dogger Bank as the location of the central hub.

For further development of the NSI, more detailed research is needed.

The research gap is recognized that there is not sufficient research on proposing new HVDC grids in the North Sea considering optimization (e.g. following a cost-related objective) of different topology structures within a scope of six surrounding countries (BE, DE, DK, GB, NL and NO), with sensitivity tests regarding uncertainties (e.g. in meteorological condition, load, or industry development).

Therefore, the main research objective of this thesis project is to evaluate CAPEX, overall OPEX of participating countries and other operational performances (e.g. energy mix, nodal price, EENS) of possible topologies of HVDC network in the North Sea, including NSI (with a central North Sea Wind Power Hub at the Dogger Bank) and other two competitive topologies, considering uncertainties in green energy technology development, European coordination, load and meteorological condition (e.g. wind speed, solar radiation and hydrology).

Three specific research questions were studied in order to achieve the aforementioned research objective: How to define 3 topologies of the North Sea HVDC network with different feasible structures? What are the criteria to optimize each topology and to compare the topologies? What are the implications of each topology, when evaluated against a wide range of uncertainties, on the overall CAPEX and OPEX of countries involved?

The simulation considers the scenario in the year 2030. Software PowerGAMA and PowerGIM are used for operation simulation and topology optimization. When calculating OPEX throughout the lifetime of the equipment (assuming 30 years), the year 2030 is taken as a representative year and the 30-year OPEX is obtained by multiplying OPEX in 2030 by an annuity factor.

In short, 3 topologies of the North Sea HVDC grid, with hub-and-spoke structure (for the NSI), point-to-point structure and meshed (without central energy hub) structure, respectively, are defined. They are then optimized towards and compared for the lowest overall cost (i.e. the sum of CAPEX and OPEX including CO₂ prices) throughout the

lifetime. Simulating under different uncertainties/selected critical scenarios (4 Visions from ENTSO-E's Ten Year Network Development Plan which reflect different RES share target and European coordination level, and extreme RES inflow and load conditions), the optimized NSI design stays most socio-economically preferable (with lowest overall cost) topology.

It is also recognized that NSI is able to realize its expected functions, namely transmission of renewable energy, enhancement of system security and price convergence. On the other hand, the launching of NSI brings in challenges such as grid congestion and benefit asymmetry.

Main contributions of this thesis include:

- Creation of the baseline model/dataset for European power system in 2030 as a background/environment for the North Sea HVDC grid planning;
- Design and optimization of the North Sea HVDC grid topologies in three different feasible structures;
- Verification of NSI's advantage in cost saving, compared to two competitors, in 4 Visions reflecting different green energy transition and European coordination level, and under extreme RES inflow and load conditions;
- Verification of NSI's function in improving energy sustainability, affordability and security;
- Realization of Non-Homogeneous Markov Chain algorithm in Excel to generate wind power inflow time series.

ABBREVIATIONS

AC	alternating current
BE	Belgium
DC	direct current
DE	Germany
DK	Denmark
EENS	expected energy not supplied
ENTSO-E	European Network of Transmission System Operators for Electricity
GB	Great Britain
FI	Finland
FR	France
LP	linear programming
MILP	mixed-integer linear programming
NL	Netherlands
NO	Norway
NSCOGI	North Sea Countries' Offshore Grid Initiative
NSI	North Sea Infrastructure
NSWPH	North Sea Wind Power Hub
OPF	optimal power flow
PowerGAMA	Power Grid and Market Analysis
PowerGIM	Power Grid Investment Model
PV	photovoltaic
RES	renewable energy sources
ROI	return on investment
SE	Sweden
TSO	transmission system operator
TYNDP	Ten Year Network Development Plan
UNFCCC	United Nations Framework Convention on Climate Change

CONTENTS

Acknowledgements	v
Abstract	vii
Abbreviations	ix
List of Figures	xv
List of Tables	xvii
1 Introduction	1
1.1 Background	1
1.2 State of the art	3
1.3 Research objective and research questions	6
1.4 Outline	6
2 Creation of baseline model of 2030 European power system	11
2.1 Introduction	11
2.2 Data sources	12
2.2.1 Grid topology	12
2.2.2 Generators and consumers	14
2.3 Assumptions	19
2.3.1 Cross-border transmission capacity	20
2.3.2 New HVDC links for scenario 2030	20
2.3.3 Prediction of development of energy storage system	21
2.3.4 4 Visions of scenario 2030 in TYNDP 2016	21
2.3.5 Storage value of Nordic reservoirs	21
2.4 Operation simulation	23
2.4.1 Working process of PowerGAMA	23
2.4.2 Optimization problem	25
2.4.3 Operation simulation of baseline model	27
2.5 Conclusion	29

3	Design and optimization of HVDC grid topologies in the North Sea	31
3.1	Introduction	31
3.2	Initial design of the North Sea Infrastructure	32
3.2.1	Input data	32
3.2.2	Assumptions	36
3.2.3	Conclusion and output	41
3.3	Optimization of NSI topology	43
3.3.1	Working process of PowerGIM	43
3.3.2	Optimization Problem	44
3.3.3	Topology optimization procedure	46
3.4	Design and optimization of HVDC grid in the North Sea with other structures	55
3.4.1	Introduction	55
3.4.2	Development of point-to-point topology and meshed topology	55
3.5	Conclusion	60
4	Sensitivity test under different RES inflow and load conditions	63
4.1	Introduction	63
4.2	Extreme RES inflow and load conditions	64
4.2.1	Possible extreme RES inflow and load conditions	64
4.2.2	Realization of extreme conditions in simulations	66
4.3	Generation of probabilistic wind power inflow time profiles: Non-Homogeneous Markov Chain algorithm	67
4.3.1	Introduction	67
4.3.2	Wind power inflow time profile variation features	67
4.3.3	Algorithm to generate variable wind inflow time series	68
4.3.4	Conclusion	76
4.4	Result analysis of simulations under extreme RES inflow and load conditions	76
4.4.1	Introduction	76
4.4.2	Result analysis of simulations under extreme wind conditions	76
4.4.3	Result analysis of simulations under extreme solar conditions	80
4.4.4	Result analysis of simulations under extreme NO and SE hydro inflow conditions	82
4.4.5	Result analysis of simulations of extreme load deviations	84
4.5	Conclusion	86

5	Other details in operation simulation	87
5.1	Advantages of NSI	87
5.2	Challenges brought by NSI	89
5.3	Conclusion	92
6	Conclusion	93
6.1	Summaries of conclusions	93
6.1.1	Conclusions in answer to the research questions	93
6.1.2	Conclusions related to other simulation results	94
6.2	Main contributions of this thesis	95
6.3	Suggestions for future research	96
6.3.1	Development of flexibility (energy storage devices and ancillary services market).	96
6.3.2	Compliance with future expansion.	97
6.3.3	Solution for benefit asymmetry among involved countries.	97
	Bibliography	99
	Appendix	104
.1	runpowergama.py	104
.2	runpowergim.py	106

LIST OF FIGURES

1.1	North Sea Infrastructure vision by TenneT [1]	3
1.2	Mean wind speed in the North Sea at the Netherlands' exclusive economic zone[2]	4
1.3	Expected central location of the North Sea Wind Power Hub in the North Sea[3]	4
1.4	Flow chart of Chapter 2 *[4][5][6][7][8][9][10][11], **[11]	7
1.5	Optimization procedure of HVDC topologies in Chapter 3 *[3][11]	8
1.6	Flow chart of Chapter 3 *[3], **[10], **[12]	9
1.7	Simulations performed in Chapter 4 for all 4 topologies (yellow area)	10
2.1	Flow chart of Chapter 2 *[4][5][6][7][8][9][10][11], **[11]	12
2.2	Partial screenshot in Excel of nodes.csv for PowerGAMA	13
2.3	Partial screenshot in Excel of branches.csv for PowerGAMA	14
2.4	Partial screenshot in Excel of hvdc.csv for PowerGAMA	14
2.5	Partial screenshot in Excel of generators.csv for PowerGAMA	16
2.6	Partial screenshot in Excel of profiles.csv for PowerGAMA	16
2.7	An example of $\hat{v}_{filling}$ as a relative coefficient dependent on the filling level of the reservoir [13]	17
2.8	Partial screenshot in Excel of profiles_storval_filling.csv for PowerGAMA	18
2.9	An example of \hat{v}_{time} as a relative coefficient dependent on the time of the year [13]	18
2.10	Partial screenshot in Excel of profiles_storval_time.csv for PowerGAMA	18
2.11	Partial screenshot in Excel of consumers.csv for PowerGAMA	20
2.12	4 Visions of scenario 2030 of European power system [14]	22
2.13	$\hat{v}_{filling}$ as a relative coefficient dependent on the filling level of the reservoir	22
2.14	\hat{v}_{time} as a relative coefficient dependent on the time of the year	23
2.15	PowerGAMA working process flow chart [13]	24
2.16	Baseline model of scenario 2030	28
3.1	Optimization procedure of HVDC topologies in Chapter 3 *[3][11]	32
3.2	Flow chart of Chapter 3 *[3], **[10], **[12]	33

3.3	NSI initial design topology	42
3.4	PowerGIM working process flow chart	43
3.5	Detailed model in PowerGAMA (left) and aggregated model in PowerGIM (right)	50
3.6	Point-to-point topology	56
3.7	Meshed (without a central energy hub) topology	58
4.1	Simulations performed in Chapter 4 for all 4 topologies (yellow area) . . .	64
4.2	France wind power inflow time series and its autocorrelation function . .	68
4.3	Probability distribution of different wind speed models [15]	69
4.4	Monthly-average wind speed synthesized by different wind speed models [15]	69
4.5	Flow chart of using NHMC algorithm to generate variable RES power inflow time series	70
4.6	Synthesized (by NHMC) France wind power inflow time series and its autocorrelation function	75
4.7	Accuracy tests for synthesized series compared to original (France)	75
4.8	Topologies to be studied and their correspondent CAPEX	77
4.9	Total cost of the system under annual mean wind speed -25% in 4 Visions	78
4.10	Total cost of the system under normal wind condition in 4 Visions	78
4.11	Total cost of the system under annual mean wind speed +25% in 4 Visions	79
4.12	Total cost of the system under different solar conditions in Vision 2	80
4.13	Total cost of the system under different solar conditions in Vision 4	81
4.14	Total cost of the system under different NO and SE hydro inflow conditions in Vision 2	82
4.15	Total cost of the system under different NO and SE hydro inflow conditions in Vision 4	83
4.16	Total cost of the system with different load in Vision 2	84
4.17	Total cost of the system with different load in Vision 4	85
5.1	Comparison of annual average nodal price by area between NSI and base-line(Vision 2)	89
5.2	Branch utilization before and after application of flexible load	90

LIST OF TABLES

2.1	Parameters in nodes.csv for PowerGAMA	13
2.2	Parameters in branches.csv for PowerGAMA	13
2.3	Parameters in hvdc.csv for PowerGAMA	14
2.4	Parameters in generators.csv for PowerGAMA	15
2.5	Parameters in consumers.csv for PowerGAMA	19
2.6	Parameters (regarding flexible load) in consumers.csv for PowerGAMA	19
2.7	Implemented HVDC links in scenario 2030 in the North Sea region	20
2.8	Base storage value chosen for Nordic reservoirs	21
2.9	Variables in PowerGAMA optimization problem.csv	26
2.10	Lifetime OPEX of six countries in total in baseline model	29
3.1	Parameters in nodes.csv for PowerGIM	34
3.2	Parameters in branches.csv for PowerGIM	34
3.3	Parameters in consumers.csv for PowerGIM	35
3.4	Parameters in generators.csv for PowerGIM	35
3.5	Installed wind power capacity (MW) [11]	37
3.6	Percentage of offshore wind installed capacity out of total installed capacity [11] [16]	37
3.7	Installed offshore wind power capacity (MW)	37
3.8	Wind power capacity supposed to be connected to the NSWPH according to the ratio (MW)	37
3.9	Wind power capacity from each country to be connected to the NSWPH (MW)	38
3.10	Remaining offshore wind power capacity to be connected to each country (MW)	38
3.11	Onshore wind power capacity for each country (MW)	38
3.12	Annual mean wind speed difference between the Dogger Bank and near shore Dutch offshore wind farms	40
3.13	Output parameters of a typical wind turbine [17]	41
3.14	Wind power density at the Dogger Bank relative to near shore wind farms	41
3.15	Initial capacity of each HVDC branch in the NSI design	41

3.16 Variables in PowerGIM optimization problem.csv	46
3.17 Parameters of nodes in parameters.xml for PowerGIM	47
3.18 Parameters of branches (1) in parameters.xml for PowerGIM	47
3.19 Parameters of branches (2) in parameters.xml for PowerGIM	47
3.20 Parameters of branches (3) in parameters.xml for PowerGIM	48
3.21 CO2 emission rate per generation type in parameters.xml for PowerGIM	48
3.22 Other parameters in parameters.xml for PowerGIM	48
3.23 Lifetime OPEX of six countries in total with initial NSI design	49
3.24 PowerGIM investment recommendation on the basis of initial NSI design (MW)	52
3.25 Mid-stage NSI design optimized by PowerGIM	52
3.26 PowerGIM investment recommendation on the basis of mid-stage NSI design (MW)	53
3.27 Optimized NSI Design	53
3.28 Branch utilization rate (p.u.) of the optimized NSI design	54
3.29 Comparison of optimized NSI design and baseline (billion €)	54
3.30 Comparison of initial and optimized point-to-point design (topology)(MW for capacity and billion € for CAPEX)	57
3.31 Comparison of optimized point-to-point design and baseline (billion €)	57
3.32 Generator capacity division in 5 new nodes	59
3.33 Comparison of initial and optimized meshed design (topology)(MW for capacity and billion € for CAPEX)	59
3.34 Comparison of optimized point-to-point design and baseline (billion €)	59
3.35 Total cost comparison of three competitive topologies (billion €)	60
3.36 Benefit of NSI compared to baseline (billion €)	61
4.1 Wind power inflow changes under extreme wind conditions	65
4.2 Comparison of widely used algorithm of generating wind time series ("x" for disadvantage)	70
4.3 Old and new column of l value	72
4.4 Range of states of wind power inflow series	73
4.5 Simulated extreme wind conditions (annual mean value)	77
4.6 Total cost save of three topologies with re-synthesized new profiles in Vision 2 (billion €)	79
4.7 Total cost save of three topologies with re-synthesized new profiles in Vision 4 (billion €)	79
4.8 Total cost save of the system under different solar conditions in Vision 2 (billion €)	80

4.9	Total cost save of the system under different solar conditions in Vision 4 (billion €)	81
4.10	Total system cost save under different NO and SE hydro inflow conditions in Vision 2 (billion €)	83
4.11	Total system cost save under different NO and SE hydro inflow conditions in Vision 4 (billion €)	84
4.12	Total cost save of the system with different load in Vision 2 (billion €) . . .	84
4.13	Total cost save of the system with different load in Vision 4 (billion €) . . .	85
5.1	Annual generation of 15000 MW offshore wind farm installed in NSI and baseline (TWh)	88
5.2	Annual renewable energy spillage of the 6 countries (TWh)	88
5.3	Comparison of installing NSI and baseline in EENS of 30 years from 2030 (TWh)	89
5.4	Nodal price comparison of installing NSI and baseline, Vision 2 (€)	91
5.5	Annual average power flow in NSI per branch, Vision 2 (MW)	91

1

INTRODUCTION

1.1. BACKGROUND

People are hoping to make the world a better place, for themselves and for their descendants. There are problems to be solved.

Specifically, in the energy area, the problems such as the shortage of primary energy sources and severe air pollution (e.g. SO_2 and NO_x) call for an energy transition. The most urgent problems among all might be the climate change, caused mainly by greenhouse gas emission.

Towards the climate change, efforts were made by countries world-wide. For example, the Paris Agreement is an agreement within the United Nations Framework Convention on Climate Change (UNFCCC) dealing with greenhouse gas emissions mitigation, adaptation and finance starting in the year 2020.

In response to the Paris Agreement, the EU has been at the forefront of international efforts towards a global climate deal [18]. It plans to take cost-effective steps towards its long-term objective of cutting emissions by 80-95% by 2050 in the context of necessary reductions by developed countries as a group.

As an important milestone, the year 2030 was set such key targets in EU's 2030 climate and energy framework [19]: at least 40% cuts in greenhouse gas emissions (from 1990 levels), at least 27% share for renewable energy, and at least 27% improvement in energy efficiency.

In order to significantly reduce greenhouse gas emission, large-scale integration of renewable energy sources (RES) is needed. Both wind and solar energy are needed, both

on a big scale. Some may argue that the wind farms are often distant from the load center, and therefore less preferable than solar photovoltaic (PV) solution. It should be mentioned why wind energy is necessary in future energy systems with large share of RES: the yearly variation characteristics of wind power generation is complementary with solar power generation [20], which can significantly reduce the need for seasonal storage.

Besides the advantages (low CO_2 emission, sustainability, low fuel cost), RES also bring in challenges to the conventional power system. For example, RES's variability challenges the transmission system regarding both capacity and direction; it demands more flexibility (e.g. storage, demand side response, exchange) in system so the stability can be retained. The construction and reinforcement of the facilitators call for investment.

The aforementioned challenges form the so-called "Energy Trilemma", which stands for energy sustainability, energy security and energy affordability. It is not easy to accomplish all three goals at the same time, because they are not mutually independent; instead, they work against each other.

High volumes of needed RES are unattainable by individual Member States, so there is a need for optimum cooperation. The European political declaration of 6 June 2016 on energy cooperation among the North Sea countries was an important step in this direction.

TenneT, the transmission system operator (TSO) in the Netherlands and Germany, proposed the vision of North Sea Infrastructure (NSI), as described in [21] and [3] (figure 1.1).

It creates a basis for a joint European approach up to 2050 and focuses specifically on developing the North Sea as a source and distribution hub for Europe's energy transition. TenneT expects the NSI to realize three functions:

- Transmission of renewable energy
- Enhancement of power system security and stability
- Price convergence

which deal with energy sustainability, energy security and energy affordability of the "Energy Trilemma", respectively.

The core of the NSI design is the North Sea Wind Power Hub (NSWPH) at the Dogger Bank. The surrounding wind farms, far out at sea where wind speed is relatively high, are connected to the hub using inexpensive AC connections, as they are "near shore" to the hub. HVDC interconnectors are built from NSWPH to the surrounding countries: the Netherlands (NL), Germany (GE), Denmark (DK), Norway (NO), Great Britain (GB)

and Belgium (BE). According to TenneT [3], the "wind-connector" (named by [3], for the design combines the wind farms with HVDC interconnectors, as shown in the left part of figure 1.1) design is expected to enable higher system efficiency, while the hub-and-spoke concept (right part of figure 1.1) is expected to facilitate optimal energy transmission and further European market integration.



Figure 1.1: North Sea Infrastructure vision by TenneT [1]

The location was chosen at Dogger Bank because of the following advantages:

- Shallow water: Water depth has a significant impact on the development for offshore wind. A development in shallow waters contributes significantly to cost reduction.
- Wind condition: Wind conditions get better further at sea, as in figure 1.2.
- Central location: For a European coordinated roll-out, a central location is important (figure 1.3).

Within this thesis, the term "North Sea Infrastructure", or its abbreviation "NSI", only refers to the specific design in "wind-connector" structure with the North Sea Wind Power Hub at the Dogger Bank; topologies of HVDC grid designs with other structures are not named with "NSI". Besides, within this thesis, the term "6 countries" refers only to the six countries surrounding the North Sea, i.e. BE, DE, DK, GB, NL and NO.

1.2. STATE OF THE ART

A literature review is performed to understand the state of the art of relevant research, considering both content and methodology. The research gap should also be identified to guide this thesis project.

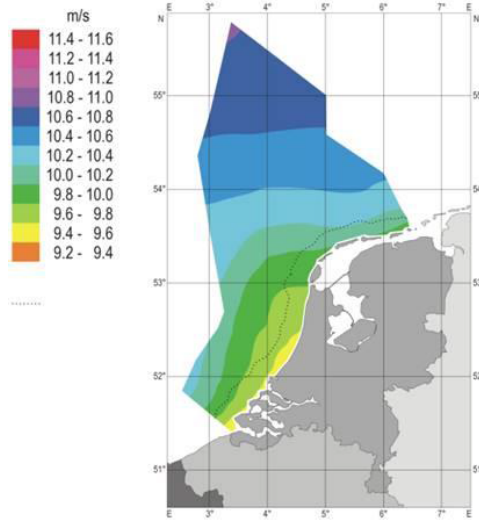


Figure 1.2: Mean wind speed in the North Sea at the Netherlands' exclusive economic zone[2]



Figure 1.3: Expected central location of the North Sea Wind Power Hub in the North Sea[3]

[22] conducts cost-benefit analysis of possible HVDC configurations (radial or multi-terminal) in the North Sea. Besides the CAPEX and OPEX (of countries involved), it also presents comparison in energy spillage and CO₂ emission, etc. However, the compared topologies are not optimized. It is not concrete to conclude whether the relative benefit of one topology, compared to the other, is because of the difference in the key feature of their structures (radial or multi-terminal), or because of lack of optimization.

[23] performs cost-benefit analysis and proposal of HVDC networks in the North Sea, considering grid robustness under 4 scenarios based on [11]. However, no extreme operation conditions (e.g. weather and resulting variable RES supply) are considered; only limited possibilities of topologies are investigated (all investigated topologies are with a central energy hub, i.e. similar structure); no budget for initial investment constraint is applied; and when importing TenneT's vision on the North Sea Infrastructure [21], it ignores one of the advantages of NSI to create "near shore" situation by connecting far shore wind farms to the energy hub using inexpensive AC connection (as an important measure for cost saving), instead it applies DC direct connections.

[24] demonstrates that the integrated North Sea grids are more beneficial than conventional point-to-point topologies (by studying three largely inter-independent regional cases: DE-NL-DK, UK-NL-BE and UK-NO), with additional focus on the distribution of benefits among participating countries. However, firstly, the investigated cases are more local than the aforementioned North Sea Infrastructure which is of interest of all six countries surrounding the North Sea; secondly, only concrete (i.e. with no optimization procedure) cases are considered in the paper.

[25] provides an initial design of a multi-terminal HVDC grid for the North Sea. It demonstrates that compared to conventional point-to-point topologies, the meshed topology can lead to higher system flexibility, security and reliability. However, it does not consider the factor of cost; neither does it consider some of the countries of interest (within the scope of this thesis), for examples, GB and BE. Similarly, [26] studies only interconnections between GB and NL. [27] optimizes European transmission system for scenario 2030, however without considering possibilities of HVDC branches across the North Sea.

The research gap is recognized that there is not sufficient research on proposing new HVDC grids in the North Sea considering optimization (e.g. following a cost-related objective) of different topology structures within a scope of six surrounding countries (BE, DE, DK, GB, NL and NO), with sensitivity tests regarding uncertainties (e.g. in meteorological condition, load, or industry development).

The answer to the research gap can be crucial to the investment decision of HVDC grid in the North Sea. If investment is used for an optimal design of HVDC grid, not only TSOs (e.g. TenneT), but also the electricity consumers in the six countries will benefit

from the decision, in the years to come after the commissioning of the grid.

1.3. RESEARCH OBJECTIVE AND RESEARCH QUESTIONS

Based on the background information from section 1.1 and research gap identified in section 1.2, the main research objective of this thesis project is determined as **to evaluate CAPEX, overall OPEX of participating countries and other operational performances (e.g. energy mix, nodal price, EENS) of possible topologies of HVDC network in the North Sea, including NSI concept ("wind-connector" with the North Sea Wind Power Hub at the Dogger Bank) and other two competitive topologies, considering different critical scenarios w.r.t green energy technology development, European coordination, load and meteorological condition (wind speed, solar radiation and hydrology).**

Three research questions have been formulated following the research objective:

- How to define 3 topologies of the North Sea HVDC network with different feasible structures?
- What are the criteria to optimize each topology and to compare the topologies?
- What are the implications of each topology, when evaluated against a wide range of uncertainties, on the overall CAPEX and OPEX of involved countries?

The starting point of the investigated time horizon is the year 2030. 2030 is chosen because: firstly, according to [3], the first part of NSI is expected to be functioning at year 2030; secondly, year 2030 is with developed database (of generations, loads and prices of fuels and CO₂) for simulation [11]; thirdly, according to [19], the year 2030 would be an important milestone of energy transition.

Due to unpredictability and complexity of developing steps of NSI, it is regarded within this thesis that NSI is built all in one stage and fully functioning by 2030. When calculating operational costs of its lifetime (assumed 30 years from 2030), 2030 is taken as a representative year, and no additional investment is considered.

1.4. OUTLINE

- Introduction

This chapter shows the background, motivation, state of the art of relevant topics, research objective, research questions and outline of the thesis.

- Creation of baseline model of 2030 European power system

Before designing topologies of HVDC grid in the North Sea, a baseline model of 2030 European power system is created in order to

- provide a background/environment for further designs;
- provide a reference to quantify performances (e.g. total cost) of the designs.

The input data format and theoretical background of the software PowerGAMA are introduced together with the elaboration of model construction procedure.

The output of the chapter is the dataset of the baseline model of European power system. The simulation results (e.g. OPEX of the 6 countries around the North Sea) would be used in further stages of the research. Simulations are performed for all 4 Visions from [11], considering different generation mix, load and CO2 price based on different assumptions of progress in green energy transition and European coordination level.

It should be noted that all operation simulations in this thesis, unless otherwise stated, are of the length of one year (8760 hours) of 2030. When calculating OPEX of the lifetime of the equipment (30 years from 2030), 2030 is taken as a representative year and 30-year OPEX is obtained by multiplying OPEX of 2030 by an annuity factor.

The working process of this chapter follows the flowchart in figure 1.4.

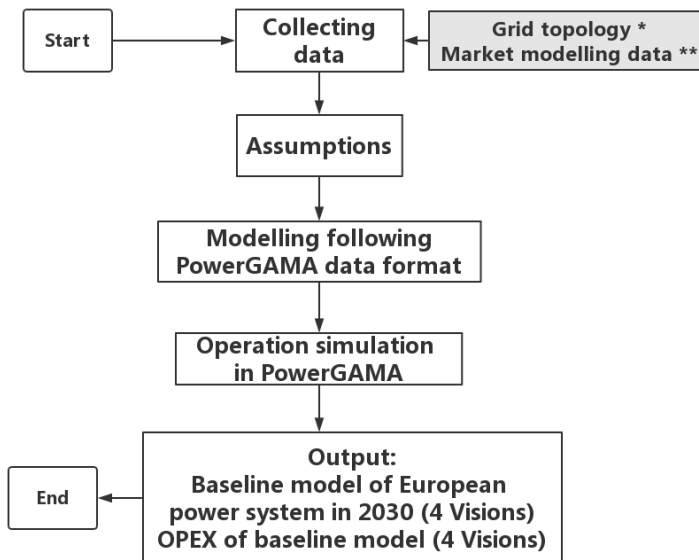


Figure 1.4: Flow chart of Chapter 2

*[4][5][6][7][8][9][10][11], **[11]

- Design and optimization of HVDC grid topologies in the North Sea

This chapter directly answers to the first and second research question, "How to define 3 topologies of the North Sea HVDC network with different feasible structures?" and "What are the criteria to optimize each topology and to compare the topologies?"

Firstly, the initial design of NSI is defined based on data sources and assumptions. Then, following the objective function in equation 1.1, the initial design is optimized by using PowerGIM and PowerGAMA (figure 1.5). The theoretical background and usage of PowerGIM are also introduced here.

$$\min(\text{Total Cost}) = \min(\text{CAPEX} + \text{OPEX}_{\text{lifetime}}) \quad (1.1)$$

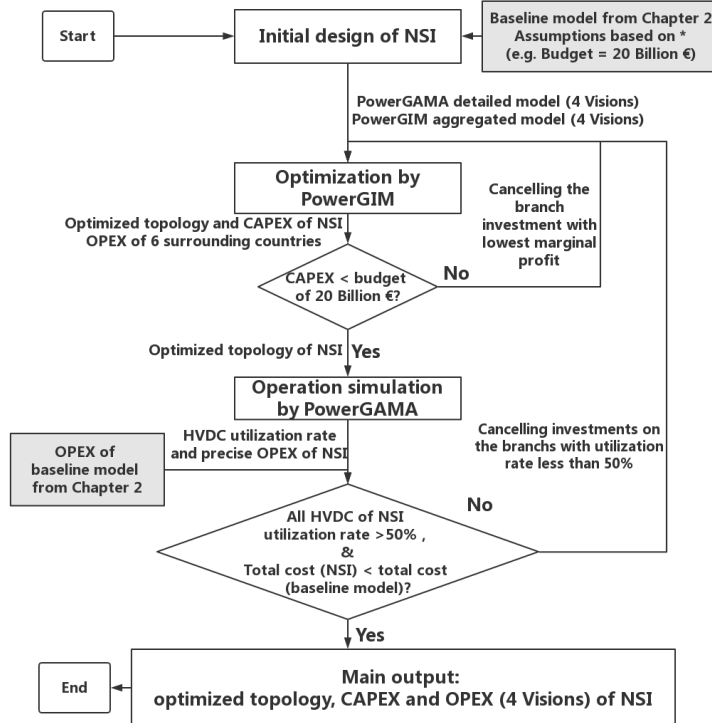


Figure 1.5: Optimization procedure of HVDC topologies in Chapter 3

*[3][11]

Then, other two topologies with point-to-point and meshed structure, respec-

tively, are defined and optimized following the same optimization procedure.

Total cost (the same concept as in equation 1.1) is chosen as the indicator to compare the three developed topologies. Results show that the NSI brings lowest *Total cost* to the 6 countries.

The working process of this chapter is shown in figure 1.6.

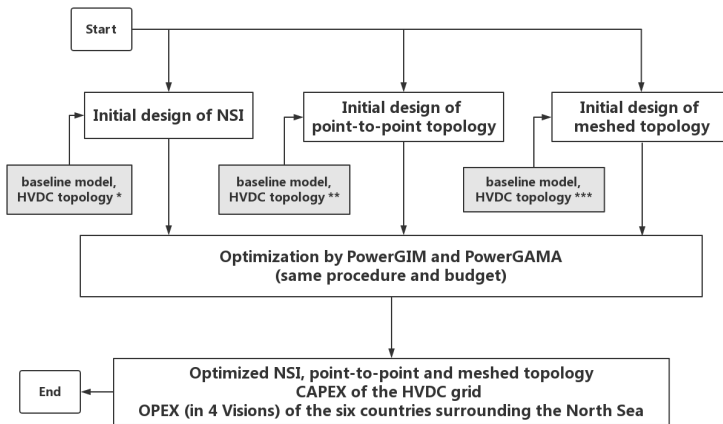


Figure 1.6: Flow chart of Chapter 3

*[3], **[10], **[12]

- Sensitivity test regarding different RES inflow and load conditions

This chapter is in answer to the third research question. European power system with proposed three HVDC designs and baseline under extreme RES inflow and load conditions are simulated to study implication of these conditions to *total cost*.

After literature review of weather anomalies, annual mean wind speed $\pm 25\%$, annual solar radiation $\pm 10\%$, annual NO and SE hydro inflow $\pm 25\%$ and annual mean load $\pm 5\%$ are chosen as extreme cases; also, two sets of re-synthesized wind power inflow time series (i.e. time profiles) are used to test the system's sensitivity to short-term randomness.

The extreme RES generation inflow and load conditions (except for re-synthesized wind power inflow time series) are simulated by scaling the power inflow factor (or annual average load, for load deviations) to the extreme annual mean value.

The two sets of re-synthesized time series of wind power inflow are generated by Non-Homogeneous Markov Chain algorithm. This creates randomness in short-

term values while still keeping statistical characteristics (e.g. yearly and daily variation characteristics) of the reference time series.

The simulations performed for all 4 topologies (three optimized HVDC grid topology and baseline) are shown in the yellow area of the figure 1.7.

	Vision 1	Vision 2	Vision 3	Vision 4
Normal	4 Topologies	4 Topologies	4 Topologies	4 Topologies
Wind speed +25%	4 Topologies	4 Topologies	4 Topologies	4 Topologies
Wind speed -25%	4 Topologies	4 Topologies	4 Topologies	4 Topologies
Wind new profiles x2		4 Topologies		4 Topologies
Solar radiation +10%		4 Topologies		4 Topologies
Solar radiation -10%		4 Topologies		4 Topologies
Nordic hydro inflow +25%		4 Topologies		4 Topologies
Nordic hydro inflow -25%		4 Topologies		4 Topologies
Load +5%		4 Topologies		4 Topologies
Load -5%		4 Topologies		4 Topologies

Figure 1.7: Simulations performed in Chapter 4 for all 4 topologies (yellow area)

As extreme (in annual mean value) wind conditions are important to the designs of the North Sea HVDC grid (with offshore wind farms), all 4 Visions of all 4 topologies are simulated. For other weather conditions, only Vision 2 and Vision 4 are simulated as examples. Vision 2 is chosen because of lower total cost difference among all investigated topologies under normal weather condition, as well as higher likelihood to happen (according to TenneT), compared to other Visions; while Vision 4 is chosen for higher proportion of RES in energy mix (and resulting higher sensitivity to RES power inflow and load changes), compared to other Visions.

- Other details in operation simulation

Besides the OPEX, other details in operation simulation can also help reveal the role of NSI. Indicators such as energy mix, nodal price and EENS are used to test if the optimized NSI design can realize the three expected functions: transmission of renewable energy, enhancement of system security and stability, and price convergence. Besides, the challenges brought by the design are also recognized.

- Conclusion

This chapter concludes the thesis, including the main findings, main contributions of the author, and suggestions for future research.

2

CREATION OF BASELINE MODEL OF 2030 EUROPEAN POWER SYSTEM

2.1. INTRODUCTION

Before designing topologies of the HVDC grid in the North Sea, it is necessary to create a baseline model of European power system of scenario 2030. The baseline model would be used as

- a background/environment for further designs of HVDC grid in the North Sea;
- a reference to quantify performances (e.g. socio-economical benefits) of the designed topologies.

After surveying several softwares, the model is decided to be built in PowerGAMA (Power Grid And Market Analysis), a Python-based lightweight simulation tool for high level analyses of renewable energy integration in large power systems. The introduction of PowerGAMA, based on the thesis author's understanding through master thesis and [13][28], is included in this chapter, alongside with the elaboration of construction of the power system model.

Data from different sources and how they are imported to PowerGAMA are introduced in section 2.2. Assumptions taken by the author of this thesis for the model creation are listed in section 2.3. Operation simulation of the model and an introduction to PowerGAMA working process are presented in section 2.4. Section 2.5 concludes the paper.

The working process of this chapter follows the flowchart in figure 2.1.

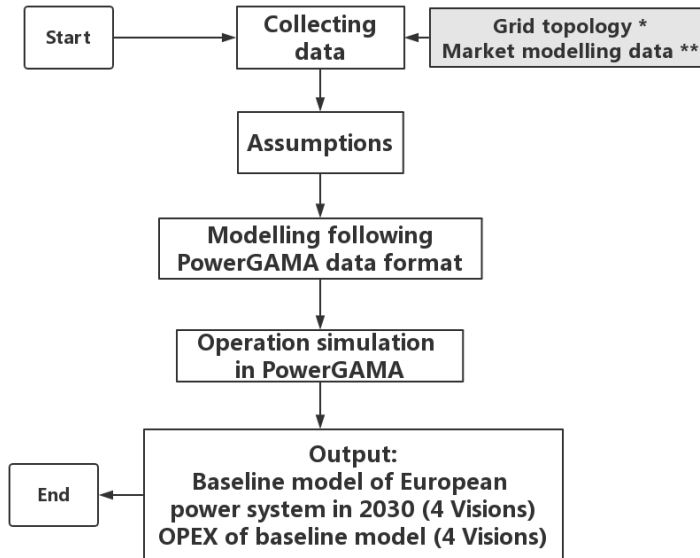


Figure 2.1: Flow chart of Chapter 2

*[4][5][6][7][8][9][10][11], **[11]

2.2. DATA SOURCES

Based on the public availability of the sources, the data used in building European power system 2030 is collected from different sources.

2.2.1. GRID TOPOLOGY

Topology of European power system is comprised of three separate models:

- Continental European network model [29];
- GB network 29-bus model [4];
- Nordic network 44-bus model [6].

In PowerGAMA, the topology is represented by the parameters of nodes and branches (AC and DC).

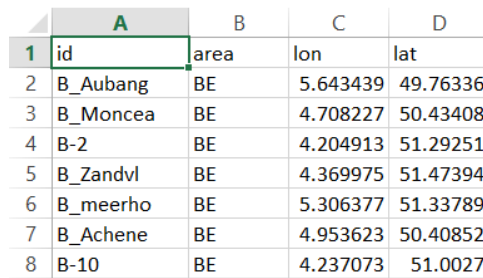
All needed input data for PowerGAMA are put in .csv files. For better presentation in this paper, the parameters are introduced in rows of each table; it should be noted that

in .csv files used for PowerGAMA, each parameter occupies one column. The order of the parameters in each .csv file can be random, i.e. does not have to follow the numbers in the first column of the tables in this sub-section. The last column of the tables in this sub-section is the unit of data in float type, or type name (in italic) of data in other types. The screenshots of .csv files are also presented in this section.

The input data used for dividing areas of nodes and creating maps are specified in "nodes.csv", as in table 2.1. Figure 2.2 is an example of part of the "nodes.csv" in Excel.

	parameter	description	unit
1	id	node name	<i>string</i>
2	area	country/region name	<i>string</i>
3	lat	latitude	degree
4	lon	longitude	degree

Table 2.1: Parameters in nodes.csv for PowerGAMA



	A	B	C	D
1	id	area	lon	lat
2	B_Aubang	BE	5.643439	49.76336
3	B_Moncea	BE	4.708227	50.43408
4	B-2	BE	4.204913	51.29251
5	B_Zandvl	BE	4.369975	51.47394
6	B_meerho	BE	5.306377	51.33789
7	B_Achene	BE	4.953623	50.40852
8	B-10	BE	4.237073	51.0027

Figure 2.2: Partial screenshot in Excel of nodes.csv for PowerGAMA

The input data for AC branches are specified in "branches.csv", as in table 2.2. Figure 2.3 is an example of part of the "branches.csv" in Excel.

	parameter	description	unit
1	node_from	name of the starting node	<i>string</i>
2	node_to	name of the end node	<i>string</i>
3	reactance	reactance of the branch	Ohm
4	capacity	capacity of the branch	MW

Table 2.2: Parameters in branches.csv for PowerGAMA

The input data for HVDC branches are specified in "hvdc.csv", as in table 2.3. Figure 2.4 is an example of part of the "branches.csv" in Excel. Compared to the "branches.csv",

	A	B	C	D
1	node_from	node_to	reactance	capacity
2	B_Zandvl	B-2	0.0052	inf
3	NL-new1	B_Zandvl	0.00776	1168.81
4	B-2	B-4	0.00434	inf
5	B-6	B-2	0.00837	inf
6	B-2	B-8	0.00753	inf
7	B-2	B-10	0.00655	inf
8	B-3	B-6	0.00666	inf

Figure 2.3: Partial screenshot in Excel of branches.csv for PowerGAMA

no information of branch reactance is mentioned in "hvdc.csv" as the HVDC branches are regarded with power electronic converters which enable full control of power flow, and therefore do not need to obey the power flow equations for AC network.

	parameter	description	unit
1	node_from	name of the starting node	<i>string</i>
2	node_to	name of the end node	<i>string</i>
3	capacity	capacity of the branch	MW

Table 2.3: Parameters in hvdc.csv for PowerGAMA

	A	B	C
1	node_from	node_to	capacity
2	FEDA_HVDC	NL-1	700
3	KRISTIA_HVDC	DK-1	1700
4	GB-Sellindge	FR	2000
5	GB-Isle of Grain	NL-15	1000
6	STENKU_HVDC	DK-2	760
7	D-4	ARRIE_HVDC	612

Figure 2.4: Partial screenshot in Excel of hvdc.csv for PowerGAMA

2.2.2. GENERATORS AND CONSUMERS

For continental Europe and GB part of the model, the sources also provided geological distribution of the generation capacity per type of technology. They are scaled to the value of the year 2030 according to Ten Year Network Development Plan (TYNDP) 2016 by ENTSO-E [11], considering 4 Visions (which will be explained further in the next

sub-section).

For Nordic power system, geological distribution of generators per type is taken from [6][7], percentage of hydro power with reservoir and run of the river are taken from [8], and reservoir energy capacity (in MWh) follows [9]. Generation capacities are also scaled to scenario 2030 according to [11].

For PowerGAMA, the input data for generators are specified in "generators.csv", as in table 2.4. An example of part of the file in Excel is figure 2.5.

	content	description	unit
1	desc	generator name/description	<i>string</i>
2	type	technology	<i>string</i>
3	node	name of the node that the generator belongs to	<i>string</i>
4	pmax	upper limit of power generation	MW
5	pmin	lower limit of power generation	MW
6	fuelcost	cost of specific fuel	€/MWh
7	inflow_fac	ratio of actual annual generation relative to full generation	p.u.
8	inflow_ref	hourly inflow value relative to annual average inflow value	p.u.
9	storage_cap	energy capacity of the storage	MWh
10	storage_price	base value of the storage	€/MWh
11	storage_ini	initial storage filling level relative to full capacity	p.u.
12	storval_filling	storage value relative coefficient dependent on filling level	p.u.
13	storval_time	storage value relative coefficient dependent on time	p.u.
14	pump_cap	power capacity of pumping	MW
15	pump_efficiency	efficiency of the pump	p.u.
16	pump_deadband	deadband of the pump	€/MWh

Table 2.4: Parameters in generators.csv for PowerGAMA

For conventional generators, the value of "inflow_ref" is set as constant 1; while the time dependent profiles are used for variable RES. The format of such a series is a column with a length of 8761 rows, while the first row is the title and the rest 8760 rows are the time profiles. The value of the time profiles are in unit of [p.u.], relative to the annual average generation/load. Therefore, average value of the total length of the time profiles is 1. Profiles for different generators (as well as consumers, which would be mentioned later in this sub-subsection) are put into the same "profiles.csv". An example of a part of "profiles.csv" in Excel is figure 2.6.

The parameters "storage_cap", "storage_price", "storage_ini", "storval_filling" and "storval_time" are specified when the generator is with storage system, for example, the hy-

	A	B	C	D	E
1	desc	type	node	pmax	pmin
2	OWEZ	wind_offs	NL-11	1977.003	
3	Princess A	wind_offs	NL-11	2196.67	
4	DR Wind	wind	NL-6	25.69005	
5	FL Wind	wind	NL-8	1455.266	
6	FR Wind	wind	NL-7	241.7887	
7	GE Wind	wind	NL-14	96.71549	

Figure 2.5: Partial screenshot in Excel of generators.csv for PowerGAMA

	DF	DG	DH	
1	wind_Poland	wind_Estonia	wind_Latvia	wind_
2	0.388108936	0.1023405	0.343933927	0.2
3	0.467871343	0.10322388	0.377059968	0.2
4	0.561257331	0.104126056	0.412140806	0.
5	0.663260355	0.105047026	0.450362387	0.3
6	0.768419214	0.105977394	0.491609131	0.3
7	0.879408346	0.106926558	0.53523279	0.3

Figure 2.6: Partial screenshot in Excel of profiles.csv for PowerGAMA

dro power plant with a reservoir. The PowerGAMA does OPF calculation for generator dispatching (which would be further elaborated in details in sub-section 2.4.1 and sub-section 2.4.2) by utilizing generators with lowest marginal cost (mainly dependent on fuel cost and efficiency for generators without storage). In this context, in order to dispatch the generators with storage together with the ones without storage, as well as to achieve better (and more realistic) utilization of energy storage, the following storage value is used:

$$v(f, t) = v_o \cdot \hat{v}_{filling}(f) \cdot \hat{v}_{time}(t) \quad (2.1)$$

where v_o is the base value, $\hat{v}_{filling}$ is the relative coefficient dependent on the filling level of the reservoir, and \hat{v}_{time} is the relative coefficient dependent on the time of the year (which, taking hydro power generators for example, lead to different water inflow).

Generally, the relative coefficient $\hat{v}_{filling}$ is high when the storage is nearly empty (therefore the storage is more likely to refill), and low when the storage is nearly full (to avoid energy spillage) (figure 2.7).

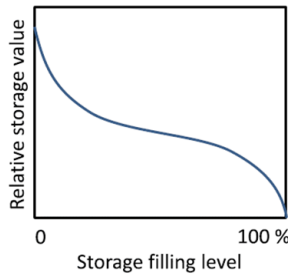


Figure 2.7: An example of $\hat{v}_{filling}$ as a relative coefficient dependent on the filling level of the reservoir [13]

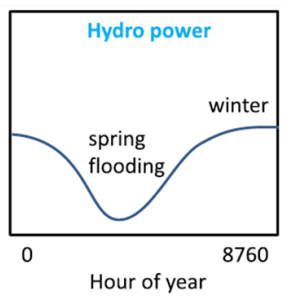
The values of the coefficients are stored in "profiles_storval_filling.csv", with a length of 101 rows (while the first row is for the names of different coefficient profiles, the rest 100 rows are for coefficient value correspondent with each of the percentage of the filling level) (figure 2.8).

Generally, the relative coefficient \hat{v}_{time} is of reversed shape of the water inflow. This is to avoid the storage being empty in the seasons when water inflow is limited (figure 2.9).

The values of the coefficients are stored in "profiles_storval_time.csv", with a length of 8761 rows (while the first row is for the names of different coefficient profiles, the rest 8760 rows are for coefficient value correspondent with each hour of the year) (figure 2.10).

	A	B	C	D
1	const	hydro_old	hydro	csp
2	1	14.3885	10	1.2
3	1	14.38831	9.6	1.195556
4	1	14.38812	9.2	1.191111
5	1	14.38723	8.8	1.186667
6	1	14.38634	8.4	1.182222
7	1	14.38282	8	1.177778
8	1	14.37929	7.6	1.173333

Figure 2.8: Partial screenshot in Excel of profiles_storval_filling.csv for PowerGAMA

Figure 2.9: An example of \hat{v}_{time} as a relative coefficient dependent on the time of the year [13]

	A	B	C	D	E	F
1	const	csp	hydro	daily_optir	weekly_t_hydro_4	
2	1	1	1	2	2.6	2.964133
3	1	0.833333	1	2	2.6	2.964663
4	1	0.666667	1	2	2.6	2.965193
5	1	0.5	1	2	2.6	2.965723
6	1	0.333333	1	2	2.6	2.966253
7	1	0.166667	1	2	2.6	2.966784
8	1	0	1	2	2.6	2.967315

Figure 2.10: Partial screenshot in Excel of profiles_storval_time.csv for PowerGAMA

The parameters "pump_cap", "pump_efficiency" and "pump_deadband" are for the generators with pump for its storage. The setting of the dead band is in order to avoid frequent switch between pumping and outputting.

The input data for consumers are specified in "consumers.csv", as in table 2.5.

	parameter	description	unit
1	node	name of the node that the consumer belongs to	<i>string</i>
2	demand_avg	annual average demand	MW
3	demand_ref	hourly demand relative to average demand	p.u.

Table 2.5: Parameters in consumers.csv for PowerGAMA

In the column of "demand_ref", the name of the reference, for example, "load_NL" is filled in. When running the simulation, it calls the time profiles of hourly demand in the file "profiles.csv", the same file where generator profiles are also stored, in which there is a column with the name of "load_NL". The length of the profiles (besides the column title) is also 8760, which provides the hourly time profiles of demand of a whole year. The real demand of a consumer at the specific time step is the value of "demand_ref" times the average demand shown in "demand_avg".

If flexible load is taken into consideration, the additional columns shown in table 2.6 can be used to specify load flexibility.

	parameter	description	unit
1	flex_fraction	fraction of demand which is flexible	p.u.
2	flex_on_off	fraction of time available for flexible load	p.u.
3	flex_storage	maximum flexibility	MWh
4	flex_basevalue	base storage value of flexible load	€
5	flex_storval_filling	storage value relative coefficient dependent on filling level	p.u.
6	flex_storval_time	storage value relative coefficient dependent on time	p.u.

Table 2.6: Parameters (regarding flexible load) in consumers.csv for PowerGAMA

The same structure as for storage system is used to follow flexible load behavior. An example can be found in section 5.2.

An example of a part of the file in Excel is figure 2.11.

2.3. ASSUMPTIONS

The assumptions taken when combining the aforementioned data are listed in the sub-sections of this section.

	A	B	C	I
1	node	demand_avg	demand_ref	flex_
2	D_185x	286.1642042	load_DE	
3	D_233	403.4108609	load_DE	
4	D_Connef	336.6149229	load_DE	
5	D_Diele	166.9262945	load_DE	
6	D_Eichst	685.2875164	load_DE	
7	D_Gronau	671.0945448	load_DE	

Figure 2.11: Partial screenshot in Excel of consumers.csv for PowerGAMA

2.3.1. CROSS-BORDER TRANSMISSION CAPACITY

The cross border power transmission capacity were taken from [11]. It is assumed by the author of this thesis that the cross-border transmission capacities are the same in both directions.

2.3.2. NEW HVDC LINKS FOR SCENARIO 2030

When considering scenario 2030, compared to the topology from original data sources, several HVDC links are added (based on information from [10][11]) as in table 2.7.

Country	Name	Capacity (MW)	Commissioning time
NL-NO	NorNed	700	2009
DK-NO	Skagerrak 4	700	2014
BE-GB	NEMO	1000	2018
DE-NO	Nord.Link	1400	2018
DK-NL	COBRA	700	2019
GB-NO	North Sea Link	1400	2021
GB-NO	NorthConnect	1400	2022

Table 2.7: Implemented HVDC links in scenario 2030 in the North Sea region

Between GB and NO, both North Sea Link and NorthConnect are considered, as a positive evaluation of advantages of Nordic reservoirs in helping integrating wind power.

Between GB and DKw, Viking Link is not considered due to its overlapping with NSI to be designed. Instead, the Viking Link is considered as part of another candidate design, which is elaborated in section 3.4.

2.3.3. PREDICTION OF DEVELOPMENT OF ENERGY STORAGE SYSTEM

According to the difficulty of prediction, the development of energy storage system (e.g. batteries) from scenario 2014 to scenario 2030 is neglected.

2.3.4. 4 VISIONS OF SCENARIO 2030 IN TYNDP 2016

The market modelling data set of TYNDP 2016 for scenario 2030 includes (but is not limited to):

- installed generation capacity in every country and of each type (technology);
- full-year load curve time profiles, with resolution of one hour (8760 hours in total), for each country;
- generation efficiency (e.g. combustion efficiency ratio of each type of fuel), fuel cost and CO2 cost.

However, as 2030 is more than ten years from now while the energy industry is under fast revolution, it is difficult to precisely predict the progress of reducing greenhouse gas emissions or the level of European coordination and cooperation. Therefore, taking these two attributes as two orthogonal axes, based on different levels, a 2*2 matrix of 4 Visions was developed by ENTSO-E, as shown in figure 2.12.

For each Vision, there are different generation mix, load curve and energy balances for each country. What's more, as an example, there is also a change in the price of CO2: for Vision 1 and Vision 2, the price of CO2 is 17 Euros per ton; while for Vision 3 and Vision 4, it is 71 Euros per ton. It is one of the reasons that the operational cost of each Vision cannot be compared directly.

TYNDP 2016 does not indicate the probability of which Vision is more likely to happen. Further discussion on which Visions to consider in simulations in this thesis can be found in section 4.1.

2.3.5. STORAGE VALUE OF NORDIC RESERVOIRS

Inspired by [23], the base storage value ν_o (table 2.8), relative coefficient $\hat{\nu}_{filling}$ (figure 2.13) and relative coefficient $\hat{\nu}_{time}$ (figure 2.14) are chosen.

Country	Norway	Sweden	Finland
Base value ν_o (€)	15	15	53

Table 2.8: Base storage value chosen for Nordic reservoirs



Figure 2.12: 4 Visions of scenario 2030 of European power system [14]

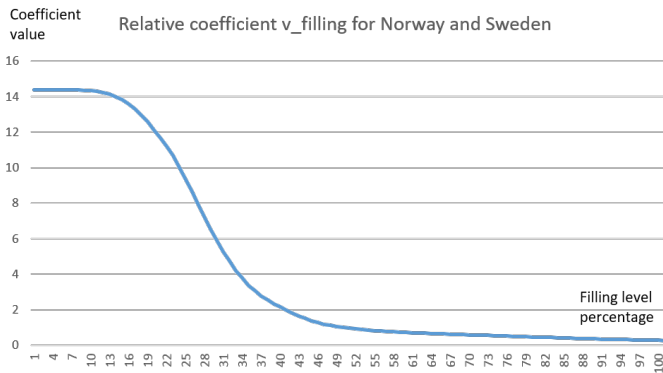


Figure 2.13: $\hat{v}_{filling}$ as a relative coefficient dependent on the filling level of the reservoir

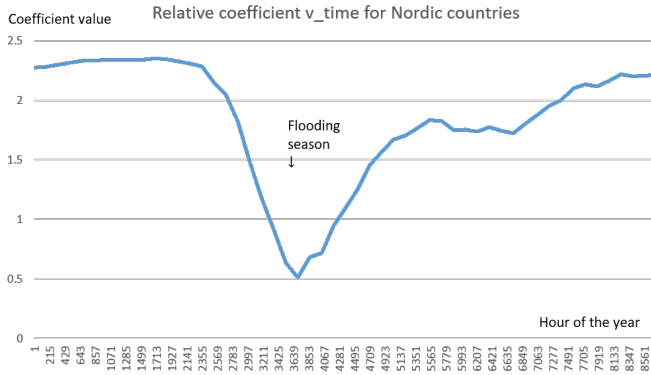


Figure 2.14: \hat{v}_{time} as a relative coefficient dependent on the time of the year

2.4. OPERATION SIMULATION

2.4.1. WORKING PROCESS OF POWERGAMA

In PowerGAMA, at each time step, based on the marginal generation cost, power outputs from all generators are optimized. Wind, solar and hydro power are considered under variable meteorological conditions. Also, the variable load curve is considered. What's more, the simulation environment is flow-based, which means that the power flow equations determine the simulated power flow in the AC grid.

Regarding the generators with energy storage device/system (e.g. hydro power station with reservoir or concentrated solar power station with thermal storage system), the optimization has to be based on the storage level (which is a part of the output from the simulation of the previous time step). Therefore, the optimization problem is solved sequentially. In order to ensure the utilization rate (and variation characteristics) of the storage system, storage values are used to control the operation of the storage. The storage values, for example, water values for Norwegian reservoirs, are dependent on the pre-set basic value and two indexes of reservoir filling level and time of the year (as mentioned in section 2.2 and section 2.3). This simplified representation leads to deviations from real behavior of the storage system.

No power market subtleties (e.g. ramping rate limits, start-up cost, unit commitment, etc.) were included in the software package. As a result, power system's ability to accommodate large-scale penetration of variable renewable energy would be overestimated; also, perfect market is assumed without nodal pricing barriers among different countries. With all such simplifications, according to the author of the software [29], PowerGAMA still provides important insights when used to guide grid planning and to

check the influence of new generations and new interconnections.

The working process of PowerGAMA is illustrated in a flow chart (figure 2.15).

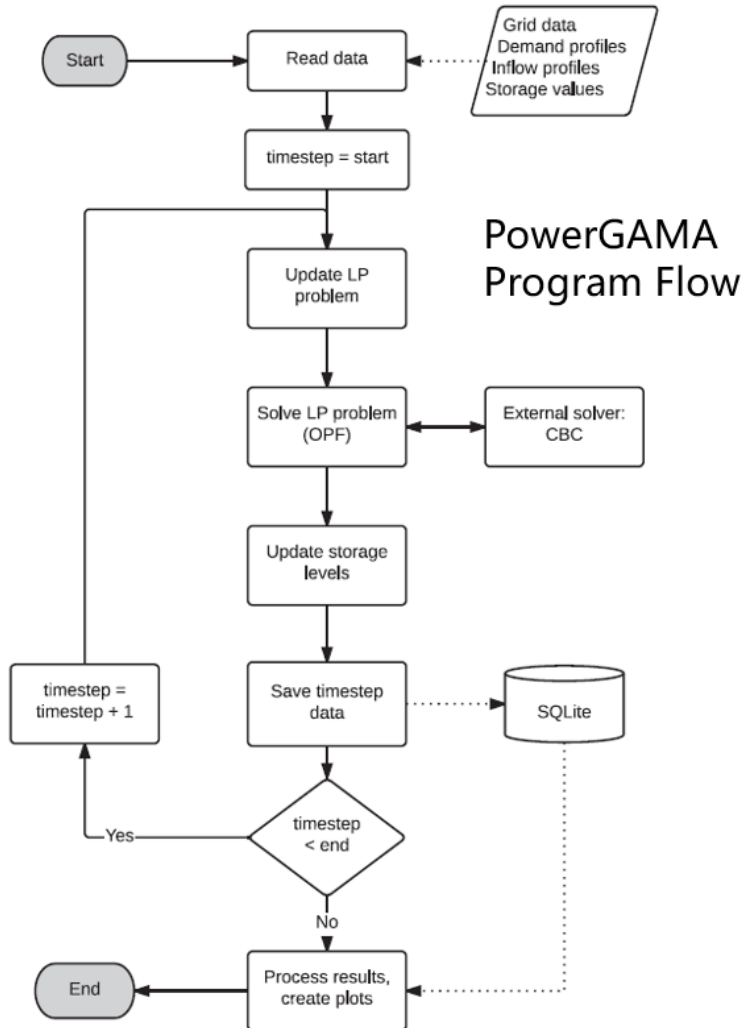


Figure 2.15: PowerGAMA working process flow chart [13]

In the "runpowergama.py" script (appendix .1), the implementation of the total process shown in the flow chart can be found.

Other scripts in the PowerGAMA package are:

"constants.py" is used for setting constant values such as load shed cost;

"GridData.py" is used for saving input data;

- "LPproblem.py" is used for solving optimal power flow;
- "database.py" is used for saving iteration results;
- "Results.py" is used for outputting results (e.g. in Excel or figures);
- "GIS.py" is used for making maps in Google Earth.

2.4.2. OPTIMIZATION PROBLEM

For solving the optimal power flow (OPF) optimization problem, the linear programming (LP) is used.

OBJECTIVE FUNCTION

The minimization of marginal cost per time step is the objective function of the simulation, as is shown in equation 2.2.

$$\min F = \min \left(\sum_n^N \text{marginal cost}_n \times \text{power output}_n \right) \quad (2.2)$$

where F refers to the total marginal costs (per time step), N for the set of generators and n is the index for generator. F is clearly represented in equation 2.3.

$$F = \sum_{g \in G} C_g^{gen} P_g^{gen} - \sum_{p \in P} C_p^{pump} P_p^{pump} - \sum_{f \in F} C_f^{flex} P_f^{flex} + \sum_{n \in N} C_n^{shed} P_n^{shed} \quad (2.3)$$

In the two equations above, all costs are in the unit of €/MWh and power outputs are in the unit of MWh. G, P, F, N are the sets of generators, pumps, flexible loads and nodes, respectively; while g, p, f, n are the indices of generator, pump, flexible load and node, respectively.

CONSTRAINTS

The first constraint is that the active power transmitted per branch has to be within the branch capacity.

$$-P_j^{max} \leq p_j \leq P_j^{max}, j \in B \quad (2.4)$$

where j is the index for branch, and B refers to the set of branches.

The second constraint is that the power generation per generator has to be within the lower and upper bounds, where the upper bound is the capacity for conventional and nuclear generators without storage, and available power for RES and other generators with storage, while the lower bound is generally (such as in this thesis) set to 0.

$$P_g^{min} \leq P_g^{gen} \leq P_g^{limit}, g \in G \quad (2.5)$$

The third constraint is that the pumping has to be within pump capacity.

$$0 \leq P_p^{pump} \leq P_p^{pump.max}, p \in P \quad (2.6)$$

The fourth constraint is that the flexible load must be lower than or equal to maximum demand.

$$0 \leq p_f^{flex} \leq P_f^{flex,max}, f \in F \quad (2.7)$$

The fifth constraint is that the net power injection per node equals to the AC power flow out of the node. Actually, the AC power flow in the network is determined by non-linear power flow equations. The linearized equation which can be used in linear programming is attained by assuming: (1)small angle differences; (2)small voltage deviations; (3)small branch resistance compared to reactance; (4)small shunt reactances (and therefore self-admittances). The equation is usually referred to as the DC power flow equation:

$$\mathbf{P}^{node} = \mathbf{B}' \Theta \quad (2.8)$$

where the \mathbf{P}^{node} is the vector of net power injections into all the nodes of the system, \mathbf{B}' is the conductance matrix, and Θ is the vector of voltage angles. An extended representation of the \mathbf{P}^{node} (at node k) is:

$$\mathbf{P}_k^{node} = \sum_{g \in G_k} P_g^{gen} - \sum_{p \in P_k} P_p^{pump} + \sum_{d \in D_k} P_k^{dc} - P_k^{cons} + P_k^{shed} \quad (2.9)$$

The sixth constraint expresses the relation between branch power inflow and nodal voltage angle differences:

$$\mathbf{P}^{ac} = \mathbf{DA} \Theta \quad (2.10)$$

where the \mathbf{D} is the diagonal matrix with elements calculated from the branch reactance $D_{mm} = -1/x_m$; \mathbf{A} is the node-branch incidence matrix which describes topology of the grid network.

VARIABLES

A recap of variables in PowerGAMA optimization problem is in table 2.9.

variable	description	unit
P_g^{gen}	power generation at generator g	MW
P_p^{pump}	pumping power at pump p	MW
P_f^{flex}	flexible load power at load f	MW
P_n^{shed}	load shedding at node n	MW
θ_n	voltage angle at node n	°
P_j	power flow at branch j (AC or DC)	MW

Table 2.9: Variables in PowerGAMA optimization problem.csv

2.4.3. OPERATION SIMULATION OF BASELINE MODEL

The initial baseline model, built by integrating three parts of models (continental Europe model, GB model and Nordic model), are of a size of more than 1500 nodes. However, the computational complexity was too high for a personal computer that the simulations were highly possible to fail/drop out (approximately 4 out of 5 times). Therefore, aggregation is used for continental Europe model: except for the models of the countries surrounding the North Sea (NL, BE, DE and DK), the topologies inside each country of continental Europe are aggregated into one node, merging all generators and consumers of that country, while keeping the cross-border branches. Models of NL, BE, DE, DK, GB and Nordic countries are kept as original size.

After aggregation, the baseline model is reduced to 387 nodes. The model still remains high resolution for six countries surrounding the North Sea, and its simulation efficiency is significantly increased: the simulation seldom fails, while the duration is about 5 hours per simulation, which is acceptable for the research of this thesis.

After 4 simulations for 4 Vision of scenario 2030, the outputs are shown below.

Figure 2.16 is the model map opened in Google Earth. While grid topology remains the same for different Visions, only one map is shown here.

An important indicator for future research would be the operational cost (OPEX, i.e. the total sum of fuel cost and CO2 cost of generation output in PowerGAMA) of 6 countries surrounding the North Sea (BE, DE, DK, GB, NL and NO) throughout the lifetime of the equipment (i.e. the North Sea HVDC grid to be designed).

Please note that in PowerGAMA, the equation to calculate operation cost is not the same with its objective function. In the objective function optimization, the marginal cost is used instead of fuel cost when calculating OPEX. The difference is that, taking hydro power station in Finland with reservoir as an example, the marginal cost is its storage value (base value 53 €/MWh), while the fuel cost is the cost of water inflow (set as 0.5 €/MWh). No investment costs of offshore wind generators are converted to operational costs.

Within this thesis, when calculating the OPEX of 6 countries throughout the lifetime, it is always to simulate for whole year at 2030 and take it as a representative year, then multiply the one-year OPEX to the annuity factor (equation 2.11 and equation 2.12).

$$OPEX_{lifetime} = OPEX_{2030} \times annuity\ factor \quad (2.11)$$

where

$$annuity\ factor = \sum_{n=1}^{lifetime} \frac{1}{(1+r)^n} \quad (2.12)$$

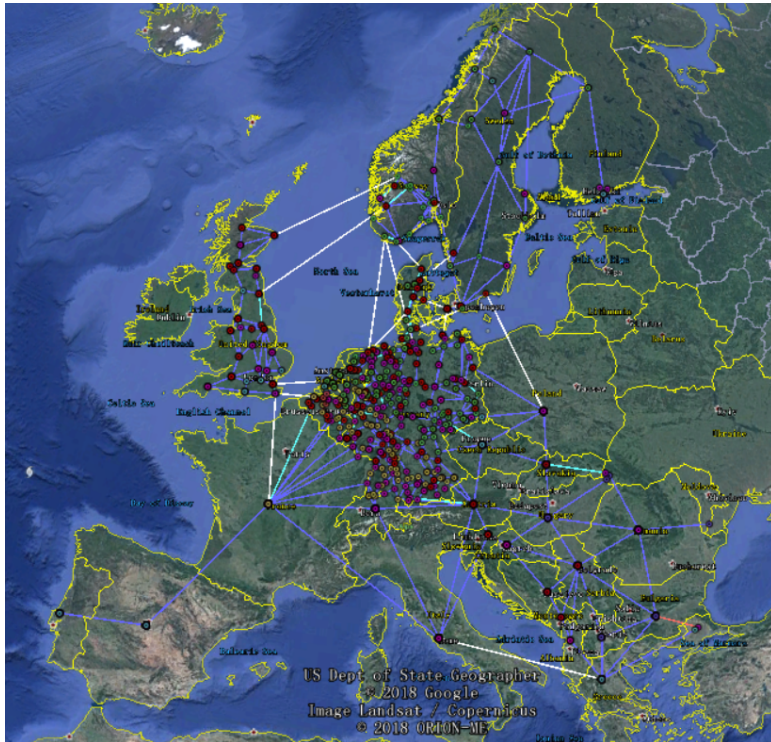


Figure 2.16: Baseline model of scenario 2030

Within this thesis, the lifetime of equipment is assumed to be 30 years and annual interest rate is 5%. The annuity factor is therefore 15.37245.

The 30-year OPEX of 6 countries in the baseline model are presented in table 2.10.

Visions	Vision 1	Vision 2	Vision 3	Vision 4
OPEX (billion €)	593	448	628	760

Table 2.10: Lifetime OPEX of six countries in total in baseline model

2.5. CONCLUSION

For the sake of providing background/environment of modelling North Sea HVDC grid design, as well as providing reference for investment decisions, the baseline model of European 2030 grid is created combining different data sources and assumptions. Theoretical background of the software, PowerGAMA, is introduced together with the modelling process of baseline case.

One important output of this chapter is the dataset of models (of 4 Visions of scenario 2030), based on which the HVDC grid in the North Sea can be designed in the next chapter. The other output would be the lifetime OPEX of the 6 countries surrounding the North Sea, which can be used in quantifying socio-economic benefits of HVDC designs in the next chapter.

3

DESIGN AND OPTIMIZATION OF HVDC GRID TOPOLOGIES IN THE NORTH SEA

3.1. INTRODUCTION

In response to the first and the second research question, i.e. "How to define 3 topologies of the North Sea HVDC network with different structures?" and "What are the criteria to optimize each topology and to compare the topologies?", the research in this chapter is conducted. On the basis of the baseline case created in the last chapter, three HVDC grid topologies in the North Sea are provided: the North Sea Infrastructure, the meshed topology (without a central energy hub) and the point-to-point topology. Please note that within this thesis, the term "North Sea Infrastructure", or its abbreviation "NSI", only refers to the specific design in "wind-connector" structure with the North Sea Wind Power Hub at the Dogger Bank; the other two topologies with other structures are not named with "NSI".

Firstly, in section 3.2, the initial design of NSI is presented, together with the input data format of PowerGIM; then, the optimization process of NSI design by using PowerGIM (of which the working process is also given) and PowerGAMA is elaborated in section 3.3, with an optimized topology (and corresponding total cost) as output; in section 3.4, the initial designs of meshed and point-to-point topology are presented, as well as, after the same optimization procedure and constraints (e.g. budget), their optimized

topologies; section 3.5 concludes the chapter.

The optimization procedure of HVDC topologies (taking NSI as an example) is shown in figure 3.1.

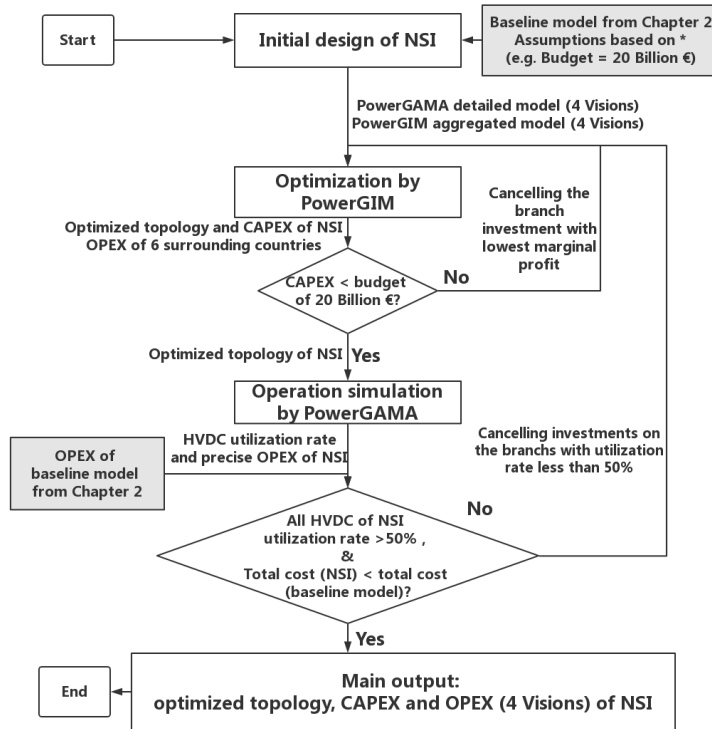


Figure 3.1: Optimization procedure of HVDC topologies in Chapter 3

*[3][11]

The working process of this chapter is shown in figure 3.2.

3.2. INITIAL DESIGN OF THE NORTH SEA INFRASTRUCTURE

Within this stage, an initial design of the North Sea Infrastructure is delivered.

3.2.1. INPUT DATA

DATA SOURCES

The input of this step includes:

- baseline model obtained from chapter 2;

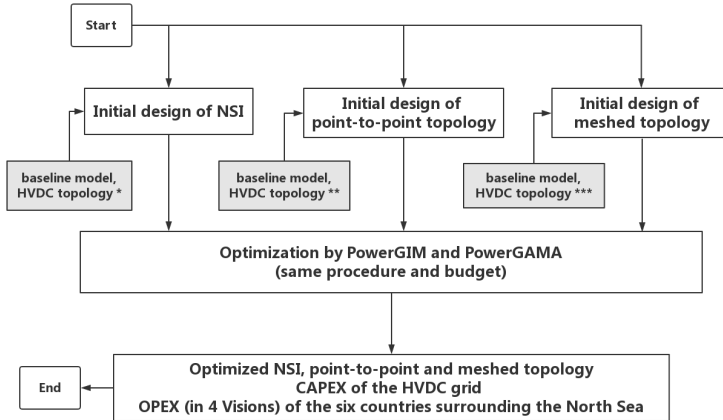


Figure 3.2: Flow chart of Chapter 3

*[\[3\]](#), **[\[10\]](#), ***[\[12\]](#)

- structure, location, installed capacity (by the year 2030) and budget of the North Sea Infrastructure from TenneT's vision [\[3\]](#).

INPUT DATA FORMAT FOR POWERGIM

The model will be built in both PowerGAMA and PowerGIM. While the input data format of PowerGAMA was already introduced in section [2.2](#), only input data format of PowerGIM would be introduced here.

As an additional module of PowerGAMA, PowerGIM (Power Grid Investment Module) offers special functions for determining socio-economically beneficial grid investments. The reason to introduce PowerGIM in a new section is that this module is documented separately from PowerGAMA. The author of this thesis wrote the introduction based on his understanding during master thesis project as well as information from [\[28\]](#)[\[30\]](#) and the author of the software.

The input data format is similar to PowerGAMA, however with specific additional information. The data is also stored in .csv files which can be edited by Excel; as screenshots of .csv files in Excel were already shown in section [2.2](#), it would not be repeated here.

In the tables of this sub-subsection, only parameters that do not exist in files for PowerGAMA would be specially introduced.

The input data for nodes are specified in "nodes.csv", as in the table [3.1](#).

The "cost_scaling" is the factor of cost scaling relative to the specified normal cost of new platform, as listed in the file "parameters.xml", the values in which are case-

	parameter	description	unit
1	id	name	<i>string</i>
2	area	country/region name	<i>string</i>
3	lat	latitude	degree
4	lon	longitude	degree
5	existing	whether the node already exists	<i>boolean</i>
6	cost_scaling	factor of cost scaling	p.u.
7	type	whether the node is for AC or DC	<i>string</i>

Table 3.1: Parameters in nodes.csv for PowerGIM

dependent. The exact values for the 2030 scenario in "parameters.xml" are shown in the chapter 3.

The input data for branches, including both AC and HVDC ones, are specified in "branches.csv", as in table 3.2.

	parameter	description	unit
1	node_from	name of the starting node	<i>string</i>
2	node_to	name of the end node	<i>string</i>
3	reactance	reactance of the branch	Ohm
4	capacity	capacity of the branch	MW
5	capacity2	externally added capacity at 2 nd stage	MW
6	expand	whether to consider expansion at 1 st stage	<i>boolean</i>
7	expand2	whether to consider expansion at 2 nd stage	<i>boolean</i>
8	max_newCap	maximum new capacity	MW
9	distance	length of the branch	km
10	cost_scaling	cost scaling factor	p.u.
11	type	AC, DC(direct) or DC(mesh)	<i>string</i>

Table 3.2: Parameters in branches.csv for PowerGIM

For the 2nd stage for "capacity 2" and "expand 2", the exact time is specified in the aforementioned "parameters.xml".

The "distance" column can be left blank. If so, the value would be calculated as the shortest distance between the starting and ending nodes, based on the node location specified in "nodes.csv".

The input data for consumers are specified in "consumers.csv", as in table 3.3.

The input data for generators are specified in "generators.csv", as in table 3.4.

	parameter	description	unit
1	node	name of the node that the consumer belongs to	<i>string</i>
2	demand_avg	annual average demand	MW
3	demand_ref	hourly demand relative to average demand	p.u.
4	emission_cap	maximum CO2 emission allowed	kg

Table 3.3: Parameters in consumers.csv for PowerGIM

	parameter	description	unit
1	desc	generator name/description	<i>string</i>
2	type	technology	<i>string</i>
3	node	name of the node that the generator belongs to	<i>string</i>
4	pmax	upper limit of power generation	MW
5	pmax2	externally added power generation capacity at 2 nd stage	MW
6	pmin	lower limit of power generation	MW
7	fuelcost	cost of specific fuel	€/MWh
8	fulecost_ref	time dependent relative profile	p.u.
9	inflow_fac	ratio of actual annual generation relative to full generation	p.u.
10	inflow_ref	hourly inflow value relative to annual average inflow value	p.u.
11	pavg	average power constraint for generators with large storage	MW
12	p_maxNew		MW
13	cost_scaling		p.u.
14	storage_cap	energy capacity of the storage	MWh
15	storage_price	base value of the storage	€/MWh
16	storage_ini	initial storage filling level relative to full capacity	p.u.
17	storval_filling	storage value relative coefficient dependent on filling level	p.u.
18	storval_time	storage value relative coefficient dependent on time	p.u.
19	pump_cap	power capacity of pumping	MW
20	pump_efficiency		p.u.
21	pump_deadband		€/MWh

Table 3.4: Parameters in generators.csv for PowerGIM

The "profiles.csv" for PowerGIM is obtained by merging information of "profiles.csv", "profiles_storval_filling.csv" and "profiles_storval_time.csv" for PowerGAMA.

3.2.2. ASSUMPTIONS

Some information acquired from TenneT's vision was already introduced, for example, the structure of "wind-connector" and the location at the Dogger Bank. In this subsection, the additional assumptions regarding the installed wind power capacity and HVDC transmission capacity are introduced.

INSTALLED OFFSHORE WIND POWER CAPACITY OF NSI

According to the development timeline in [3] (see Step 3 and Step 4), it is assumed by the author of this thesis that 15000 MW wind farm around the North Sea Wind Power Hub at the Dogger Bank is taken connected to it.

Another important assumption is that the installed capacity of 15000 MW is constant in all four different Visions.

DISTRIBUTION OF WIND POWER CAPACITY OF 6 COUNTRIES SURROUNDING THE NORTH SEA

For every surrounding country (i.e. BE, DE, DK, GB, NL and NO), offshore wind power installed capacity are divided into two parts: near shore part, which is directly connected to the on-shore nodes of the country, and far shore part, which is connected to the NSWPH at the Dogger Bank (regarded as the installed wind power capacity at the NSWPH, i.e. 15000 MW in total). It is assumed that in calculations, the cost of AC branches between the wind farms and the nodes (either at the Dogger Bank or in the country) are ignored. The division of each country of installed capacity at the hub followed the ratio of offshore wind capacity of each country (from [11], average value of 4 Visions).

It is also assumed that the division is constant for all four different Visions.

The assumptions in this sub-subsection are used to decide the installed offshore wind power capacity directly connected to the country, i.e. the residual offshore wind capacity after the data in TYNDP subtracted by the capacity connected to the hub.

Multiplying the installed wind power capacity in 2030 (table 3.5) and the percentage of offshore wind power (table 3.6), the installed offshore wind power capacity is obtained as in table 3.7.

Following the same installed offshore wind ratio of each country, the wind power capacity that is supposed to be connected to the North Sea Wind Power Hub at the Dogger Bank (15000 MW in total for all Visions) is calculated as in table 3.8.

Country	DE	DK	GB	BE	NL	NO
Vision 1	74050	6190	21870	4900	7000	2080
Vision 2	61200	8410	57300	4900	6160	2080
Vision 3	100750	10750	51090	8500	12700	2910
Vision 4	96967	12825	57901	7518	9995	2495

Table 3.5: Installed wind power capacity (MW) [11]

Country	DE	DK	GB	BE	NL	NO
percentage offshore	20.87%	48.34%	70%	42.69%	53.13%	56.14%

Table 3.6: Percentage of offshore wind installed capacity out of total installed capacity [11] [16]

Country	DE	DK	GB	BE	NL	NO
Vision 1	15454	2992	15309	2092	3719	1168
Vision 2	12772	4065	40110	2092	3273	1168
Vision 3	21027	5197	35763	3629	6748	1634
Vision 4	20237	6200	40531	3209	5310	1401

Table 3.7: Installed offshore wind power capacity (MW)

Country	DE	DK	GB	BE	NL	NO
Vision 1	5691	1102	5637	770	1370	430
Vision 2	3018	961	9478	494	773	276
Vision 3	4262	1053	7250	7368	1368	331
Vision 4	3948	1209	7907	626	1036	273

Table 3.8: Wind power capacity supposed to be connected to the NSWPH according to the ratio (MW)

As assumed, the wind power connected to the energy island from each country is supposed to be constant for all of the 4 Visions, therefore the average value per Vision is taken for each country for the constant division of wind power to be connected to the NSWPH (table 3.9).

Country	DE	DK	GB	BE	NL	NO
Capacity	4230	1081	7568	657	1137	328

Table 3.9: Wind power capacity from each country to be connected to the NSWPH (MW)

Therefore, the remaining offshore wind power capacity to be connected to each country is in table 3.10.

Country	DE	DK	GB	BE	NL	NO
Vision 1	11224	1911	7741	1435	2582	840
Vision 2	8543	2984	32542	1435	2136	840
Vision 3	16797	4115	28195	2972	5611	1306
Vision 4	16007	5118	32963	2553	4174	1073

Table 3.10: Remaining offshore wind power capacity to be connected to each country (MW)

At last, the onshore wind power capacity for each country is shown in table 3.11.

Country	DE	DK	GB	BE	NL	NO
Vision 1	58596	3198	6561	2808	3281	912
Vision 2	48428	4345	17190	2808	2887	912
Vision 3	79723	5553	15327	4871	5952	1276
Vision 4	76730	6625	17370	4309	4685	1094

Table 3.11: Onshore wind power capacity for each country (MW)

All the changes to the division of the installed capacity that are not connected to the NSWPH, are scaled to the existing generators per country per type (offshore/onshore).

BUDGET OF THE HVDC TRANSMISSION GRID TO BE DESIGNED IN THE NORTH SEA

Budget for initial investment is not unlimited. Although there might be some further investments which can lead to higher benefit within the equipment's lifetime, there is a limit of the budget for initial investment. According to [3], budget for offshore wind power development is around 10 billion Euros for NL and DE in the next ten years. Taking the sum of NL and DE as an average value, total budget for all six surrounding countries (i.e. BE, DE, DK, GB, NL, NO) is $10 / 2 * 6 = 30$ billion Euros.

It is assumed that 2/3 of the total budget for offshore wind is used for the North Sea Infrastructure (while the other 1/3 is for near shore and other preparation steps, or other offshore projects at the other side of the country, opposite to the North Sea). Therefore, the total budget for the investment cost of the North Sea Infrastructure to be designed is $2 / 3 * 30 = 20$ billion Euros.

Being difficult to predict the exact value, as well as to identify the sponsor, the non-electric part of the NSI, e.g. earthwork of the power hub, is not included in the budget. Nevertheless, it is beneficial to estimate approximately the investment cost for this part, and the answer is about 1.5 billion Euros [3] to 4.5 billion Euros. Based on this approximate answer, when comparing the optimized NSI design with other competitive topologies, a sensitivity test is performed to check if different possible investment cost of the non-electric part construction leads to different choices among topologies. This part of research is introduced in section 3.5.

TRANSMISSION CAPACITY OF HVDC GRID (FROM HUB TO THE SURROUNDING COUNTRIES)

Total transmission capacity is no lower than the installed wind capacity (15000 MW). This is taken because the HVDC lines are designed not only to transmit far shore wind power generated at the Dogger Bank, but also as interconnectors for better European coordination.

The initial design of division of transmission capacity from the NSWPH to the surrounding countries considered the ratio of offshore wind capacity of each country, benefited area of each country and advantage of Nordic reservoir. The initial design HVDC links are set with lower total capacity (and lower CAPEX) than the expected optimized result, as PowerGIM can only give investment recommendation of adding new capacity on the basis of the initial design, but not reducing capacity from it.

ONSHORE NODES TO BE CONNECTED WITH THE HUB

Besides GB (which is of special relative geographical position with the North Sea), there is only one node from each of other surrounding countries to be connected with the North Sea Wind Power Hub at the Dogger Bank.

The choice of the nodes mainly considers the nodes' geographical distance with the North Sea Wind Power Hub (i.e. generally the shorter the better). Also, it is more ideal if the nodes are at load center and are intersections of multiple branches.

WIND POWER INFLOW AT THE DOGGER BANK COMPARED TO NEAR SHORE WIND FARMS

According to TenneT's vision of NSI [3], one important advantage of constructing a central energy hub at the Dogger Bank is that the wind condition there is better than near shore wind farms. In operation simulations, it is therefore needed to quantify such

a difference of the Dogger Bank compared to near shore offshore wind farms in wind power generation inflow.

From the two versions of wind atlas, [31] for 60m above mean sea level and [2] for 90m above mean sea level, the annual mean wind speed difference between the Dogger Bank and near shore Dutch offshore wind farms can be seen, as in table 3.12.

Height above sea level (m)	60	90
Annual mean wind speed at Dogger Bank (m/s)	10.3	10.7
Annual mean wind speed at Dutch near shore wind farms (m/s)	9.4	9.8

Table 3.12: Annual mean wind speed difference between the Dogger Bank and near shore Dutch offshore wind farms

The next step would be to convert the difference of annual mean wind speed to difference in wind power generation output (between the Dogger Bank and near shore wind farms, assuming near shore wind farms in other countries surrounding the North Sea are of the same wind speed as Dutch ones).

There are different power outputting models of wind turbines [17], for example, widely used quadratic model [32][33] and cubic model [34], where wind power density \propto cube of wind speed.

In quadratic model, taking typical wind turbine model in [17] as an example, the wind power output P is:

$$P = \begin{cases} 0 & v < v_{in} \\ P_N(A + Bv + Cv^2) & v_{in} \leq v < v_N \\ P_N & v_N \leq v < v_{out} \\ 0 & v_{out} \leq v \end{cases} \quad (3.1)$$

where

$$A = \frac{1}{(v_{in} - v_N)^2} [v_{in}(v_{in} + v_N) - 4v_{in}v_N(\frac{v_{in} + v_N}{2v_N})^3] \quad (3.2)$$

$$B = \frac{1}{(v_{in} - v_N)^2} [4(v_{in} + v_N)(\frac{v_{in} + v_N}{2v_N})^3 - (3v_{in} + v_N)] \quad (3.3)$$

$$C = \frac{1}{(v_{in} - v_N)^2} [2 - 4(\frac{v_{in} + v_N}{2v_N})^3] \quad (3.4)$$

In equation 3.1 to 3.4, v , v_{in} , v_N and v_{out} are wind speed, cut-in wind speed, nominal wind speed and cut-out wind speed, respectively.

Parameters of a typical wind turbine from data in [17] are considered (table 3.13).

cut-in wind speed (m/s)	nominal wind speed (m/s)	cut-out wind speed (m/s)
3	12.5	25

Table 3.13: Output parameters of a typical wind turbine [17]

Importing data from table 3.12 and 3.13 to equation 3.1 to 3.4, wind power density at the Dogger Bank and near shore wind farms can be obtained (by the quadratic model). Combining the results of cubic model [34], the results are in table

Height above mean sea level (m)	60	90
mean wind speed at the Dogger Bank/near shore (m/s)	10.3/9.4	10.7/9.8
Wind power of the Dogger Bank relative to near shore (quadratic) (p.u.)	1.312	1.292
Wind power of the Dogger Bank relative to near shore (cubic) (p.u.)	1.316	1.302

Table 3.14: Wind power density at the Dogger Bank relative to near shore wind farms

As a result, the inflow of wind power at the Dogger Bank is assumed to be multiplied by 1.3 when importing from "profiles.csv".

3.2.3. CONCLUSION AND OUTPUT

The output of this step of initial design of the NSI is shown in figure 3.3.

The HVDC branches with a yellow node at center and a yellow number nearby, are NSI branches; the node with a yellow point at its center is the the North Sea Wind Power Hub at the Dogger Bank. The initial capacity of each HVDC branch is shown in table 3.15.

Number	from	to	Initial Capacity (MW)
1	GB-2	Dogger Bank	1000
2	GB-7	Dogger Bank	2000
3	GB-16	Dogger Bank	2000
4	NL	Dogger Bank	2000
5	DE	Dogger Bank	2000
6	DKw	Dogger Bank	2000
7	NO	Dogger Bank	2000
8	BE	Dogger Bank	2000

Table 3.15: Initial capacity of each HVDC branch in the NSI design

The numbers of the HVDC links are randomly chosen and do not indicate any order.

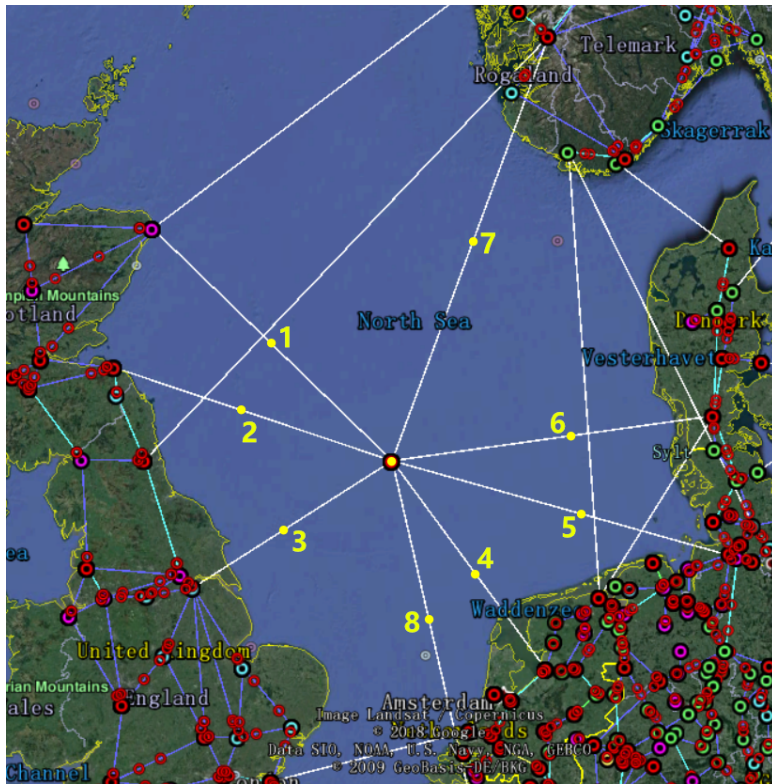


Figure 3.3: NSI initial design topology

3.3. OPTIMIZATION OF NSI TOPOLOGY

Before recognizing the role of the North Sea Infrastructure, the design of NSI should be optimized at first. PowerGIM is helpful in providing such functions. While PowerGAMA solves linear programming (LP) problem, PowerGIM solves mixed-integer linear programming (MILP) problem, which enables the consideration of binary and integer investment variables. However, the computational complexity of MILP is heavier than LP, and only aggregated models are used for the research of this master thesis for acceptable simulation duration.

3.3.1. WORKING PROCESS OF POWERGIM

The working process of PowerGIM is illustrated in the flow chart (figure 3.4).

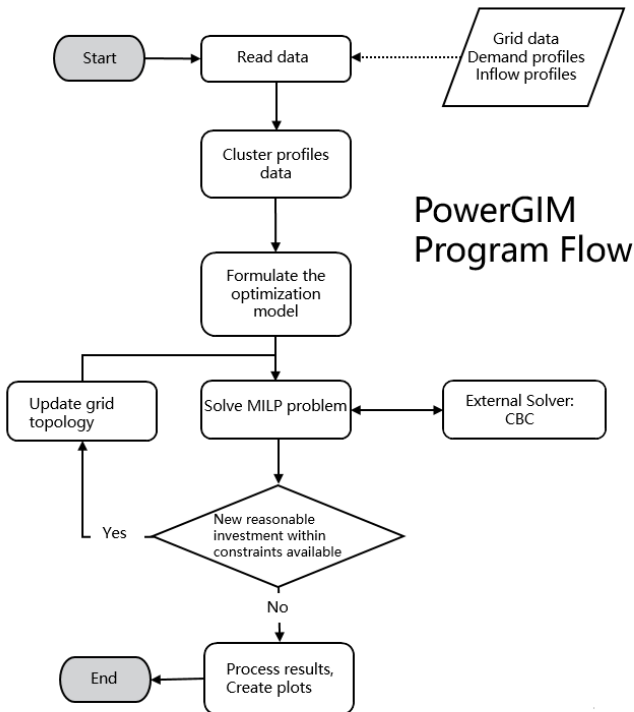


Figure 3.4: PowerGIM working process flow chart

The implementation of such process can be found in the script "runpowergim.py" (appendix .2).

3.3.2. OPTIMIZATION PROBLEM

OBJECTIVE FUNCTION

The optimal solution (of investment) is attained by the optimization process of minimizing the net present value (NPV) of the total cost (i.e. investment cost of new transmission branches and new generators and operational cost). Therefore, the objective function of the problem is:

$$\min (Total\ Cost) = \min (CAPEX + a \cdot OPEX) \quad (3.5)$$

Where a is the annuity factor that converts the annual operational costs (calculated for one representative year) of lifetime to the NPV.

The equations to calculate the investment cost (CAPEX) and operation cost (OPEX) are as follows:

$$CAPEX = \sum_{b \in B} (C_b^{fix} y_b^{num} + C_b^{var} y_b^{cap}) + \sum_{n \in N} C_n^{bus} z_n + \sum_{i \in G} CX_i x_i \quad (3.6)$$

$$OPEX = \sum_{t \in T} \omega_t (\sum_{i \in G} (MC_i + CO2_i) g_{it} + \sum_{n \in N} VOLL s_{nt}) \quad (3.7)$$

where b, n, i, t are indices or branch, node, generator and time step, respectively; B, N, G, T are the sets of branches, nodes, generators and time steps, respectively; C_b^{fix} and C_b^{var} would be explained later in the next paragraph; y_b^{num} is the number of new transmission lines at branch b ; y_b^{cap} is the new transmission capacity at branch b ; C_n^{bus} is the cost for a new platform; z_n is the new platform at node n ; $CX_i x_i$ is the investment cost for every unit of generation capacity at generator i ; ω_t is the number of hours per cluster (for the aggregated time profile); MC_i and $CO2_i$ are the marginal cost and CO2 emission cost of power generation at generator i , respectively; g_{it} is the generation dispatch of generator i at hour t ; $VOLL$ is the value of lost load (i.e. load shedding cost); s_{nt} is load shedding at node n at hour t .

For the two parameters without explanation in the previous paragraph, C_b^{fix} and C_b^{var} , hereby the extended representation:

$$C_b^{fix} = B + B^d D_b + 2CL/CS, b \in B \quad (3.8)$$

$$C_b^{var} = B^{dp} D_b + 2CL^p/CS^p, b \in B \quad (3.9)$$

where B, B^d and B^{dp} are the branch mobilization cost, fixed cost (dependent only on the length of the branch) and variable cost (dependent on both length and power capacity of the branch); D_b is the length or distance of the branch b ; CL and CL^p are the fixed and variable (dependent on power capacity) cost of onshore switchgear, respectively; CS and CS^p are the fixed and variable (dependent on power capacity) cost of offshore switchgear, respectively.

CONSTRAINTS

The first constraint is that for a given node n , at time step t , the sum of generation, net power flow injection (subtracted by branch power loss) and load shedding equals sum of demand:

$$\sum_{i \in G_n} g_{it} + \sum_{b \in B_n^{in}} f_{bt}(1 - l_b) - \sum_{b \in B_n^{out}} f_{bt} + s_{nt} = \sum_{l \in L_n} D_{lt}, n \in N, b \in B \quad (3.10)$$

where f_{bt} refers to power flow at branch b at time step t , l_b is the branch loss at branch b , B_n^{in} and B_n^{out} are injecting branch and outputting branch of node n , and D_{lt} refers to demand at load l at time step t . Other indices which were already mentioned in the last sub-subsection would not be repeatedly introduced again here.

The second constraint is that the load shedding at node n at time step t must be lower than or equal to the sum of demand at node n :

$$s_{nt} \leq \sum_{l \in L_n} D_{lt} \quad (3.11)$$

The third constraint is that for the given generator i , the power generation has to be within lower limit and upper limit:

$$P_i^{min} \leq g_{it} \leq \gamma_{it}(P_i^e + x_i) \quad (3.12)$$

where γ_{it} is factor for available generator capacity at generator i at time step t ; P_i^e and x_i are the existing and new generation capacity at generator i at time step t , respectively.

The fourth constraint is that for the generator i , the power generated whole year must be lower than or equal to the yearly disposable energy:

$$\sum_{t \in T} \omega_t g_{it} \leq E_i \quad (3.13)$$

where E_i is the yearly disposable energy of generator i .

The fifth constraint is that the power flow at branch b at time step t should be within the power capacity in both directions:

$$-(P_b^e + y_b^{cap}) \leq (P_b^e + y_b^{cap}) \quad (3.14)$$

where P_b^e and y_b^{cap} are existing and new transmission capacity at branch b , respectively.

The sixth constraint is that the new transmission capacity at branch b must be lower than or equal to the product of maximum new line capacity and number of new transmission lines:

$$y_b^{cap} \leq P_b^{n,max} y_b^{num} \quad (3.15)$$

The seventh constraint is that a node facility (e.g. an offshore platform) is forced to be implemented if it does not exist at the node n where there are branches connected to:

$$\sum_{b \in B_n} y_b^{num} \leq M z_n \quad (3.16)$$

where M is a sufficiently large number; z_n is a binary variable used to reflect whether to install a new platform.

The eighth constraint is to specify the value range of all variables:

$$x_i, y_b^{cap}, g_{it}, f_{bt}, s_{nt} \geq 0, y_b^{num} \in Z^+, z_n \in \{0, 1\} \quad (3.17)$$

VARIABLES

A recap of all variables for the optimization problem in PowerGIM is in table 3.16.

variable	description	unit
y_b^{num}	number of new transmission lines at branch b	<i>integer</i>
y_b^{cap}	new power transmission capacity at branch b	MW
z_n	new platform at node n	<i>boolean</i>
x_i	new power generation capacity at generator i	MW
g_{it}	power generation at generator i at time step t	MW
f_{bt}	power flow at branch b at time step t	MW
s_{nt}	load shedding at node n at time step t	MW

Table 3.16: Variables in PowerGIM optimization problem.csv

3.3.3. TOPOLOGY OPTIMIZATION PROCEDURE

In answer to research question 2, "What are the criteria to optimize each topology and to compare the topologies?", the optimization objective function as well as the comparison indicator are the same as in equation 3.5.

The CAPEX of the NSI design is calculated in PowerGIM, following equation 3.6, 3.8 and 3.9. The details of the specific "parameters.xml", which is used for CAPEX and OPEX calculation, are listed in table 3.17, table 3.18, table 3.19, table 3.20, table 3.21 and table 3.22. Values in the "parameters.xml" are determined mainly based on [35], while prices for CO2 emission from [11]. The exact meaning of each parameter can be found in subsection 3.3.2.

Under this condition, the CAPEX of initial NSI design is **13.66808 billion Euros**. It is not dependent on the choice of Visions. Distribution of offshore generators are pre-set and fixed for all different Visions, of which the investment costs are not included in

CAPEX within this thesis. All compared topologies (i.e. NSI and two other topologies to be designed in section 3.4) are of the same installed capacity (15000 MW), therefore whether to calculate investment costs of wind turbines would not lead to difference in preference of topologies.

Please note the initial design is intended to be lower than the budget (20 billion Euros), for that PowerGIM can only give new investment guidance in addition to the current topology (but not reduce capacity/lines from the current topology).

node type	S(€)
AC	50000000
DC	406000000

Table 3.17: Parameters of nodes in parameters.xml for PowerGIM

branch type	B(€)	Bdp(€/km*MW)	Bd(€/km)
AC	312000	1416	1193000
meshed DC	312000	578	1236000
direct DC	312000	578	1236000
converter	0	0	0
AC OHL	0	394	1187000

Table 3.18: Parameters of branches (1) in parameters.xml for PowerGIM

branch type	CL(€)	CLp(€/MW)	CS(€)	CSp(€/MW)
AC	1562000	0	4813000	0
meshed DC	1562000	0	4813000	0
direct DC	58209000	93200	452499000	107800
converter	28323000	46600	20843000	53900
AC OHL	1562000	0	0	0

Table 3.19: Parameters of branches (2) in parameters.xml for PowerGIM

The OPEX of the six countries surrounding the North Sea (BE, DE, DK, GB, NL NO) through out the lifetime of equipment of NSI can be calculated in both PowerGAMA, as was shown in sub-section 2.4.3, and in PowerGIM.

In PowerGIM, OPEX is also calculated as equation 3.7 for one representative year. The results is automatically multiplied by the annuity factor (calculated as in equation 2.12), therefore the OPEX PowerGIM outputs to "results.xlsx" is the OPEX throughout

branch type	maximum capacity(MW)	loss constant	loss per km
AC	400	0	0.00005
meshed DC	1000	0	0.00003
direct DC	1000	0.032	0.00003
converter	2000	0.016	0
AC OHL	4000	0	0.00003

Table 3.20: Parameters of branches (3) in parameters.xml for PowerGIM

generation type	CO2 emission (ton/MWh)
wind offshore	0
wind	0
solar PV	0
hydro	0
bio	0
nuclear	0
gas	0.4215
coal	0.8605
oil	0.7167

Table 3.21: CO2 emission rate per generation type in parameters.xml for PowerGIM

parameter type	value
interest rate	0.05
lifetime	30 years
operation/maintenance rate relative to investment	0.02
CO2 price	17(Vision 1/2) or 71(Vision 3/4) €/ton
value of lost load	1000 €/MW
stage2TimeDelta	0 year
stages	1 stage

Table 3.22: Other parameters in parameters.xml for PowerGIM

the equipment's lifetime. Besides the fuel cost and CO₂ cost of the generation output, compared to PowerGAMA, PowerGIM also considers branch loss and maintenance cost.

There is a deviation between the OPEX calculation results from PowerGAMA and PowerGIM. Besides the differences of branch loss and maintenance cost, the main reason is that PowerGIM uses aggregated model to reduce computational complexity (and therefore precision is sacrificed). This would be elaborated later in this sub-section. In short, OPEX calculated by PowerGIM is only used during optimization process, and OPEX calculated by PowerGAMA is the final version for result checking and for comparison between different topologies.

The lifetime OPEX (calculated by PowerGIM) of the six countries surrounding the North Sea with initial NSI design under 4 Visions is shown in the table 3.23.

Visions	Vision 1	Vision 2	Vision 3	Vision 4
OPEX (billion €)	747	612	697	805

Table 3.23: Lifetime OPEX of six countries in total with initial NSI design

One might find it counter-intuitive that with the same initial design (**CAPEX = 13.66808 billion €**), the OPEX for Vision 4 is higher while it assumes great progress in both achieving green energy goals and European coordination/cooperation (and is therefore supposed to be of lowest OPEX, with much lower fuel cost of RES compared to conventional energy sources). However, the OPEX results cannot be directly compared this way. For example, the annual load per country is highest in Vision 4, so is the CO₂ cost (71 €/ton, while for Vision 1 and 2 it is 17 €/ton). Such differences should not be ignored, and the result of Vision 4 with high OPEX is easier to understand if taking them into consideration.

As is shown in the topology optimization procedure flow chart (figure 3.1), the input of the topology optimization is European model with initial NSI design, and both PowerGIM and PowerGAMA are used for optimization iterations.

A recap of the functions and features of PowerGIM and PowerGAMA is given at first, in order to guide two softwares to cooperate.

(1) PowerGIM:

PowerGIM, in this step, is mainly used for giving investment advice and calculating CAPEX of the system.

MILP problem is of high computational complexity. In order to obtain useful simulation results within acceptable time duration, the aggregated model is in need. The aggregation is performed regarding both the grid topology and the time profiles.

In the aggregated model, the onshore nodes of each country were merged into one or only a few representative nodes. In addition, the corresponding intra-area onshore

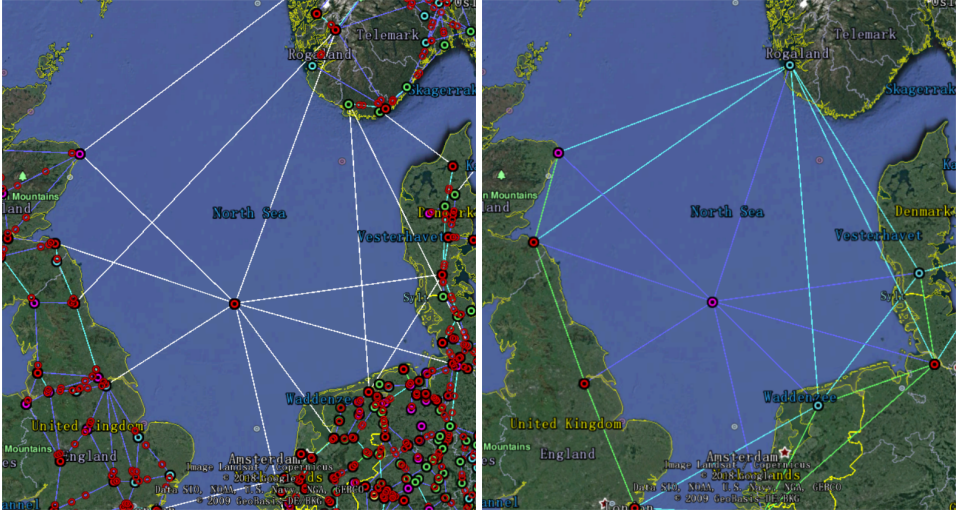


Figure 3.5: Detailed model in PowerGAMA (left) and aggregated model in PowerGIM (right)

AC branches (which are generally with infinite capacity in the full-size model) were neglected. At last, only six countries surrounding the North Sea were kept in this model. The cross-border AC branches and the HVDC branches (among the six countries) were kept as before. Comparison of original model and the aggregated one is shown in figure 3.5.

As is shown, the GB nodes were merged into 4 nodes, while 2 nodes for DK, and 1 node for each of BE, DE, NL, and NO. The decision of the location of each node follows the rule that the resulting HVDC topology remains almost the same shape as in the original model, for the sake of keeping similar CAPEX (which highly depends on the length of the HVDC branches).

As for the aggregation of time profiles (for the generation output and load at each hour), 1200 out of 8760 hours were randomly chosen as sampling points. While it is difficult to keep continuous water level given randomly chosen discrete time points, reservoirs are considered as fully dispatchable to imitate real reservoir behavior as much as possible.

The aggregation of time profiles lead to severe deviation. Sensitivity tests done by the author of this thesis show that when running simulation for several times for the same model, the deviations in OPEX results can be ± 20 billion Euros. This deviation is as large as the budget of HVDC branches in the North Sea. Therefore, the OPEX results from PowerGIM are not useful in topology comparisons.

Nevertheless, although deviations in OPEX results between different times of simu-

lations are large, PowerGIM provides consistent (and useful, which is tested later in this chapter) investment advice.

Standard of stopping iterations in PowerGIM is when there is no further reasonable investment possibility (that can be paid back within the lifetime of 30 years) missing, or the investment cost is beyond the budget.

(2) PowerGAMA:

PowerGAMA, in this step, is mainly used for giving precise operational simulation and therefore calculating operational cost (OPEX) accurately. Also, it can give advice on adjusting transmission capacity of HVDC branches by recording branch utilization rate.

The computational complexity of LP problem in PowerGAMA is lighter than MILP in PowerGIM. Therefore, the full year operation simulation with resolution of per hour (8760 hours in total) and 388-bus European model (with high-resolution for 6 countries surrounding the North Sea and lower resolution for other European countries) can be performed. Each simulation takes about 5 hours.

Based on the above analysis, the following cooperation mode between PowerGIM and PowerGAMA is implemented:

(1) One can use PowerGIM to add new capacity/lines to the current NSI design before reaching the budget, and use PowerGAMA to decrease redundant capacity/lines based on their utilization rate when the budget is exceeded.

(2) OPEX results from PowerGIM are only used during optimization process, and OPEX from PowerGAMA are used as final results and for topology comparison.

(3) When the investment decision from PowerGIM contradicts with PowerGAMA output, results from PowerGIM are of higher priority. As is aforementioned, the PowerGAMA can only help by tracing utilization rate per branch. Firstly, a branch with relatively low utilization rate does not necessarily mean its investment cannot be paid back within its lifetime. What's more, the adjustment of one specific branch is not independent of other branches. The expansion and reduction of one branch, which based on the result of its utilization rate, may lead to changes of other branches. To understand the influence of adjustment of this single branch, an overall simulation should be performed. However, each iteration per Vision by PowerGAMA takes 5 hours on a personal computer, while PowerGIM can provide hundreds of iterations within one hour.

The difference of priority can be applied by, for example, setting a loose criterion for stopping iteration when the result from PowerGIM is processed by PowerGAMA.

Giving PowerGIM the initial NSI design as input, and setting 2 stages of investment in "parameters.xml" (2nd stage at year = 10; for more insights of preferable investments), after hundreds of iterations, the table 3.24 is attained as the investment recommendation.

"DB" refers to the Dogger Bank; "ini.cap." refers to the initial capacity; "v1_step1"

number	1	2	3	4	5	6	7	8
from	GB-2	GB-7	GB-16	NL	DE	DKw	NO	BE
to	DB	DB	DB	DB	DB	DB	DB	DB
ini.cap.	1000	2000	2000	2000	2000	2000	2000	2000
vi1_step1	0	1000	1000	1000	1000	0	1000	1000
vi1_step2	0	0	1000	0	1000	0	1000	0
vi2_step1	1000	1000	1000	1000	1000	1000	1000	1000
vi2_step2	0	0	1000	1000	1000	0	1000	0
vi3_step1	1000	0	1000	1000	1000	0	1000	1000
vi3_step2	0	0	0	1000	1000	0	1000	0
vi4_step1	1000	0	1000	1000	1000	1000	1000	1000
vi4_step2	1000	0	0	1000	0	0	1000	1000
times	4	2	6	7	7	2	8	5

Table 3.24: PowerGIM investment recommendation on the basis of initial NSI design (MW)

refers to, as an example, investment recommendation for step 1 of Vision 1; "times" sums the investment recommendation each branch receives for 2 steps in each of the 4 Visions.

As PowerGIM is not able to find the optimal solution under given budget, the alternative here is to adjust manually by counting investment recommendations, and doing CAPEX calculation again to check if budget is followed.

Based on the counting in "times", which reflects tendency of preferable investment, a line with capacity 1000 MW is added to each of the branches with "times" higher than or equal to 5, and an additional 1000 MW line is added to each branch with full "times", i.e. equal to 8.

The resulting capacities of branches are shown in table 3.25.

number	1	2	3	4	5	6	7	8
from	GB-2	GB-7	GB-16	NL	DE	DKw	NO	BE
to	DB	DB	DB	DB	DB	DB	DB	DB
capacity (MW)	1000	2000	3000	3000	3000	2000	4000	3000

Table 3.25: Mid-stage NSI design optimized by PowerGIM

However, after calculating the CAPEX of the new NSI design, the result is **23.5009 billion €** and therefore beyond the budget.

The procedure is repeated to check the investment tendency from the new NSI de-

sign (table 3.26).

number	1	2	3	4	5	6	7	8
from	GB-2	GB-7	GB-16	NL	DE	DKw	NO	BE
to	DB	DB	DB	DB	DB	DB	DB	DB
exs.cap.	1000	2000	3000	3000	3000	2000	4000	3000
vi1_step1	0	1000	1000	1000	1000	0	1000	0
vi1_step2	0	0	1000	0	0	0	1000	0
vi2_step1	1000	1000	1000	1000	1000	1000	1000	0
vi2_step2	1000	0	0	1000	1000	0	1000	0
vi3_step1	1000	0	1000	1000	1000	0	1000	0
vi3_step2	0	0	0	0	0	0	1000	0
vi4_step1	1000	0	1000	1000	1000	0	1000	1000
vi4_step2	0	0	0	1000	0	0	1000	0
times	4	2	5	6	5	1	8	1

Table 3.26: PowerGIM investment recommendation on the basis of mid-stage NSI design (MW)

It is shown in "times" that the investment tendency for branch 6 and 8 is low, reflecting redundancy. At this time when the design is beyond budget, 1000MW capacity is taken from each of the branch (table 3.27).

number	1	2	3	4	5	6	7	8
from	GB-2	GB-7	GB-16	NL	DE	DKw	NO	BE
to	DB	DB	DB	DB	DB	DB	DB	DB
capacity (MW)	1000	2000	3000	3000	3000	1000	4000	2000

Table 3.27: Optimized NSI Design

CAPEX result is **19.81483 billion €** and this latest NSI topology can be regarded as an optimized NSI design.

After the optimization procedure from PowerGIM, PowerGAMA is used to check if there is significant idleness of optimized branches by tracing the utilization rate.

The criteria for an acceptable utilization rate is, according to the average value of utilization rate of existing HVDC projects [36], 50%.

For the optimized design of NSI, the utilization rate of each branch in 4 Visions is as in the table 3.28.

It can be seen that the utilization rates of all branches in all Visions are higher than the criterion.

number	from	Vision 1	Vision 2	Vision 3	Vision 4
1	GB-2	0.80	0.84	0.80	0.77
2	GB-7	0.90	0.90	0.90	0.91
3	GB-16	0.92	0.91	0.93	0.92
4	NL	0.88	0.88	0.88	0.88
5	DE	0.87	0.89	0.87	0.87
6	DKw	0.93	0.94	0.92	0.92
7	NO	0.81	0.81	0.82	0.79
8	BE	0.99	0.99	0.99	0.99

Table 3.28: Branch utilization rate (p.u.) of the optimized NSI design

It is therefore concluded that the NSI design as in the table 3.27 is the optimized NSI design.

At last, a final check needs to be done by comparing OPEX calculated by PowerGAMA (i.e. accurate result) of optimized NSI design and the baseline case. The comparison is given as in table 3.29. It is clear that for each Vision, compared to the baseline, the optimized NSI design brings much lower total cost.

Optimized NSI	CAPEX	OPEX	Total Cost
Vision 1	19.82	558	578
Vision 2	19.82	409	429
Vision 3	19.82	577	597
Vision 4	19.82	711	731
Baseline	CAPEX	OPEX	Total Cost
Vision 1	0	593	593
Vision 2	0	448	448
Vision 3	0	628	628
Vision 4	0	760	760

Table 3.29: Comparison of optimized NSI design and baseline (billion €)

3.4. DESIGN AND OPTIMIZATION OF HVDC GRID IN THE NORTH SEA WITH OTHER STRUCTURES

3.4.1. INTRODUCTION

In answer to the first and the second research question, the topologies with structures different from NSI are designed, optimized and compared with NSI.

When recognizing the role of the the North Sea Wind Power Hub, the influence of this hub in cost-benefit is an important aspect. It is worth research whether the hub brings intrinsic economic advantage, the conclusion of which determines whether the hub is an essential part of the design.

Correspondingly, two competitive HVDC grid topologies of the North Sea are developed in this stage. The first one comprised of only point-to-point direct HVDC links (e.g. the Viking Link under planning), while the second one uses meshed HVDC links (inspired by [12]).

The result of the comparison among the three topologies with different structures (point-to-point structure, meshed structure without a central hub, and star-like structure with a central North Sea Wind Power Hub) can show strongly the role of the energy hub.

To make the topologies comparable, the budget limit for investment cost for the point-to-point design and meshed design remains the same as for the North Sea Infrastructure design of 20 billion Euros, and the optimization iteration procedure is similar to NSI.

The output of this section are the optimized design of the two competitive topologies and the simulated total cost throughout lifetime (the same as was used in the previous section), which means the sum of CAPEX (same value in all 4 Visions) and OPEX (throughout lifetime of 30 years, different value in different Visions).

$$Total\ Cost = CAPEX + OPEX_{lifetime} \quad (3.18)$$

3.4.2. DEVELOPMENT OF POINT-TO-POINT TOPOLOGY AND MESHED TOPOLOGY

Besides "hub and spoke" structure of NSI, there are also to other kinds of structures of HVDC grid, e.g. the point-to-point interconnectors and the meshed HVDC grid (without a central energy hub). If the socio-economical parameters (i.e. Total cost of lifetime) of the proposed NSI with NSWPH can exceed both the point-to-point and meshed (without a central hub) topology, the role of the North Sea Wind Power Hub can be strongly proved.



Figure 3.6: Point-to-point topology

Inspired by the Viking Link connecting GB and DK under planning (however ignored in the baseline model because of overlapping with NSI), the point-to-point topology is developed. As is shown in the flow chart, following the same optimization procedure by both PowerGIM and PowerGAMA, an optimized point-to-point topology (with same budget as NSI) is proposed (figure 3.6).

The offshore wind farm of 15000 MW, which was counted on the NSWPH while designing, is divided and scaled to the surrounding countries following table 3.9.

The comparison between initial design and optimized design is in table 3.30.

The comparison between optimized point-to-point topology and baseline is in table 3.31 using OPEX results from PowerGAMA. Regarding the total cost, it can be seen that in Vision 1, the HVDC investment cannot be paid back before the end of lifetime. For Vision 2, 3 and 4, the point-to-point design is still a reasonable investment; compared to baseline, it reveals its advantage in the Visions when RES ratio is higher.

Then, inspired by the topology in [12], a meshed HVDC design without a central en-

number	from	to	Initial	Optimized
1	GB-15	DKw	2000	2000
2	GB-16	DE	2000	4000
3	GB-19	NL	2000	4000
CAPEX			10.81	19.76

Table 3.30: Comparison of initial and optimized point-to-point design (topology)(MW for capacity and billion € for CAPEX)

Optimized point-to-point	CAPEX	OPEX	Total Cost
Vision 1	19.76	578	598
Vision 2	19.76	427	447
Vision 3	19.76	604	624
Vision 4	19.76	735	755
Baseline	CAPEX	OPEX	Total Cost
Vision 1	0	593	593
Vision 2	0	448	448
Vision 3	0	628	628
Vision 4	0	760	760

Table 3.31: Comparison of optimized point-to-point design and baseline (billion €)

ergy hub is proposed (figure 3.7).

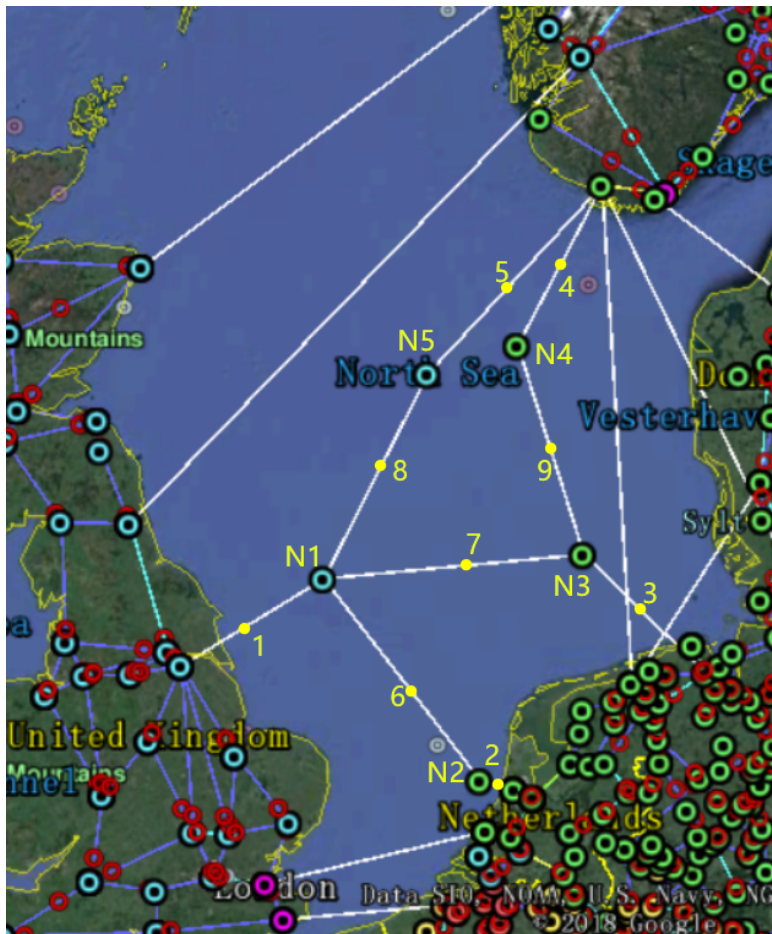


Figure 3.7: Meshed (without a central energy hub) topology

The off-shore wind farm of 15000 MW, which was counted on NSWPH while designing NSI, is divided and scaled to the surrounding countries following table 3.32 for GB, NL, DE and NO, and following table 3.9 for DK and BE.

The comparison between initial design and optimized design is in table 3.33.

The comparison between optimized meshed topology and baseline is in table 3.34 using OPEX results from PowerGAMA. As there is also a node at the Dogger Bank in this topology, the advantage of higher wind speed than near shore wind farms is also considered. Although it cannot be paid back within lifetime in Vision 1 either (the same as point-to-point topology), it bears an advantage compared to baseline in most Visions.

country	GB	NL	DE	NO	NO
name	Dogger Bank	Ijmuiden	Gaia	Ægir	Idunn
node	N1	N2	N3	N4	N5
longitude (°)	1.66	4.2	6.08	5.12	3.5
latitude (°)	54.5	52.5	54.68	56.75	56.5
capacity (MW)	7568	1137	4230	149	179

Table 3.32: Generator capacity division in 5 new nodes

number	from	to	Initial	Optimized
1	N1	GB-16	5000	5000
2	N2	NL	2000	3000
3	N3	DE	4000	3000
4	N4	NO-Feda	2000	4000
5	N5	NO-Blafalli	2000	4000
6	N1	N2	2000	2000
7	N1	N3	2000	2000
8	N1	N5	2000	4000
9	N3	N4	2000	4000
CAPEX			14.05	19.80

Table 3.33: Comparison of initial and optimized meshed design (topology)(MW for capacity and billion € for CAPEX)

Optimized point-to-point	CAPEX	OPEX	Total Cost
Vision 1	19.80	574	594
Vision 2	19.80	422	442
Vision 3	19.80	592	612
Vision 4	19.80	726	746
Baseline	CAPEX	OPEX	Total Cost
Vision 1	0	593	593
Vision 2	0	448	448
Vision 3	0	628	628
Vision 4	0	760	760

Table 3.34: Comparison of optimized point-to-point design and baseline (billion €)

3.5. CONCLUSION

Following the same procedure of optimization by PowerGIM and PowerGAMA, the optimized NSI, point-to-point topology and meshed topology (without a central hub) are developed in this chapter. The baseline model created in chapter 2 is used as starting point for the designs and to quantify the absolute value of socio-economic benefit of each topology.

The cost-benefit comparison of three topologies in 4 Visions of scenario 2030 is as in the table 3.35.

Total cost	NSI	point-to-point	meshed	baseline
Vision 1	578	598	594	593
Vision 2	429	447	442	448
Vision 3	597	624	612	628
Vision 4	731	755	746	760

Table 3.35: Total cost comparison of three competitive topologies (billion €)

From the data in the table, it is clear that the proposed NSI design with the North Sea Wind Power Hub outperforms two other optimized topologies with different structure.

However, it is assumed in sub-section 3.2.2 that the investment cost of non-electric part of the power hub, e.g. earthwork, is ignored. A sensitivity test is needed here to check if different cost of non-electric constructions will lead to different preference of topology.

Calculating the the difference of total cost between NSI and two other topologies, it can be found that the smallest difference appears at Vision 2 between NSI and meshed topology.

This smallest difference, $442 - 429 = 13$ billion €, is the maximum investment cost for the non-electric constructions of the NSWPH without influencing the topology preference. The approximate cost of the earthwork is 1.5 billion € to 4.5 billion €, which is only about 11.5% to 35% of the acceptable difference. In fact, if taken construction cost of new nodes in meshed topology into consideration (which is previously ignored), the advantage of NSI is even larger.

Therefore, it can be concluded that the proposed NSI design provides best cost-benefit performance among all developed topologies.

Compared to the baseline situation, the benefit that NSI can entail through its life-time is shown in table 3.36.

Vision	Vision 1	Vision 2	Vision 3	Vision 4
Benefit (€)	15	19	31	29

Table 3.36: Benefit of NSI compared to baseline (billion €)

4

SENSITIVITY TEST UNDER DIFFERENT RES INFLOW AND LOAD CONDITIONS

4.1. INTRODUCTION

In the simulations in chapter 2 and chapter 3, for 2030 scenario, the time profiles of variable generation (wind, solar and hydro) and load are taken from [29] for scenario 2014, with installed capacity scaled to scenario 2030 [11].

However, systematic (e.g. climate change) or random (i.e. anomalies) changes in weather conditions may happen from 2014 to 2030 (and to 2060, the end of the lifetime of the equipment). It is necessary to perform sensitivity tests for the HVDC designs to test their behavior (e.g. OPEX) under weather conditions significantly different from scenario 2014.

Extreme weather conditions considered in this chapter as well as their realization in the model are introduced in section 4.2; as wind power is of special interest in this thesis, the algorithm to generate wind power inflow profiles and its realization in Excel are introduced in section 4.3; results of simulations under extreme conditions are analyzed in section 4.4; section 4.5 concludes the chapter.

The simulations performed for all 4 topologies (three optimized HVDC grid topology and baseline) in this chapter are shown in the yellow area of figure 4.1.

As extreme (in annual mean value) wind conditions are important to the designs of

	Vision 1	Vision 2	Vision 3	Vision 4
Normal	4 Topologies	4 Topologies	4 Topologies	4 Topologies
Wind speed +25%	4 Topologies	4 Topologies	4 Topologies	4 Topologies
Wind speed -25%	4 Topologies	4 Topologies	4 Topologies	4 Topologies
Wind new profiles ×2		4 Topologies		4 Topologies
Solar radiation +10%		4 Topologies		4 Topologies
Solar radiation -10%		4 Topologies		4 Topologies
Nordic hydro inflow +25%		4 Topologies		4 Topologies
Nordic hydro inflow -25%		4 Topologies		4 Topologies
Load +5%		4 Topologies		4 Topologies
Load -5%		4 Topologies		4 Topologies

Figure 4.1: Simulations performed in Chapter 4 for all 4 topologies (yellow area)

the North Sea HVDC grid (which are considered with offshore wind farms), all 4 Visions of all 4 topologies are simulated. For other weather conditions, only Vision 2 and Vision 4 are simulated as examples.

The reasons to choose Vision 2 are that

- according to the results in table 3.35, the lowest total cost difference between NSI and other topologies under normal weather condition exists in Vision 2 (between NSI and meshed topology), therefore Vision 2 is regarded as an interesting Vision where changes in generation and load might influence the topology reference (i.e. whether NSI leads to lowest total cost of 6 countries, compared to other topologies);
- according to TenneT, Vision 2 is recognized most likely to happen in the future, compared to other Visions in ENTSO-E's TYNDP [11];

while the reason to choose Vision 4 is that

- it represents the most radical "green evolution" where there is highest proportion (compared to other Visions in [11]) of RES in energy mix, and therefore more likely to be influenced by changes in RES power inflow and load (which consumes RES generation).

4.2. EXTREME RES INFLOW AND LOAD CONDITIONS

4.2.1. POSSIBLE EXTREME RES INFLOW AND LOAD CONDITIONS

WIND POWER INFLOW

According to [37][38], within this century in Europe, the multi-year annual mean wind speed could be under the change of $\pm 25\%$.

The changes in wind speed can be converted to changes in wind power inflow by using the quadratic or cubic model as in chapter 3. The results are shown in table 4.1.

Change in wind speed	-25%	+25%
Change in wind power inflow	-59.514%	+92.308%

Table 4.1: Wind power inflow changes under extreme wind conditions

Besides the deviations in annual mean wind speed, the system's sensitivity to the short-term randomness, which can be provided by re-synthesized wind inflow time profiles, is also tested. In this case, the new wind inflow time profiles are with the same statistical features (e.g. annual mean value, seasonal and daily variation characteristics) which are extracted from reference profile, but different/random short-term behavior (which are determined by random number within the re-synthesis process), with regard to each hour. The algorithm of re-synthesis and its realization is introduced in section 4.3.

SOLAR POWER INFLOW

Basically, PV cells' generation output is positively proportional to solar radiation (W/m^2), and negatively and linearly correlated to temperature [39].

According to [40], in Europe, maximum annual mean solar radiation deviation during 1939-2012 are $\pm 10\%$ from the 1971-2012 mean value. Assuming fixed annual mean temperature, the deviations of solar radiation lead to $\pm 10\%$ of solar power inflow.

According to [41], the efficiency of PV cells falls 0.5% when temperature increases per $^{\circ}C$; while annual temperature of Europe changes 1 $^{\circ}C$ for the past 100 years [42], the deviation of solar power inflow caused by temperature changes is much lower compared to deviations of solar radiation.

Therefore, $\pm 10\%$ deviation of annual mean solar power inflow from normal case is considered as the extreme condition to be studied in this chapter.

HYDRO POWER INFLOW

According to [43], from 1950 to 2002, the extreme deviation of annual hydro inflow of Norwegian and Swedish hydro power stations are $\pm 25\%$.

Only deviations of NO and SE power inflow are considered in the simulations of this chapter since that the capacity of Norwegian and Swedish hydro power is 3 times the sum of hydro power of other countries surrounding the North Sea.

When considering the influence of temperature to the hydro power inflow, [44] claims that increased temperature leads to higher hydro inflow, while [45] states the opposite. The influence of temperature is therefore neglected in this thesis.

LOAD

The annual load of Europe from 1990 experienced a process of increasing, and has been slightly fluctuating since 2008 [46]. In scenario 2030 predicted by TYNDP 2016 [11], there are two Visions (Vision 1 and 4) with load higher than scenario 2020, and two Visions with load lower than scenario 2020, which indicated that there is not an obvious trend of whether the load will increase or decrease.

Therefore, in the simulations of this thesis, besides considering load difference given by 4 Visions, deviation of $\pm 5\%$ is considered according to the extreme deviation in [46] from 2008.

It should be noted that fluctuations in load are not necessarily due to weather change; development and electrification level of the country [47] may also play an important role. Nevertheless, the implications of load deviation to *Total cost* are worth studying, and are therefore included in this chapter.

CORRELATION AMONG DIFFERENT WEATHER AND LOAD PARAMETERS

With in a year, the correlation among variations of different parameters are inherently presented in the time profiles. For example, in winter, wind speed is usually higher (compared to the annual mean value), while solar radiation is usually lower; at the same time, the load is usually higher partly due to use of heat at lower temperature.

However, when considering multi-year trend, no aforementioned parameters are considered correlated within this thesis. There are mainly three reasons.

- Weak correlation, e.g. correlation between wind and solar power inflow [48];
- Minor influence, e.g. the multi-year temperature change in PV output as mentioned earlier in this section;
- Unclear influence, e.g. influence of temperature change in hydro inflow.

4.2.2. REALIZATION OF EXTREME CONDITIONS IN SIMULATIONS

In order to create extreme conditions in power system simulations in PowerGAMA, it can be directly realized by scaling inflow factor of the specific type of generator. For example, in order to simulate the situation when solar radiation increases by 10%, it is realized by multiplying inflow factor of solar generators by 1.1. The same method is used for simulating extreme hydro and load changes.

Since that the wind condition is of special interest in this thesis (HVDC grid is designed with offshore wind farms), the system's sensitivity to short-term randomness is also tested by using re-synthesized wind inflow time series (with same statistical features as reference profiles, e.g. seasonal and daily variation characteristics). The time

series is re-synthesized by Non-Homogeneous Markov Chain algorithm. The algorithm can be applied in an Excel file, which will be elaborated in section 4.3.

For extreme cases in wind, solar and load conditions, the changes in power inflow/load are considered the same for all countries in the model, for no long-term predictions in RES generation/load with higher geographic resolution are found. However, for extreme conditions in hydro power, only changes in Norwegian and Swedish area are considered, for the reason claimed in sub-section 4.2.1.

4.3. GENERATION OF PROBABILISTIC WIND POWER INFLOW TIME PROFILES: NON-HOMOGENEOUS MARKOV CHAIN ALGORITHM

4.3.1. INTRODUCTION

As is mentioned in chapter 2 and chapter 3, time profiles (time series) of variable generation and load, with length of whole year and resolution of one hour, are imported in PowerGAMA and PowerGIM for power system simulations.

The format of such time series, as is shown in figure 2.6, is a column (for each time series) with a length of 8761 rows, while the first row is the title and the rest 8760 rows are the profiles. The time profiles are in unit of [p.u.], relative to the annual average generation/load. Therefore, the average value of the total length of the time profiles is 1, for each column.

Considering short-term uncertainty of wind power inflow, new time series is needed (while there is only one-year historical data available, as mentioned in 4.1). Series generated by Non-Homogeneous Markov Chain algorithm is expected to provide randomness in short-term values without hurting statistical characteristics (e.g. probability distribution, yearly and daily variation characteristics) of the reference time series.

In sub-section 4.3.2, the variation characteristics of wind power inflow time series are analyzed; in sub-section 4.3.3, the details to use NHMC algorithm to generate wind power inflow time profiles, and how the algorithm is applied by using widely available software (i.e. in this thesis, Microsoft Office Excel), are introduced. The developed Excel file can, given a reference profile (taken from historical data or already validated model), generate a full-length new profile fully automatically. The procedure to adjust the algorithm for this project and the Excel file are developed by the author of this thesis.

4.3.2. WIND POWER INFLOW TIME PROFILE VARIATION FEATURES

Within this sub-section, the time variation characteristics of variable generation and demand are analyzed.

Figure 4.2 A shows the normalized wind power inflow in France for one year (i.e. 8760 hours). Wind generation is clearly lower in summer than in winter, which indicates the seasonal variation of wind generation.

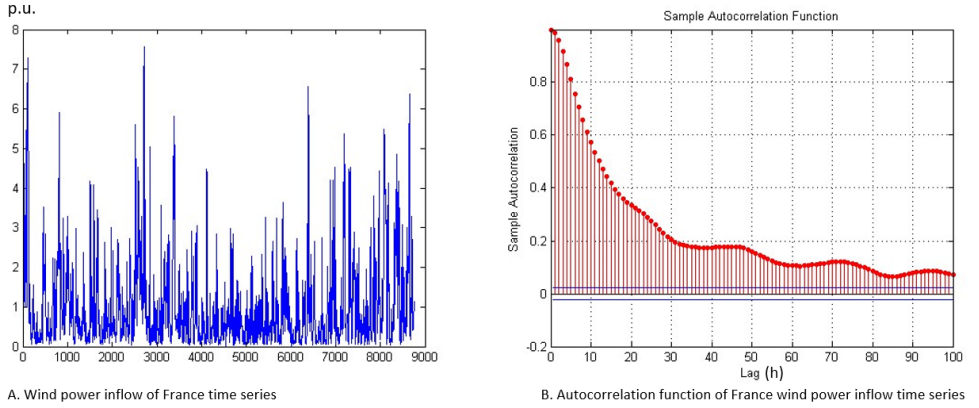


Figure 4.2: France wind power inflow time series and its autocorrelation function

Figure 4.2 B is the result of autocorrelation analysis of the time series in 4.2 A.

Autocorrelation function measures the correlation between y_t and y_{t+k} , where $k = 0, \dots, K$.

The formula for the autocorrelation for lag k is [49]:

$$r_k = \frac{c_k}{c_0} \quad (4.1)$$

$$c_k = \frac{1}{(T-1)} \sum_{t=1}^{T-k} (y_t - \bar{y})(y_{t+k} - \bar{y}) \quad (4.2)$$

where c_0 is the sample variance of the time series.

Bulges can be recognized when lag = 24, 48, 72, 96h, which indicates daily (period = 24h) variation.

4.3.3. ALGORITHM TO GENERATE VARIABLE WIND INFLOW TIME SERIES

After analyzing the variation characteristics of time profiles, an algorithm to generate such profiles is to be chosen.

The accuracy test of time series generated and synthesized by widely used algorithms was performed in [15], of which the results are shown in figure 4.3 and figure 4.4.

"NHMC", "FOMC", "SOMC" and "ARMA" refer to Non-Homogeneous Markov Chain, First-Order Markov Chain, Second-Order Markov Chain and Autoregressive Moving Average algorithm, respectively.

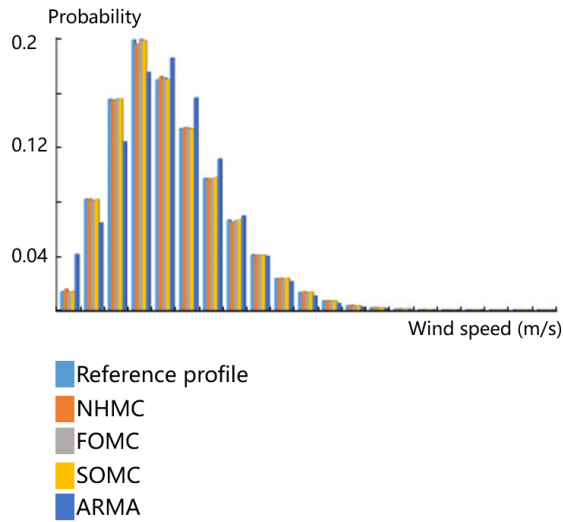


Figure 4.3: Probability distribution of different wind speed models [15]

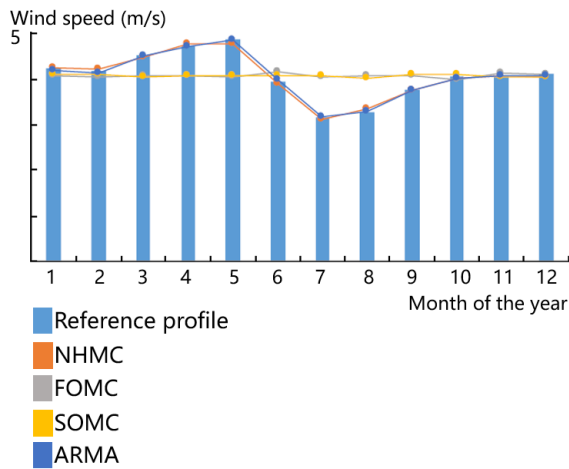


Figure 4.4: Monthly-average wind speed synthesized by different wind speed models [15]

From the accuracy results shown in figure 4.3 and figure 4.4, the conclusions in the table 4.2 regarding the comparison of algorithms can be attained [15].

<p>Autoregressive Moving Average (ARMA)</p> <p>× Significant error in probability distribution when the data is not in normal distribution</p> <p>Reliable autocorrelation performance</p>
<p>Markov Chain (1st/2nd Order)</p> <p>Reliable probability distribution performance</p> <p>× Time-homogeneous and only short-term autocorrelation</p>
<p>Non-Homogeneous Markov Chain</p> <p>Reliable probability distribution performance</p> <p>Reliable long-term (daily to seasonal) autocorrelation</p>

Table 4.2: Comparison of widely used algorithm of generating wind time series ("×" for disadvantage)

With reliable performance regarding both probability distribution and autocorrelation, the Non-Homogeneous Markov Chain algorithm is therefore chosen for the research of this thesis project.

Within this subsection, both algorithm and its realization in Excel are introduced.

The flow chart of the algorithm is shown in figure 4.5. Detailed explanation of content in each block is in the following sub-subsections.

Probabilistic Profile: Non-Homogeneous Markov Chain

Modelling and synthesis algorithm of variable generation time profiles

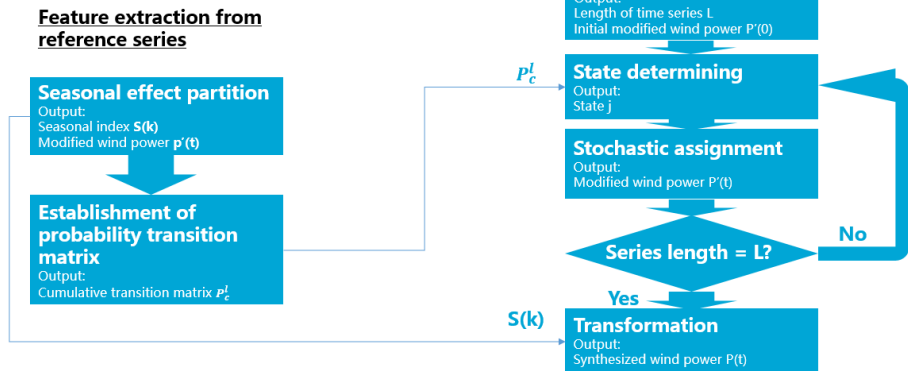


Figure 4.5: Flow chart of using NHMC algorithm to generate variable RES power inflow time series

SEASONAL EFFECT PARTITION

Firstly, the wind power inflow time series is partitioned into several segments;
Then, the seasonal index $S(k)$ of each segment is calculated following the equation:

$$S(k) = \frac{\bar{p}_k}{\bar{p}} \tag{4.3}$$

At last, the original time series is modified as:

$$p'(t) = \frac{p(t)}{S(k_t)} \tag{4.4}$$

\bar{p}_k and \bar{p} are the mean values of the k th segment and the whole year, respectively;
 $p(t)$ and $p'(t)$ are the actual and the modified wind power output at time t , respectively;
 k_t is the segment number corresponding to time instant t .

Within this thesis, the seasonal index is taken monthly (assuming each month is of same length). Therefore there are 12 indexes extracted from 12 equally long partitioned segments (each of length $8760/12 = 730$). This leads to enough precision to reflect seasonal variation characteristics of the wind time series (the output is tested in figure 4.7).

In Microsoft Office Excel, the extraction of seasonal index can be easily done by using "AVERAGE" function to calculate the average value of each of the 730-row segments. As the unit of the profile used in this thesis is [p.u.], each monthly average value equals the seasonal index.

ESTABLISHMENT OF PROBABILITY TRANSITION MATRIX

At first, the time-related variable $l = 0, 1, \dots, R-1$ is defined;

Then, the time set,

$$T_l = \{t | \text{mod}(t, R) = l\} \tag{4.5}$$

the transition probability,

$$p_{ij}^l = \frac{f_{ij}^l}{\sum_{t \in T_l} f_{ij}^l} \tag{4.6}$$

and the matrix,

$$P^l = (p_{ij}^l) = \begin{pmatrix} p_{11}^l & p_{12}^l & \dots \\ p_{21}^l & p_{22}^l & \dots \\ \vdots & \vdots & \ddots \end{pmatrix} \tag{4.7}$$

are calculated;

At last, the cumulative transition matrix is obtained by

$$P_c^l = p_{c,ij}^l = \sum_{k=1}^j p_{ik}^l \tag{4.8}$$

It can be seen in equation 4.8 that for each value of l (total number = R), a separate transition matrix is built.

In [15], it is recommended to use $R = 24$ to reflect the period of daily variation: 24 hours. However, in real application of this algorithm within this thesis, it is found that if the reference profile is divided into 24 segments, there would be too few elements (i.e. sample capacity) for building each matrix. If so, in (especially corners of) each matrix, the values may not reflect useful statistical probability.

Therefore, instead of using $R = 24$, the research in this thesis uses $R = 8$. In order to still keep the variation period of 24 hours, in the Excel, the “ROUNDDOWN” function is used. In a new column, column “new_l”, every old l value (when $R = 24$) is divided by 3 and rounded down to the nearest integer (table 4.3).

old_l (recommended in [15])	new_l (applied in this thesis)
1	0
2	0
3	1
4	1
5	1
6	2
7	2
...	...

Table 4.3: Old and new column of l value

In each day, the three profiles of same l value share the same transition matrix. Therefore, the sample size in $R = 8$ situation for each matrix is three times larger than in the old $R = 24$ situation, which is now sufficient; meanwhile, the matrix keeps reflecting daily variation.

As a result, the number of transition matrices is 8.

Another important issue is about the division of states. The rule should be to divide the reference profile in a way that the range of each state is not too large so the precision is remained, and not too small so there is still sufficient sample size for each state.

The number of profiles fall in a given value range can be counted by using “COUNTIF” function in Excel. Following the rule mentioned in the last paragraph (it should be noted that the range of each state does not have to be the same), the wind power generation profile is divided into states listed in table 4.4 (11 states in total).

In the research of this thesis, each of the state transition matrix occupies one sheet. In order to achieve fully automatic filling of each matrix, the steps below are followed (taking the matrix for $l = 5$ for example):

state range	state number
[0, 0.1]	0
(0.1, 0.2]	1
(0.2, 0.4]	2
(0.4, 0.7]	3
(0.7, 1]	4
(1, 1.3]	5
(1.3, 1.6]	6
(1.6, 2]	7
(2, 3]	8
(3, 4]	9
(4, 7]	10

Table 4.4: Range of states of wind power inflow series

(1) The modified wind power inflow time series is assumed to be saved in the first sheet. In a new column, for example, column I, using “LOOKUP” function to output the state of row in the modified series. The length of this column is also 8761 (1 row for title and 8760 rows for content). Then, in column J next to column I, output the next state of each of the state in the same row in column I. For example, the equation to be filled in cell J2 is “=I3”.

(2) In a new sheet, for example, sheet 5 (where the transition matrix for $l = 5$ is saved), “IF” function is used to copy the states in column I and column J in the first sheet, outputting the states if the value in column “new_l” is 5, otherwise outputting “skip”. The first two columns of this sheet 5 are therefore occupied, as column “state” and column “state_next”.

(3) The content of the first two columns, i.e. column A “state” and column B “state_next”, is merged to the third column, namely column “merge”, by filling in, for example, in cell C2, “=A2” ”B2”. As a result, the content in each cell of column C “merge” is either state transition (pair of states at current and next time step) for profiles of $l = 5$ (representing 14:00 to 17:00 of each day), or “skip skip” for profiles that are of other l values.

(4) A new matrix is built, using “COUNTIF” function in each corresponding cell to calculate the times each state transition occurs in column C “merge”.

(5) A new matrix is built, calculating the cumulative probability as described in equation 4.8.

The steps aforementioned can be performed by calling the output of the previous step, therefore it can be fully-automatic in Excel.

INITIALIZATION

The length of time series to be synthesized is determined; a modified wind power output at initial time, $P'(o)$, is generated.

Within this thesis, the series length is chosen as 8760, i.e. one year with hourly resolution. The value of reference series at time = 1h, is taken also as the initial value of the simulated time profile.

STATE DETERMINING

Firstly, the row in P_c^l related to current time step is found, assuming row i ;

Secondly, a uniformly distributed variable $r \in (0, 1)$ is generated and compared in turns to the cumulative probabilities in row i ;

Thirdly, if the value of r is between the j th and $j + 1$ th cumulative probability, the wind power state at next time step is assigned as state j .

The determining can be realized by either "LOOKUP" function or, as is used in this thesis, by nesting "IF" functions. It should be noted that for different time steps with different value at column "new_1", the transition matrix to be called is different.

The needed uniformly distributed variable is generated by "RAND" function in Excel.

STOCHASTIC ASSIGNMENT

A new uniformly distributed variable, $r' \in (0, 1)$, is generated;

Then, the modified wind power output at next time step is calculated:

$$P'(t) = P_{lj} + r'(P_{uj} - P_{lj}) \quad (4.9)$$

The P_{uj} and P_{lj} are the upper and lower bound of probability at stage j , respectively.

The same as for r , r' is also generated by "RAND" function in Excel.

TRANSFORMATION

Following the reversed process of the first stage, the modified series $P'(t)$ is multiplied with the seasonal index for the synthesized $P(t)$.

$$P(t) = P'(t)S(k_t) \quad (4.10)$$

An additional step is added by the author of this thesis to avoid deviations from needed average value: every cell (row) of $P(t)$ needs to be divided by \bar{P} , the average value of $P(t)$, so that the annual average value remains 1 (please recall that the time profiles are in unit of [p.u.] relative to the annual average value).

When the profiles of extreme condition, e.g. wind speed -25% (which leads to wind power inflow drop by 59.514%) are needed, the final output can be acquired by multiplying the output $P(t)$ with a scaling factor of $1 - 59.514\% = 40.486\%$.

OUTPUT

Figure 4.6 A shows the synthesized wind power inflow time series for France. Figure 4.6 B is the result of autocorrelation analysis of the time series in figure 4.6 A. Compared to profiles in figure 4.2, same yearly and daily variation characteristics can be recognized.

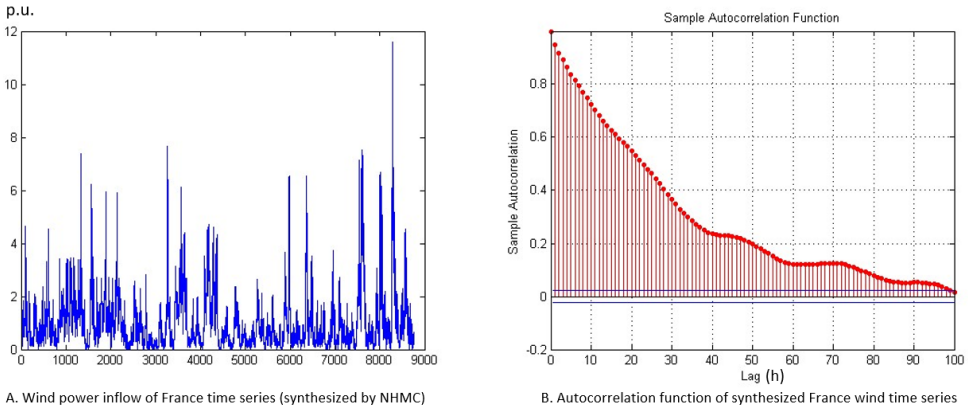


Figure 4.6: Synthesized (by NHMC) France wind power inflow time series and its autocorrelation function

Figure 4.7 shows the accuracy tests (following [15]) done for the synthesized series. Series re-generated by NHMC shows acceptable similarity to the original series, compared to series generated by other methods in figure 4.3 and figure 4.4.

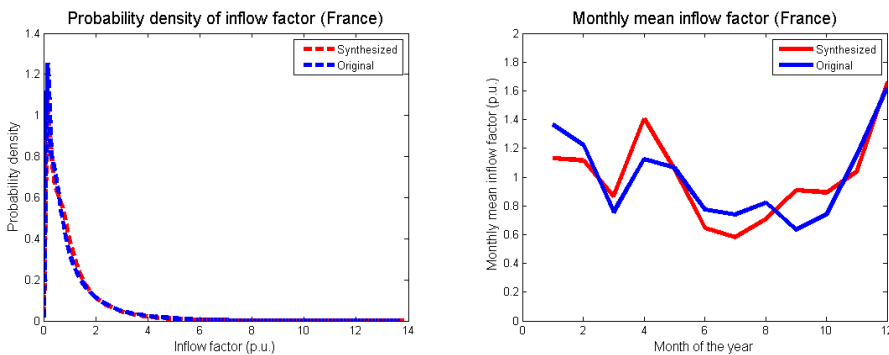


Figure 4.7: Accuracy tests for synthesized series compared to original (France)

4.3.4. CONCLUSION

Within this section, firstly, the time variation characteristics of wind power inflow time profiles are analyzed. They are recognized with seasonal (yearly) and daily variation.

Then, after comparison of widely used algorithms, the Non-Homogeneous Markov Chain is chosen for the research of this thesis because of the reliable performance in both probability distribution and autocorrelation of the time profiles generated by it.

After that, the detailed methodology to generate variable generation time series is introduced. Adjustments are taken to develop a methodology suitable for the research of this thesis. An Excel file to automatically generate new wind power inflow time profiles is also developed and described.

4.4. RESULT ANALYSIS OF SIMULATIONS UNDER EXTREME RES INFLOW AND LOAD CONDITIONS

4.4.1. INTRODUCTION

Within this section, the socio-economic benefit of 4 topologies (3 proposed design of HVDC grid in the North Sea and the baseline) under extreme RES generation inflow and load conditions would be compared.

Hereby a recap of the comparing standard among the topologies is given. The indicator for comparison is the total cost of each design, calculated as in equation 4.11.

$$Total\ Cost = CAPEX + OPEX_{lifetime} \quad (4.11)$$

Please bear in mind that the CAPEX is the investment cost of the designed HVDC transmission network in the North Sea, and OPEX is the operational cost of the six countries surrounding the North Sea (i.e. BE, DE, DK, GB, NL and NO) for 30 years from 2030. Details of calculating CAPEX and OPEX can be found in chapter 3.

The topologies and their CAPEX are as listed in figure 4.8.

In the sub-sections for the rest of this section, total cost under "normal" condition will also be given, as a reference. The term "normal" refers to the simulation results with profiles used in chapter 2 and chapter 3, without scaling or re-generation.

4.4.2. RESULT ANALYSIS OF SIMULATIONS UNDER EXTREME WIND CONDITIONS

UNDER EXTREME WIND CONDITIONS W.R.T ANNUAL MEAN WIND POWER INFLOW

The extreme wind conditions (w.r.t annual mean value) to be studied in this sub-section are listed in table 4.5.

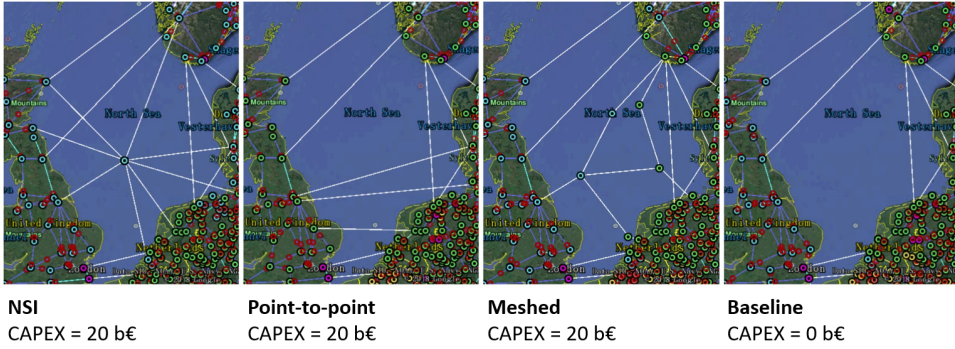


Figure 4.8: Topologies to be studied and their correspondent CAPEX

Change in wind speed	-25%	+25%
Change in wind power inflow	-59.514%	+92.308%

Table 4.5: Simulated extreme wind conditions (annual mean value)

The simulation result of system total cost under the conditions of annual mean wind speed -25%, normal situation and +25% are shown in figure 4.9, figure 4.10 and figure 4.11, respectively.

Variable RES generators (wind, solar and hydro power) are of much lower fuel cost (0.5 €/MWh) compared to conventional generators (e.g. fuel cost of gas generators are 83.3 €/MWh). What’s more, no CO2 emission is considered for RES generation. These lead to the situation that generally, the higher RES penetration in the power system, the lower the system OPEX.

Under the condition of wind speed -25%, the wind power inflow drops almost 60%. Although the three proposed HVDC topologies still lead to lower OPEX for the 6 countries compared to baseline, their influence in helping integrate variable RES becomes so weak that when CAPEX is added, they can not be paid back within lifetime of 30 years (except for NSI in Vision 3). Nevertheless, NSI still brings lower overall cost in all Visions compared to the two competitors (point-to-point and meshed).

Under the condition of wind speed +25%, the system with proposed HVDC topologies presented great benefit compared to the baseline. NSI ranks first in all Visions, followed by meshed topology; their performances not only thank to the optimized HVDC topology, but also to the higher wind speed at the Dogger Bank (where there is a node for both NSI and meshed topology).

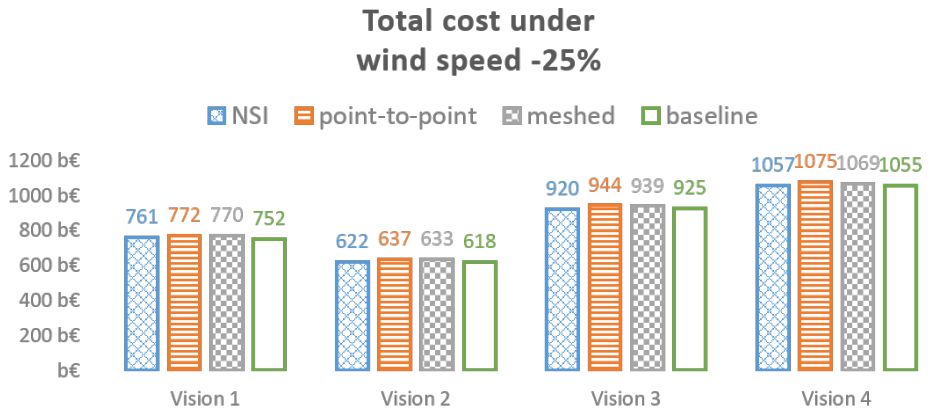


Figure 4.9: Total cost of the system under annual mean wind speed -25% in 4 Visions

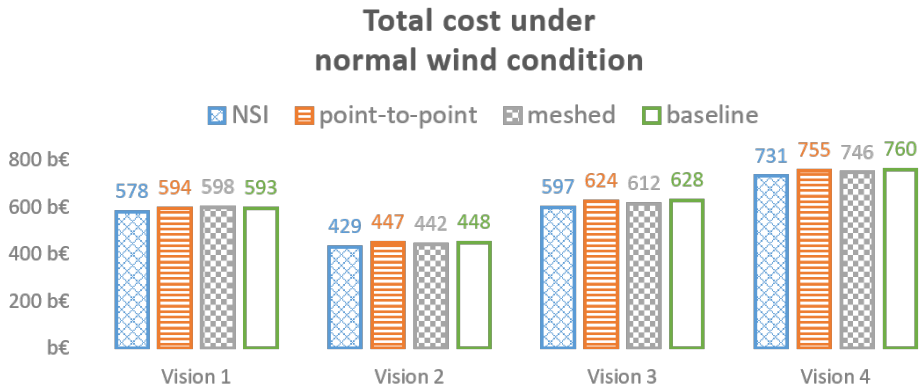


Figure 4.10: Total cost of the system under normal wind condition in 4 Visions

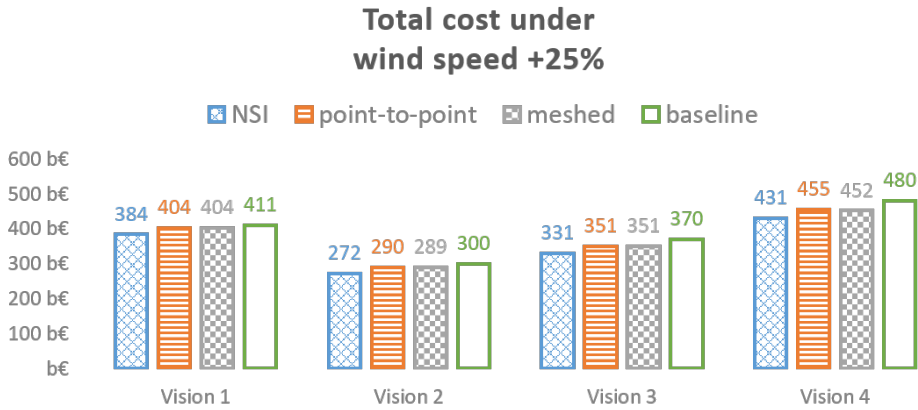


Figure 4.11: Total cost of the system under annual mean wind speed +25% in 4 Visions

SENSITIVITY TEST W.R.T SHORT-TERM RANDOMNESS

When importing re-synthesized time series (with same statistical features as reference time series, including annual mean value, yearly and daily variation characteristics) in simulations for Vision 2 and Vision 4, the results in total cost save of 3 optimized HVDC grid topologies (compared to the total cost of baseline) are shown in table 4.6 and table 4.7, respectively.

Total cost save	NSI	point-to-point	meshed
reference	19	1	6
new profiles 1	22	1	7
new profiles 2	21	2	8

Table 4.6: Total cost save of three topologies with re-synthesized new profiles in Vision 2 (billion €)

Total cost save	NSI	point-to-point	meshed
reference	29	5	14
new profiles 1	34	7	16
new profiles 2	32	7	17

Table 4.7: Total cost save of three topologies with re-synthesized new profiles in Vision 4 (billion €)

It can be seen that for different time series (reference and 2 sets of re-synthesized) with same statistical features, no significant differences in total cost save are recognized.

Comparison of the designs is therefore regarded as not sensitive to short-term randomness.

4.4.3. RESULT ANALYSIS OF SIMULATIONS UNDER EXTREME SOLAR CONDITIONS

The extreme solar conditions to be studied in this sub-section are annual mean solar radiation (as well as solar power inflow) $\pm 10\%$ (for all countries in the model), as is explained in section 4.2.1.

The simulated total system cost under the conditions of solar radiation -10% , normal situation and $+10\%$ in Vision 2 and Vision 4 are shown in figure 4.12 and figure 4.13, respectively.

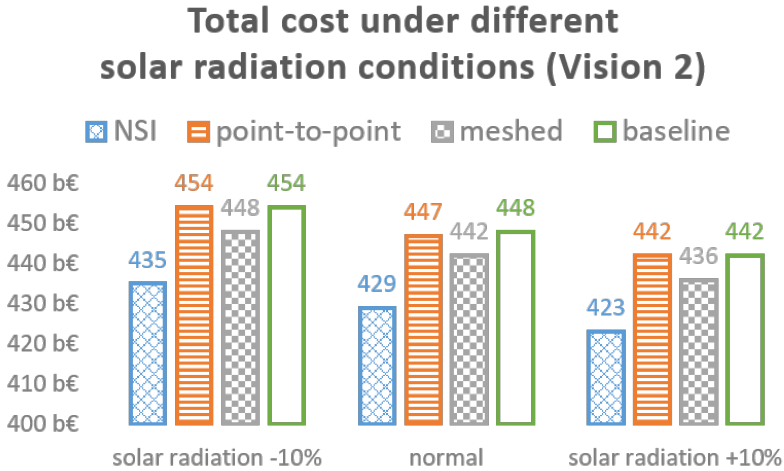


Figure 4.12: Total cost of the system under different solar conditions in Vision 2

If calculating the cost save of three proposed topologies compared to baseline, the results are as in table 4.8 for Vision 2 and table 4.9 for Vision 4.

Total cost save (b€)	NSI	point-to-point	meshed
solar radiation -10%	19	0	6
normal	19	1	6
solar radiation +10%	19	0	6

Table 4.8: Total cost save of the system under different solar conditions in Vision 2 (billion €)

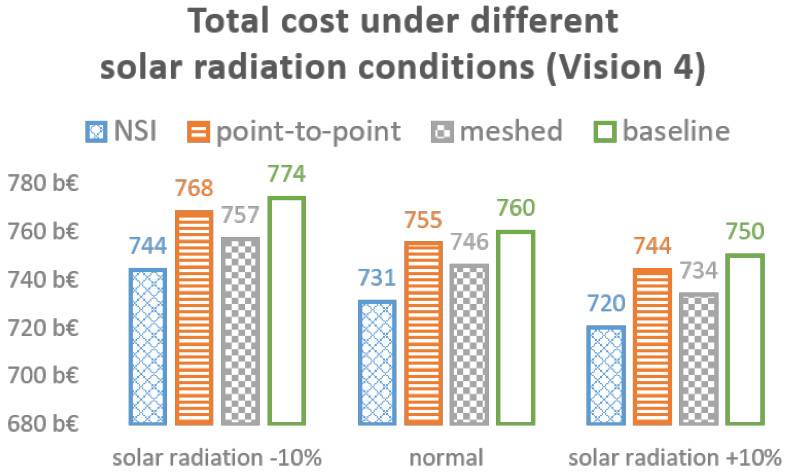


Figure 4.13: Total cost of the system under different solar conditions in Vision 4

Total cost save (b€)	NSI	point-to-point	meshed
solar radiation -10%	30	6	17
normal	29	5	14
solar radiation +10%	30	6	16

Table 4.9: Total cost save of the system under different solar conditions in Vision 4 (billion €)

It can be seen that there are no clear differences in total cost save under different solar conditions. The reasons are:

- The changes in power inflow are low (especially when compared with extreme wind conditions);
- The role of solar energy in the energy mix of the six countries is minor. According to the energy mix result, under normal weather conditions, the wind energy is three times of solar energy in the six countries;
- Unlike offshore wind generators, solar PV generators are installed nearer to the load center. Therefore, the dependency of HVDC interconnectors to help integrated variable solar energy is lower compared to wind energy.

4.4.4. RESULT ANALYSIS OF SIMULATIONS UNDER EXTREME NO AND SE HYDRO INFLOW CONDITIONS

The extreme hydro inflow conditions to be studied in this sub-section are hydro power inflow $\pm 25\%$ (for Norway and Sweden), as explained in section 4.2.1.

The simulated total system cost under the conditions of hydro inflow -25% , normal situation and $+25\%$ in Vision 2 and Vision 4 are shown in figure 4.14 and figure 4.15, respectively.

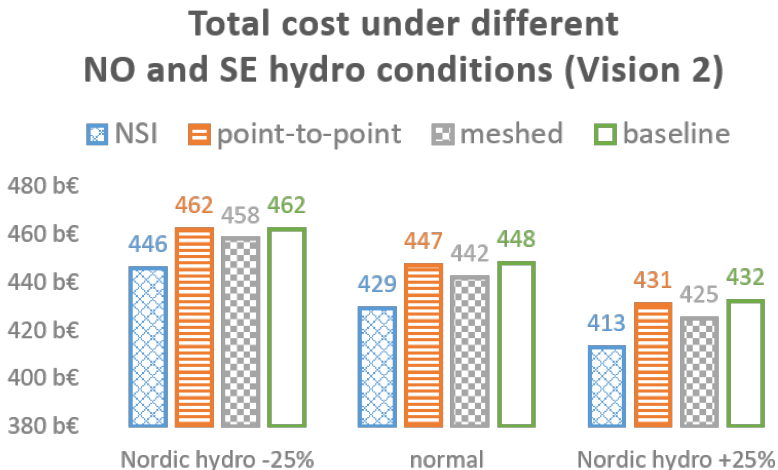


Figure 4.14: Total cost of the system under different NO and SE hydro inflow conditions in Vision 2

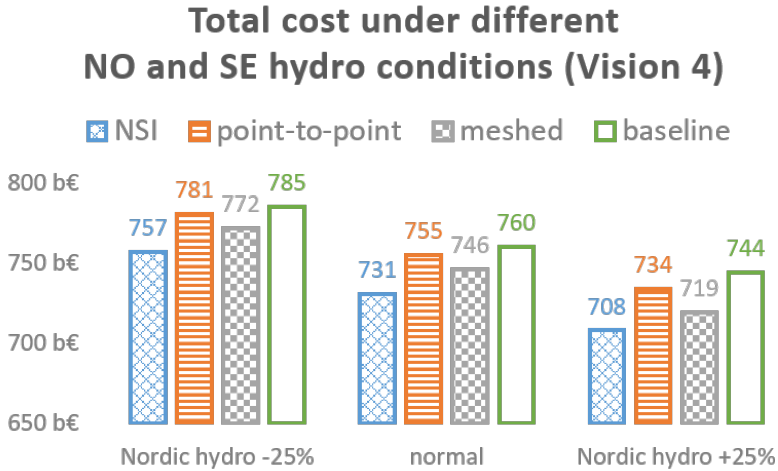


Figure 4.15: Total cost of the system under different NO and SE hydro inflow conditions in Vision 4

If calculating the cost save of three proposed topologies compared to baseline, the results are as in table 4.10 for Vision 2 and table 4.11 for Vision 4.

Total cost save (b€)	NSI	point-to-point	meshed
hydro inflow -25%	16	0	4
normal	19	1	6
hydro inflow +25%	19	1	7

Table 4.10: Total system cost save under different NO and SE hydro inflow conditions in Vision 2 (billion €)

The three proposed HVDC topologies keep advantage in total cost compared to baseline, while NSI ranks first among all topologies again.

It can be seen that as hydro inflow increase, the cost save of proposed HVDC grid increases too. Higher hydro inflow help reduce OPEX of the 6 countries by:

- generating hydro power (of low fuel cost);
- feeding reservoirs which provide flexibility to help integrate variable RES.

Results (between proposed HVDC grid and baseline) show that HVDC interconnectors are needed to deliver such functions from Nordic countries to other areas.

Total cost save (b€)	NSI	point-to-point	meshed
hydro inflow -25%	28	4	13
normal	29	5	14
hydro inflow +25%	36	10	25

Table 4.11: Total system cost save under different NO and SE hydro inflow conditions in Vision 4 (billion €)

4.4.5. RESULT ANALYSIS OF SIMULATIONS OF EXTREME LOAD DEVIATIONS

The extreme load deviations to be studied in this sub-section are load $\pm 5\%$ (for all countries in the model), as is explained in section 4.2.1.

The simulation result of total cost of the system with load +5%, normal load and load -5% in Vision 2 and Vision 4 are shown in figure 4.16 and figure 4.17, respectively.

Total cost with different load (Vision 2)

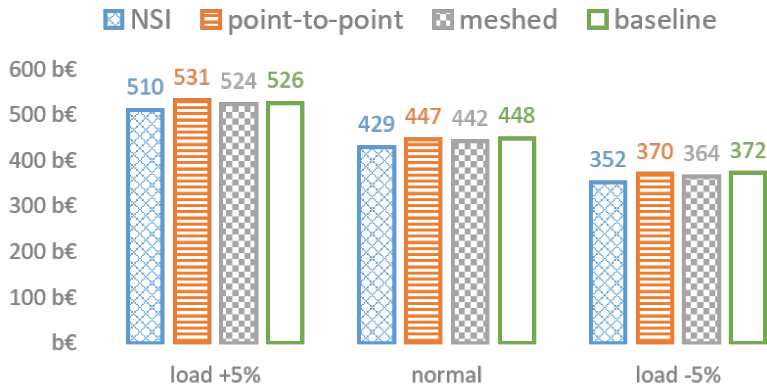


Figure 4.16: Total cost of the system with different load in Vision 2

If calculating the cost save of three proposed topologies compared to baseline, the results are as in table 4.12 for Vision 2 and table 4.13 for Vision 4.

Total cost save (b€)	NSI	point-to-point	meshed
load +5%	16	-5	2
normal	19	1	6
load -5%	20	2	8

Table 4.12: Total cost save of the system with different load in Vision 2 (billion €)

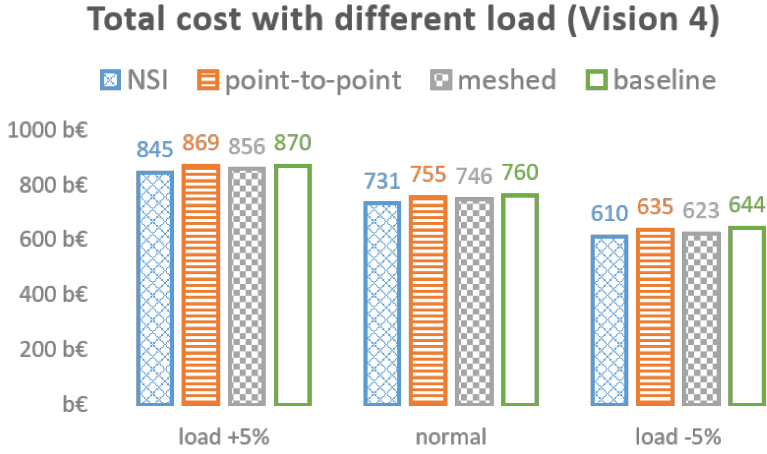


Figure 4.17: Total cost of the system with different load in Vision 4

Total cost save	NSI	point-to-point	meshed
load +5%	25	1	14
normal	29	5	14
load -5%	34	9	21

Table 4.13: Total cost save of the system with different load in Vision 4 (billion €)

NSI, in extreme load conditions, still leads to lowest overall costs.

It can also be seen that with lower load, the role of HVDC network to help integrate variable RES becomes more significant.

4.5. CONCLUSION

In answer to the third research question, extreme deviations in RES inflow and load are considered in simulations. Wind speed $\pm 25\%$, solar radiation $\pm 10\%$, Nordic hydro inflow $\pm 25\%$ and load $\pm 5\%$ are recognized as possible extreme cases during the lifetime of the designed HVDC grid.

All 4 Visions are simulated for extreme wind conditions (deviations w.r.t annual mean wind speed), while only Vision 2 and Vision 4 are simulated for other extreme cases; besides, the system's sensitivity to short-term randomness in wind power inflow is also tested (in Vision 2 and Vision 4).

It can be concluded that the proposed NSI design with the North Sea Wind Power Hub at the Dogger Bank not only leads to lower overall cost for the six surrounding countries under normal conditions (i.e. conclusion of chapter 3), but also shows robustness in keeping its advantage under extreme wind, solar, hydro conditions and load deviations, compared to point-to-point and meshed (without central hub) topology.

However, under wind speed - 25% condition (and if the conditions lasts for 30 years), it is possible that the investment of NSI cannot be paid back within lifetime.

5

OTHER DETAILS IN OPERATION SIMULATION

In chapter 3 and chapter 4, the socio-economic advantage in of NSI is validated. Compared to other topologies of the North Sea HVDC grid (with same budget of 20 billion Euros), no matter meshed or point-to-point topology, the North Sea Infrastructure with the North Sea Wind Power Hub at Dogger Bank has lower overall cost throughout its lifetime, in all simulated Visions and under extreme RES inflow and load conditions.

However, besides the cost, other performance indicators (e.g. nodal price and EENS) of the proposed NSI design are also of interest. In partial response of the research objective, research in this stage is performed.

5.1. ADVANTAGES OF NSI

It is necessary to review the expected functions of the proposed NSI design before verification. The three functions are:

- (1) Transmission of renewable energy (which improves energy sustainability)
- (2) Price convergence (which improves energy affordability)
- (3) Security of supply (which improves energy security)

In fact, the result of chapter 3 and chapter 4, in which the proposed NSI design is of lowest overall cost, already provided an intuitive expectation that the NSI can realized the three functions. The more renewable energy it transmits (while fuel cost of renewable energy is much lower than fossil fuel), the more coordination the NSI provides

(which leads to price convergence), and the better security of supply (which avoids high charge of load shedding), the lower OPEX (and total cost, given same CAPEX) is expected.

However, after all, the lower OPEX is not a sufficient condition of each of the three expected functions. Also, it is unclear if all three functions play roles in lowering the OPEX. Therefore, each of the expected functions needs to be verified separately and quantitatively.

TRANSMISSION OF RENEWABLE ENERGY

Comparisons between NSI and baseline are shown in table 5.1 and table 5.2.

generation (TWh)	Vision 1	Vision 2	Vision 3	Vision 4
NSI	65	56	59	57
baseline	50	47	46	45

Table 5.1: Annual generation of 15000 MW offshore wind farm installed in NSI and baseline (TWh)

spillage (TWh)	Vision 1	Vision 2	Vision 3	Vision 4
NSI	15	31	46	49
baseline	19	39	55	58

Table 5.2: Annual renewable energy spillage of the 6 countries (TWh)

As is mentioned in chapter 2 and 3, the wind farms of 15000 MW are installed in both NSI (around the NSWPH at the Dogger Bank) and baseline (at each of the 6 countries) situation.

It can be seen that, compared to the baseline, when NSI is installed, the 15000 MW wind farms can generate more energy, while the 6 countries surrounding the North Sea suffered from less renewable energy spillage. Providing more generation while leading to less waste, NSI's ability to transmit renewable energy is therefore verified.

PRICE CONVERGENCE

Considering the comparison between NSI and baseline, NSI presented satisfactory price convergence performance. There are two main features:

Convergent prices: Compared to baseline, when NSI is launched, the differences of prices between different countries become lower.

Lower overall price: On the whole (considering all 6 surrounding countries), the price becomes lower. The value is 62.492€ with NSI and 62.798€ in baseline situation.

The two features could be recognized in all 4 Visions of 2030. Taking Vision 2 as an example, The difference in annual average nodal price by area is presented in figure 5.1.

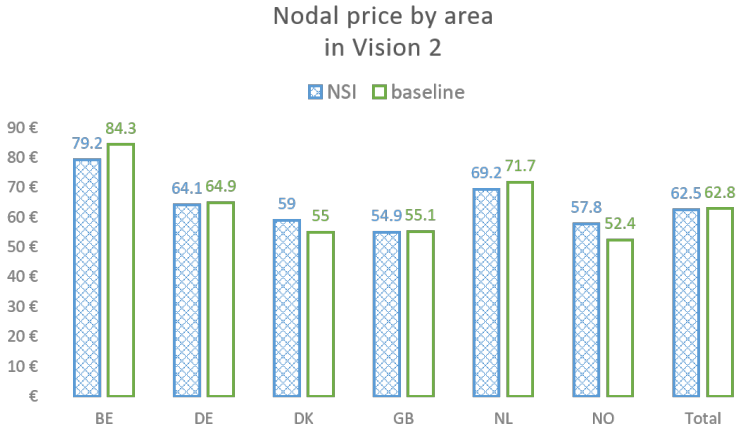


Figure 5.1: Comparison of annual average nodal price by area between NSI and baseline(Vision 2)

SECURITY OF SUPPLY

Calculating EENS (Expected energy not supplied) of 30 years, for NSI and baseline case, the comparison is as in table 5.3.

EENS (TWh)	NSI	baseline
Vision 1	17.3	39.0
Vision 2	14.4	29.6
Vision 3	16.1	29.4
Vision 4	18.2	28.2

Table 5.3: Comparison of installing NSI and baseline in EENS of 30 years from 2030 (TWh)

Although the absolute value of EENS in TWh might not be reliable (due to aggregation and approximation of the software), the relative comparison between NSI and baseline design can show clearly that NSI strongly improves the system security of supply.

5.2. CHALLENGES BROUGHT BY NSI

CONGESTION

Congestion is often recognized when the system is integrating large-scale variable RES (figure 5.2 A).

Grid reinforcement and demand-side response are regarded as possible solutions of grid congestion. As is shown in figure 5.2 B, when implementing flexible load (specif-

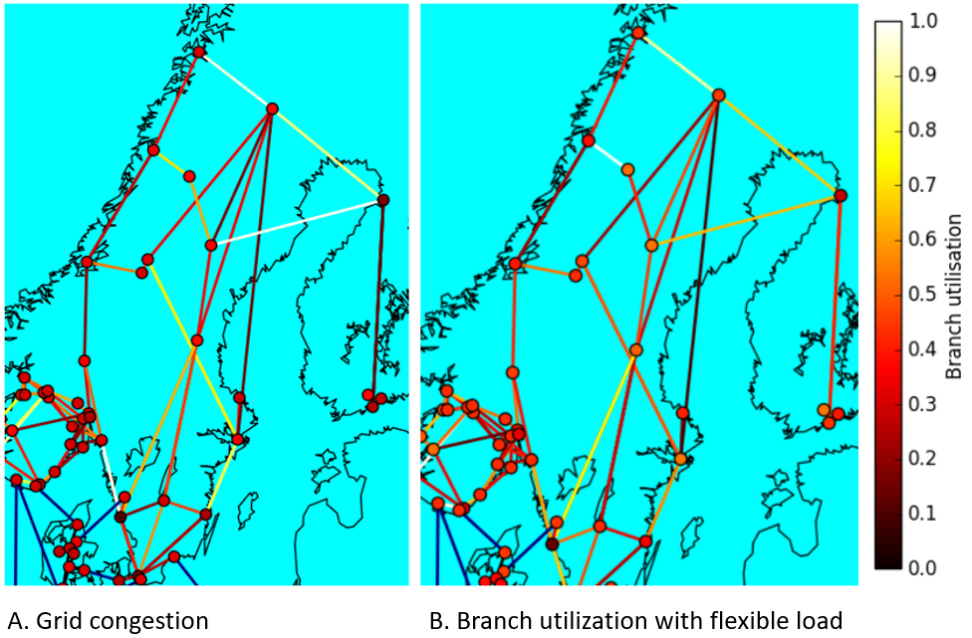


Figure 5.2: Branch utilization before and after application of flexible load

ically, it is set within this thesis that 10% demand is flexible and 20% of the total time flexible demand can be used) in Nordic power system, the grid congestion is relieved.

ASYMMETRY

It is easy to imagine that the interconnection can lead to asymmetry of benefit.

From table 5.4, when installing NSI, although the overall nodal price is lower, for specific countries, such as DK and NO, the nodal price becomes higher.

Table 5.5 shows clearly the direction and value of annual average power flow in all NSI HVDC branches. It can be seen that the flow from NO to the Dogger Bank is higher than the flow in the opposite direction. Please note that in this table, the values in "total" column are rounded to the nearest integer based on their original values, which will lead to deviation up to 1 from the direct sum of rounded values in columns "positive" and "negative".

The solutions for the asymmetry, for instance, a scientific side payment mechanism, need to be developed to better incentivize the investment from all the surrounding countries.

Nodal price (€)	NSI	baseline
BE	79.2	84.3
DE	64.1	64.9
DK	59.0	55.0
GB	54.9	55.1
NL	69.2	71.7
NO	57.8	52.4
Total	62.5	62.8

Table 5.4: Nodal price comparison of installing NSI and baseline, Vision 2 (€)

from	to	capacity (MW)	positive (MW)	negative (MW)	total (MW)
DB	NL	3000	2400	254	2654
DB	DE	3000	1585	1071	2656
DB	DK	1000	573	363	936
DB	NO	4000	1608	1645	3252
DB	GB-16	3000	2061	661	2722
DB	GB-7	2000	1037	760	1796
DB	BE	2000	1972	3.5	1976
DB	GB-2	1000	348	491	839

Table 5.5: Annual average power flow in NSI per branch, Vision 2 (MW)

5.3. CONCLUSION

In chapter 3 and chapter 4, the research focuses on the cost-benefit analysis of the HVDC grids. Nevertheless, other details in the operation simulation also reveal interesting implications of NSI.

15000 MW wind farms around the North Sea Wind Power Hub in NSI generated more energy than near shore wind farms (of the same capacity) in baseline; at the same time, NSI leads to lower renewable energy spillage in 6 countries; nodal prices in 6 countries become convergent and lower (as a whole) when NSI is installed; EENS becomes much lower with than without NSI.

It can be concluded that the three functions TenneT expects on NSI, i.e. transmission of renewable energy, price convergence and enhancement of system security can be realized.

It should also be noted that if NSI is installed, grid reinforcement and/or flexible load are needed to relieve the grid congestion and to release the potential of NSI; a scientific side payment mechanism is in need to boost the construction of NSI by incentivising investment from countries involved.

6

CONCLUSION

6.1. SUMMARIES OF CONCLUSIONS

6.1.1. CONCLUSIONS IN ANSWER TO THE RESEARCH QUESTIONS

At this last chapter of the thesis, the three research questions raised at the first chapter can be answered.

HOW TO DEFINE 3 TOPOLOGIES OF THE NORTH SEA HVDC NETWORK WITH DIFFERENT FEASIBLE STRUCTURES?

HVDC grid topologies with three different structures are put forward in this thesis.

The North Sea Infrastructure in a hub-and-spoke structure with the North Sea Wind Power Hub at the Dogger Bank, is proposed based on TenneT's vision [3].

The point-to-point topology is put forward based on Viking Link [10], which is comprised of only DC direct branches.

The meshed topology is defined based on the topology in [12], without a central energy hub.

As the common constraints, the three topologies are limited to a budget of 20 billion Euros and 15000 MW of installed offshore wind farms.

A baseline model is created as a background/environment for HVDC designs and as a reference to quantify the performance (especially in cost-benefit) of the designs.

WHAT ARE THE CRITERIA TO OPTIMIZE EACH TOPOLOGY AND TO COMPARE THE TOPOLOGIES?

The three topologies are optimized by using PowerGIM and PowerGAMA towards the objective of minimizing overall cost throughout lifetime (i.e. sum of CAPEX and OPEX of six surrounding countries, including CO₂ cost). The overall costs of three optimized topologies are compared to determine the most socio-economically preferable topology (with lowest overall cost).

In the considered 4 Visions from [11], the total cost of optimized NSI design stays at least 13 billion Euros lower than other designs. The possible cost of non-electric construction (e.g. earthwork) of the North Sea Wind Power Hub up to 4.5 billion Euros, which is much lower than 13 billion Euros, would not influence the preference of the topologies.

WHAT ARE THE IMPLICATIONS OF EACH TOPOLOGY, WHEN EVALUATED AGAINST A WIDE RANGE OF UNCERTAINTIES, ON THE OVERALL CAPEX AND OPEX OF COUNTRIES INVOLVED?

The aforementioned 4 Visions from [11], with different generation capacity, load and CO₂ price, are based on different predictions in green energy transition progress and European coordination level. These are some of the uncertainties considered in this thesis.

Besides, extreme deviations in annual mean value of RES inflow and load are considered in simulations. Wind speed $\pm 25\%$, solar radiation $\pm 10\%$, NO and SE hydro inflow $\pm 25\%$ and load $\pm 5\%$ are recognized as possible extreme cases within the lifetime of the designed HVDC grid.

Simulations are performed in all 4 Visions for extreme wind conditions, while only in Vision 2 and Vision 4 for other extreme cases; besides, the system's sensitivity to short-term randomness in wind power inflow is tested (in Vision 2 and Vision 4).

In all simulated cases, NSI leads to lowest total cost among the three HVDC designs.

However, under wind speed - 25% condition (and if the condition lasts for 30 years), it is possible that the investment of NSI cannot be paid back within lifetime.

6.1.2. CONCLUSIONS RELATED TO OTHER SIMULATION RESULTS

Advantages of the proposed NSI design (besides the lowest overall cost already mentioned in section 6.1.1) are recognized as:

- Transmission of renewable energy (by generating wind power with high wind speed, and by connecting surrounding countries to provide flexibility needed for integrating variable RES): Compared to baseline, the NSI can generate more energy (transmission from NSI to surrounding countries) while leading to less spillage (transmission between surrounding countries) in all 4 Visions.

- Security of supply: Compared to the baseline, the NSI can lead to lower EENS, in all 4 Visions.
- Price convergence: Compared to the baseline, the NSI can lead to convergent (and lower, on the whole) average area prices, in all 4 Visions.

Therefore, the proposed design is useful in enhancing energy sustainability, affordability and security.

Challenges brought by the proposed design are identified as:

- Grid congestion: NSI leads to increasing need in grid reinforcement or demand side flexibility to deal with the grid congestion.
- Benefit asymmetry: Although the overall welfare (lower overall system cost) is expected, there will be certain countries suffering from increase of operational cost and nodal price.

6.2. MAIN CONTRIBUTIONS OF THIS THESIS

Main contributions of this thesis include:

- Creation of baseline model/dataset for European power system 2030 as background/environment for the North Sea HVDC grid planning.
- Design and optimization of the North Sea HVDC grid topologies in three different feasible structures. The optimization methodology by using both PowerGIM and PowerGAMA can be useful for future research.
- Verification of NSI's advantage in cost saving, compared to two competitors, in 4 Visions reflecting different green energy transition and European coordination level, and under extreme RES inflow and load conditions.
- Verification of NSI's functions in improving energy sustainability, affordability and security; and revealing of challenges brought by NSI, such as grid congestion and benefit asymmetry.
- Realization of Non-Homogeneous Markov Chain algorithm in Excel to generate wind power inflow time series.

6.3. SUGGESTIONS FOR FUTURE RESEARCH

6.3.1. DEVELOPMENT OF FLEXIBILITY (ENERGY STORAGE DEVICES AND ANCILLARY SERVICES MARKET)

The flexibility of power system to deal with the uncertainty is crucial. It would be of even more significance in future power system with higher share of RES, most of which are variable and unpredictable.

The role of flexibility in helping integration of variable RES is already testified in some parts of this thesis project. For example, the hydro reservoir of Nordic power system, especially in Norway, is critical in coping with variability of far shore wind power generation in the North Sea. What's more, the demand side response, studied in section 5.2, is proved useful in dealing with grid bottlenecks and, therefore, in postponing investment in grid reinforcement.

Nevertheless, there could be more possibilities in flexibility, which, due to certain reasons, are less concerned or out of scope of this master thesis.

It is recommended that there should be more research in development of energy storage system and ancillary services market.

It is not easy to predict the scale of future development of energy storage in Europe. Breakthroughs in electrochemistry might lead to significant reduction in the cost of the devices and boost popularity of storage installation. Moreover, the involved countries' initiative can make a huge influence in the capacity of the storage, for example, there is a difference of 14.5 GW in predicting the hydropower generation capacity in Norwegian power system in 2030 between the data in Vision 4 of ENTSO-E's TYNDP [11] and in Statnett's "Long-Term Market Analysis-The Nordic Region and Europe 2016-2040" [50].

More specifically, the power-to-gas (hydrogen or synthetic methane) technology is of great interest within the North Sea region. The far shore wind farms can be connected to gas pipelines under the sea, and, for instance, provide fuel for onshore vehicles. However, both capacity and pricing are difficult to predict for long term scenario [51].

Another potential progress worth attention is of European ancillary services market. Ancillary services includes services such as frequency control, reserves, load following, reactive power and black start, which are "necessary to support the transmission of electric power from seller to purchaser given the obligations of control areas and transmitting utilities within those control areas to maintain reliable operations of the interconnected transmission system" [52].

As is mentioned in chapter 2, the softwares used in this thesis project, PowerGAMA and PowerGIM, do not consider market subtleties, therefore the ancillary services are out of scope of the performed simulations.

6.3.2. COMPLIANCE WITH FUTURE EXPANSION

Within the scope of this master thesis, the North Sea Infrastructure was considered as a once-for-all construction in the year of 2030, with the North Sea Wind Power Hub of 6 km^2 at the Dogger Bank, 15000 MW installed wind farm around the hub and 19000 MW HVDC between the hub and surrounding countries.

However, in the long term plan of NSI by TenneT, the construction would be continuing until around the year of 2050, with possible additional construction of 2 extra island and additional wind farms and interconnectors alongside them.

It should be noted that the optimized topology for the once-for-all situation might be different from the real life situation. For example, there might be need for redundancy in capacity of HVDC cables for future potential additions of wind farms; the situation with three energy islands in the ultimate plan by the year 2050 might be more complicated than merely replicate the one-island situation for three times.

Therefore, it is recommended that further research and design should consider compliance of possible future expansions when hoping to attain a more realistic design for the first phase – the one-island situation.

6.3.3. SOLUTION FOR BENEFIT ASYMMETRY AMONG INVOLVED COUNTRIES

As is mentioned in chapter 1, the realization of emission reduction targets needs the cooperation of all countries involved. However, according to the result of section 5.2, the asymmetry of benefits is recognized for the six countries surrounding the North Sea. Although the overall welfare is expected, there will be certain countries suffering from increase of operational cost and nodal price, which means that they would sacrifice for the “greater good” if the proposed North Sea Infrastructure is functioning, when no other side payment solutions are found.

Solutions are needed, in future research, to incentives the investment from all countries involved. The working paper [30] provides a solution by “using a capacity-planning model for transmission and generation expansion under perfect competition, in combination with cooperative game theory”.

BIBLIOGRAPHY

- [1] TenneT, “Cooperation european transmission system operators to develop north sea wind power hub,” in <https://www.tennet.eu/news/detail/cooperation-european-transmission-system-operators-to-develop-north-sea-wind-power-hub>, 2017.
- [2] J. Donkers, A. Brand, and P. Eecen, “Offshore wind atlas of the dutch part of the north sea,” *EWEA 2011 Annual Event, Brussels*, 2011.
- [3] A. Croes, “Future north sea infrastructure,” in <https://www.kivi.nl/uploads/medial/589ddf177d345>, 2016.
- [4] M. Belivanis, “Reduced gb network,” in <http://www.maths.ed.ac.uk/optenergy/NetworkData/reducedGB>, 2013.
- [5] ENTSO-E, “Yearly statistics adequacy retrospect,” in <https://www.entsoe.eu/publications/statistics/yearly-statistics-and-adequacy-retrospect/Pages/default.aspx>, 2017.
- [6] L. Vanfretti, S. H. Olsen, V. N. Arava, G. Laera, A. Bidadfar, T. Rabuzin, S. H. Jakobsen, J. Lavenius, M. Baudette, and F. J. Gómez-López, “An open data repository and a data processing software toolset of an equivalent nordic grid model matched to historical electricity market data,” *Data in Brief*, vol. 11, pp. 349–357, 2017.
- [7] Wikipedia, “Category: Renewable energy power stations in norway,” in https://en.wikipedia.org/wiki/Category:Renewable_energy_power_stations_in_Norway, 2017.
- [8] W. E. Council, “Hydropower,” in <https://www.worldenergy.org/data/resources/country/sweden/hydropower/>, 2017.
- [9] N. Pool, “Market data,” in <http://www.nordpoolspot.com/Market-data1/nordic/table>, 2017.
- [10] O. D. Adeuyi and J. Wu, “The north sea grid,” *Proceedings of the Institution of Civil Engineers-Energy*, vol. 168, no. 3, pp. 160–165, 2015.
- [11] ENTSO-E, “Ten year network development plan 2016,” in <http://tyndp.entsoe.eu/reference/#downloads>, 2016.

- [12] H. Farahmand, S. Jaehnert, T. Aigner, and D. Huertas-Hernando, "Nordic hydropower flexibility and transmission expansion to support integration of north european wind power," *Wind Energy*, vol. 18, no. 6, pp. 1075–1103, 2015.
- [13] H. G. Svendsen and O. C. Spro, "Powergama: A new simplified modelling approach for analyses of large interconnected power systems, applied to a 2030 western mediterranean case study," *Journal of Renewable and Sustainable Energy*, vol. 8, no. 5, p. 055501, 2016.
- [14] ENTSO-E, "Future system perspectives," in <http://tyndp.entsoe.eu/insight-reports/future-system>, 2016.
- [15] K. Xie, Q. Liao, H.-M. Tai, and B. Hu, "Non-homogeneous markov wind speed time series model considering daily and seasonal variation characteristics," *IEEE Transactions on Sustainable Energy*, 2017.
- [16] E. W. E. Association, "Wind energy scenarios for 2030," in <https://www.ewea.org/fileadmin/files/library/publications/reports/EWEA-Windenergy-scenarios-2030.pdf>, 2016.
- [17] G. Zhang, B. Zhang, *et al.*, "Wind speed and wind turbine output forecast based on combination method [j]," *Automation of Electric Power Systems*, vol. 18, pp. 92–95, 2009.
- [18] J. Rogelj, M. Den Elzen, N. Höhne, T. Fransen, H. Fekete, H. Winkler, R. Schaeffer, F. Sha, K. Riahi, and M. Meinshausen, "Paris agreement climate proposals need a boost to keep warming well below 2 c," *Nature*, vol. 534, no. 7609, pp. 631–639, 2016.
- [19] E. C. D.-G. for Energy and E. M. P. (Greece), *European energy and transport: Trends to 2030*. European Communities, 2003.
- [20] ENTSO-E, "Monthly statistics reports," in <https://www.entsoe.eu/publications/statistics/monthly-statistics/Pages/default.aspx>, 2017.
- [21] TenneT, "North sea infrastructure," in <https://www.tennet.eu/our-key-tasks/innovations/north-sea-infrastructure/>, 2017.
- [22] T. Houghton, K. Bell, and M. Doquet, "Offshore transmission for wind: Comparing the economic benefits of different offshore network configurations," *Renewable Energy*, vol. 94, pp. 268–279, 2016.
- [23] A. Larrañaga Arregui, "Cost benefit analysis of different offshore grid topologies in the north," Master's thesis, NTNU, 2017.

- [24] I. Konstantelos, D. Pudjianto, G. Strbac, J. De Decker, P. Joseph, A. Flament, P. Kreutzkamp, F. Genoese, L. Rehfeldt, A.-K. Wallasch, *et al.*, “Integrated north sea grids: The costs, the benefits and their distribution between countries,” *Energy Policy*, vol. 101, pp. 28–41, 2017.
- [25] R. Irnawan, F. F. da Silva, C. L. Bak, and T. C. Bregnhøj, “An initial topology of multi-terminal hvdc transmission system in europe: A case study of the north-sea region,” in *Energy Conference (ENERGYCON), 2016 IEEE International*, pp. 1–6, IEEE, 2016.
- [26] J. Kester, E. Wiggelinkhuizen, M. Ars, E. Kontos, P. Bauer, J. Gazendam, and F. Nieuwenhout, “Electrical integration of north sea wind power plants using interconnectors,” *Wind Energy*, vol. 2016, p. 2015, 2017.
- [27] T. Brown, P.-P. Schierhorn, E. Tröster, and T. Ackermann, “Optimising the european transmission system for 77% renewable electricity by 2030,” *IET Renewable Power Generation*, vol. 10, no. 1, pp. 3–9, 2016.
- [28] H. G. Svendsen, “Powergama user guide v1.1,” 2017.
- [29] H. G. Svendsen, “Powergama/home,” in https://bitbucket.org/harald_g_svendsen/powergama/wiki/Home, 2017.
- [30] M. Kristiansen, F. D. Munoz, S. Oren, and M. Korpås, “Efficient allocation of monetary and environmental benefits in multinational transmission projects: North seas offshore grid case study,” in *Heading Towards Sustainable Energy Systems: Evolution or Revolution?, 15th IAEE European Conference, Sept 3-6, 2017*, International Association for Energy Economics, 2017.
- [31] A. Brand, “Offshore wind atlas of the dutch part of the north sea,” *Global Wind Power 2008, Beijing*, 2008.
- [32] T. Senjyu, D. Hayashi, N. Urasaki, and T. Funabashi, “Optimum configuration for renewable generating systems in residence using genetic algorithm,” *IEEE Transactions on Energy Conversion*, vol. 21, no. 2, pp. 459–466, 2006.
- [33] R. Karki, P. Hu, and R. Billinton, “A simplified wind power generation model for reliability evaluation,” *IEEE transactions on Energy conversion*, vol. 21, no. 2, pp. 533–540, 2006.
- [34] R. E. Science and Technology, “Wind power, a clean and renewable energy,” in <http://www.renewableenergyst.org/wind.htm>, 2018.

- [35] P. Härtel, T. K. Vrana, T. Hennig, M. von Bonin, E. J. Wiggelinkhuizen, and F. D. Nieuwenhout, "Review of investment model cost parameters for vsc hvdc transmission infrastructure," *Electric Power Systems Research*, vol. 151, pp. 419–431, 2017.
- [36] M. Bennett, N. Dhaliwal, and A. Leirbukt, "A survey of the reliability of hvdc systems throughout the world during 2009-2010," *44rd CIGRE Session, Paris, France*, 2012.
- [37] C. Chen and G. Ren, "The updated understanding of the change in near-surface and upper air wind and wind energy," 2016.
- [38] O. Edenhofer, R. Pichs-Madruga, Y. Sokona, K. Seyboth, S. Kadner, T. Zwickel, P. Eickemeier, G. Hansen, S. Schlömer, C. von Stechow, *et al.*, *Renewable energy sources and climate change mitigation: Special report of the intergovernmental panel on climate change*. Cambridge University Press, 2011.
- [39] Q. Chen, "Model and algorithm research of operation optimization of active distribution system." XJTU, 2015.
- [40] A. Sanchez-Lorenzo, M. Wild, M. Brunetti, J. A. Guijarro, M. Z. Hakuba, J. Calbó, S. Mystakidis, and B. Bartok, "Reassessment and update of long-term trends in downward surface shortwave radiation over europe (1939–2012)," *Journal of Geophysical Research: Atmospheres*, vol. 120, no. 18, pp. 9555–9569, 2015.
- [41] R. Pašičko, "Impacts of climate change on renewable energy sources in croatia," in *Joint ICTP-IAEA Workshop on Vulnerability of Electricity Systems to Climate Change and Extreme Events, UNDP Croatia*, 2010.
- [42] E. E. Agency, "Global and european temperature," 2010.
- [43] N. Andersson, "Managing the business of hydropower," in <http://slideplayer.com/slide/7258670/>, 2008.
- [44] cqvip.com, "Introduction to the influen of climate change to hydro power," in <http://www.cqvip.com/read/read.aspx?id=666048356>, 2016.
- [45] weather.com, "Climate change leads to less hydro power," in <http://www.weather.com.cn/climate/2016/01/qhbhyw/2460973.shtml>, 2016.
- [46] Enerdata, "Global energy statistical yearbook 2017," in <https://yearbook.enerdata.net/electricity/electricity-domestic-consumption-data.html>, 2017.
- [47] Wikipedia, "World energy consumption," in https://en.wikipedia.org/wiki/World_energy_consumption, 2018.

- [48] P. E. Bett and H. E. Thornton, "The climatological relationships between wind and solar energy supply in Britain," *Renewable Energy*, vol. 87, pp. 96–110, 2016.
- [49] G. E. Box, G. M. Jenkins, G. C. Reinsel, and G. M. Ljung, *Time series analysis: forecasting and control*. John Wiley & Sons, 2015.
- [50] Statnett, "Long-term market analysis-the nordic region and Europe 2016-2040," in http://www.statnett.no/Documents/Nyheter_og_media/Nyhetsarkiv/2016/Longterm%20Market%20Analysis%20The%20Nordic%20Region%20and%20Europe%202016-2040.pdf, 2016.
- [51] E. Consulting, "The potential of power-to-gas: Technology review and economic potential assessment," in <http://www.enea-consulting.com/wp-content/uploads/2016/01/ENEAConsulting-The-potential-of-power-to-gas.pdf>, 2016.
- [52] U. F. E. R. Commission *et al.*, "Promoting wholesale competition through open access non-discriminatory transmission services by public utilities; recovery of stranded costs by public utilities and transmitting utilities," *Order*, vol. 888, p. 24, 1996.

.1. RUNPOWERGAMA.PY

```

1 # -*- coding: utf-8 -*-
2 ### This file is mainly built by the author of PowerGAMA, Harald Svendsen
3
4 ## 1. Data importing and initialization
5 # importing necessary components for simulation and plotting
6 from __future__ import division
7 import powergama
8 import powergama.GIS
9 import powergama.scenarios
10 import time
11 import matplotlib.pyplot as plt
12
13 # setting simulation time
14 timerange=range(0,8760)
15
16 data = powergama.GridData()
17 # setting the path of reading data, and of saving data and figure
18 datapath= "data/"
19 resultpath= "result/"
20 scenarioPrefix = "2030_"
21 # if no new optimization of the beginning wanted, set rerun=False for analyzing
    already existing file
22 rerun = True
23 # saving the optimization result in an sqlite3 file
24 sqlfile = "2030.sqlite3"
25
26 data.readGridData(nodes=datapath + scenarioPrefix + "nodes.csv",
27                  ac_branches=datapath + scenarioPrefix + "branches.csv",
28                  dc_branches=datapath + scenarioPrefix+ "hvdc.csv",
29                  generators=datapath + scenarioPrefix + "generators.csv",
30                  consumers=datapath + scenarioPrefix + "consumers.csv")
31 data.readProfileData(filename=datapath+"profiles.csv",
32                      storagevalue_filling=datapath+"profiles_storval_filling.csv",
33                      storagevalue_time=datapath+"profiles_storval_time.csv",
34                      timerange=timerange,
35                      timedelta=1.0)
36
37 ## 2. Running optimization
38 lp = powergama.LpProblem(data)
39 if rerun:
40     res = powergama.Results(data, resultpath+sqlfile, replace=True)
41     start_time = time.time()
42     lp.solve(res)
43     end_time = time.time()
44     print("\nExecution time = "+str(end_time - start_time)+"seconds")

```

```

45 else:
46     res = powergama.Results(data, resultpath+sqlfile ,replace=False)
47
48 ## 3. Analyzing the results
49 # saving result to a .kml file which can be opened in Google Earth.
50 powergama.GIS.makekml(resultpath+"2030.kml",data,res=res,
51                       nodetype="nodalprice",branchtype="flow",
52                       title="2030")
53 # plotting grid map with nodal color indicating energy balance and branch color
54   indicating utilization rate
55 res.plotMapGrid(nodetype="energybalance",branchtype="utilisation", show_node_labels=
56                 False, dotsize=60, draw_par_mer=False, showTitle=False)
57 # plotting grid map with nodal color indicating nodal price and branch color
58   indicating power flow
59 res.plotMapGrid(nodetype="nodalprice",branchtype="flow", show_node_labels=False,
60                 dotsize=60, draw_par_mer=False, showTitle=False)
61 # plotting generation mix in NL
62 res.plotGenerationPerArea('NL', fill=True)
63 # plotting demand curve in six countries around the North Sea
64 res.plotDemandPerArea(areas=('NL', 'DE', 'GB', 'DK', 'BE', 'NO'))
65 # plotting energy mix for all countries
66 res.plotEnergyMix(relative=True,showTitle=False)
67 # plotting spilled renewable energy in relevant areas (six surrounding countries and
68   Dogger Bank)
69 res.plotEnergyMix(variable='spilled', relative=False, areas=('NL', 'DE', 'GB', 'DK', 'BE',
70   'NO', 'DB'),showTitle=False, gentypes=['hydro', 'wind', 'wind_offshore', 'solar_pv',
71   'solar_csp'])
72 # plotting yearly area price change by color
73 res.plotTimeseriesColour(('NL', 'DE', 'GB', 'DK', 'BE', 'NO'),value='nodalprice')
74 # plotting yearly area price change by curve
75 res.plotAreaPrice(areas=['NL', 'DE', 'DK', 'GB', 'BE', 'NO'])
76
77 # saving power flow in HVDC connectors results (value of average power flow in both
78   directions)
79 dc=res.getAverageBranchFlows(branchtype='dc')
80 import pandas as pd
81 dem_dc=pd.DataFrame(dc)
82 dem_dc.to_csv(resultpath+'dcpowerflow.csv')
83
84 # saving area price (resolution = per hour)
85 ap=res.getAreaPrices(area='NL')
86 import pandas as pd
87 dem_ap=pd.DataFrame(ap)
88 dem_ap.to_csv(resultpath+'NLprice.csv')
89
90 # saving Norwegian hydro reservoir level in percentage
91 area = 'NO'
92 genType = 'hydro'

```

```

85 timeMaxMin = [res.timerange[0],res.timerange[-1]+1]
86 storCap = 0
87 genTypeIdx = res.grid.getGeneratorsPerAreaAndType()[area][genType]
88 reservoirPerc = [i*100 for i in
89 res.db.getResultStorageFillingMultiple(genTypeIdx,
90 timeMaxMin, storCap)]
91 import pandas as pd
92 dem_dfreper = pd.DataFrame(reservoirPerc)
93 dem_dfreper.to_csv(resultpath+"NOhydro.csv")
94
95 # saving system operational cost of every country
96 sc=res.getSystemCost()
97 import pandas as pd
98 dem_sc=pd.DataFrame(sc)
99 dem_sc.to_csv(resultpath+'systemcost.csv')

```

.2. RUNPOWERGIM.PY

```

1 # -*- coding: utf-8 -*-
2 ### This file is mainly built by the author of PowerGIM, Martin Kristiansen
3
4 ## 1. Data importing and initialization
5
6 # importing necessary components for simulation and plotting
7 from __future__ import division
8 import Model
9 import Model.powergim as pgim
10 import Model.GIS
11 import pyomo.environ as pyo
12 import pandas as pd
13 import numpy as np
14 import time
15
16 # additional script to rewrite the function from Results.py
17 # CAPEX calculation (NPV) of specific branches
18 def computeCostBranch(model,b,include_om=False):
19
20     stage=1
21     ar = 1
22     br_num=int(model.branchExistingCapacity[b]/700)
23     br_cap=model.branchExistingCapacity[b]
24     b_cost = 0
25
26     salvagefactor = (int(stage-1)*model.stage2TimeDelta/model.financeYears)*(
27         1/((1+model.financeInterestrate)
28             *(model.financeYears-model.stage2TimeDelta*int(stage-1))))
29     discount_t0 = (1/((1+model.financeInterestrate)
30         *(model.stage2TimeDelta*int(stage-1))))

```



```

79 generators = "data/generators.csv",
80 consumers = "data/consumers.csv")
81 grid_data.readProfileData(filename = "data/profiles.csv",
82 timerange = range(8760),
83 timedelta = 1.0)
84
85 # reducing the size of the time series (i.e. sampling or clustering)
86 print("sampling new time steps...")
87 samplesize = 400
88 timerange = pd.np.random.choice(8760, size=samplesize, replace=False)
89 pd.np.random.seed(2017)
90 grid_data.readProfileData(filename="data/profiles.csv",
91 timerange = timerange,
92 timedelta = 1.0)
93
94 ## 2. Optimization formulating and running
95
96 # formulating the optimization model
97 print("formulating model...")
98 sip = pgim.SipModel()
99 dict_data = sip.createModelData(grid_data,
100 datafile='data/parameters.xml',
101 maxNewBranchNum=4,
102 maxNewBranchCap=10000)
103 model = sip.createConcreteModel(dict_data)
104 df_res = pd.DataFrame(columns=['Costs'])
105
106 # running optimization
107 print("solving optimization model")
108 opt = pyo.SolverFactory('cbc')
109 results = opt.solve(model, tee=True,
110 keepfiles=True,
111 symbolic_solver_labels=True)
112 print("Finished!")
113 i=0
114
115 ## 3. Analyzing the results
116
117 # outputting CAPEX of specific branches
118 branches=[0,1,2,3,4,5,6,7]
119 df_res.loc[i, 'Costs'] = sum(computeCostBranch(model,b,include_om=True) for b in
    branches)/10**9
120 writer = pd.ExcelWriter('data/results/CAPEX.xlsx')
121 df_res.to_excel(writer, 'CAPEX')
122 writer.save()
123
124 # saving results (investment recommendation, results operational cost, etc.) to Excel
    file

```

```
125 sip.saveDeterministicResults(model=model, excel_file='data/results/results.xlsx')
126
127 # saving the results in the so called pg_res variable, for visualization
128 grid_res = sip.extractResultingGridData(grid_data, model=model)
129 pg_res = Model.Results(grid_res, databasefile='data/results/results.sqlite3', sip=
    True)
130
131 # creating two .kml files for analysing the results in Google Earth.
132 # saving input grid topology to "inputgrid.kml"
133 Model.GIS.makekml("data/results/inputgrid.kml", grid_data=grid_data,
134 nodetype='powergim_type', branchtype='powergim_type',
135 res=None, title='inputgrid')
136 # saving output grid topology to "outputgrid.kml"
137 Model.GIS.makekml("data/results/outputgrid.kml", grid_data=grid_res,
138 nodetype='powergim_type', branchtype='powergim_type',
139 res=None, title='outputgrid')
```